INVEST. BUILD. GROW.

MANITOBA

GEOSCIENTIFIC REPORT GR2021-1

BEDROCK GEOLOGY OF THE CENTRAL SIPIWESK LAKE AREA, PIKWITONEI GRANULITE DOMAIN, CENTRAL MANITOBA (PART OF NTS 63P4)

Manitoba Geological Survey

Manitoba

Geoscientific Report GR2021-1

Bedrock geology of the central Sipiwesk Lake area, Pikwitonei granulite domain, central Manitoba (part of NTS 63P4)

by C.G. Couëslan
Manitoba Geological Survey
Winnipeg, 2021

Couëslan, C.G. 2021: Bedrock geology of the central Sipiwesk Lake area, Pikwitonei granulite domain, central Manitoba (part of NTS 63P4); Manitoba Agriculture and Resource Development, Manitoba Geological Survey, Geoscientific Report GR2021-1, 47 p. plus 1 appendix and 1 map at 1:20 000 scale.

NTS grid: 63P4

Published by:

Manitoba Agriculture and Resource Development
Manitoba Geological Survey
360–1395 Ellice Avenue
Winnipeg, Manitoba
R3G 3P2 Canada

Telephone: 1-800-223-5215 (General Enquiry)
204-945-6569 (Publication Sales)
Fax: 204-945-8427
E-mail: minesinfo@gov.mb.ca
Website: manitoba.ca/minerals

ISBN: 978-0-7711-1628-5

This publication is available to download free of charge at manitoba.ca/minerals.

Cover illustrations:

Left: Pseudotachylite vein crosscutting gneissic trondhjemite.

Right: Hematite alteration along joints in gneissic trondhjemite.

Abstract

A mapping campaign of the Pikwitonei granulite domain was initiated with work in the central Sipiwesk Lake area in the summer of 2012. The purpose of the study was to remap the area using protolith interpretation and determine any relationships between the Pikwitonei domain and adjacent domains of the Superior province. Rocks of the gneissic tonalite suite are the most volumetrically dominant in the map area and consist of a gneissic tonalite unit and a gneissic trondhjemite unit. A sample of gneissic trondhjemite yielded a magmatic age of ca. 2784 Ma, and this suite is tentatively interpreted as the basement upon which all other units were deposited or into which they were emplaced. The mafic gneiss suite consists of interlayered leucocratic and mesocratic mafic gneiss with local layers of iron formation. It is interpreted as a mafic volcanic assemblage with dominantly arc-tholeiite to calcalkaline affinity. The mafic gneiss suite is locally associated and interlayered with rocks of the shoshonitic gneiss suite. The shoshonitic gneiss suite consists of mafic and intermediate gneisses with shoshonitic geochemistry that are interpreted to be part of the same volcanic assemblage as the mafic gneiss suite.

Spatially associated with the volcanic assemblage are exposures of siliciclastic rocks consisting of arkosic arenite, arkosic wacke and mudstone. The three varieties of siliciclastic rocks are commonly interlayered. Rare layers of mafic gneiss, interpreted as mafic tuff or sandstone, occur within the siliciclastic package. Sparse occurrences of gneisses with unusual bulk compositions are present but not resolvable at map scale. One variety is Al and Mg rich, and characterized by abundant cordierite and orthopyroxene, and local sapphirine. It may be a product of volcanogenic massive sulphide (VMS)–style hydrothermal alteration. Another gneiss of unusual composition is enriched in Al and Ca. It is tentatively interpreted as a metamorphosed epidosite. The preceding units are intruded by variably foliated granitoids that are assumed to be Archean, and a swarm of unmetamorphosed Paleoproterozoic ultramafic to mafic dikes. Geochemistry of the mafic dikes is similar to that of contaminated mid-ocean–ridge basalt, and the larger dikes typically trend north-northeast, suggesting they are part of the Molson dike swarm.

The majority of Archean rocks are characterized by an S_1 gneissosity that was transposed by an S_2 foliation. The S_2 foliation is axial planar to minor F_2 folds. Leucosome and ultrahigh-temperature metamorphic assemblages (sillimanite-orthopyroxene-quartz±sapphirine) are overprinted by the S_2 foliation, suggesting that D_2 outlasted high-grade metamorphism. Peak metamorphic conditions are estimated to have reached 1025–1070°C and 8.0–9.5 kbar. Microtextures and retrograde mineral assemblages suggest a clockwise pressure-temperature-time path, and high-temperature decompression and D_2 were likely underway by ca. 2645 Ma. Paleoproterozoic brittle structures consist of pseudotachylite veins and breccias, which are interpreted to be coincident with the mafic-dike magmatism and later fault gouge–lined fracture zones.

Lithological associations, and whole-rock lithogeochemistry and Sm-Nd isotope geochemistry suggest a correlation between the volcanic assemblage, comprising the mafic gneiss and shoshonitic gneiss suites, and the Oxford Lake group of the Oxford Lake–Knee Lake greenstone belt of the adjacent Oxford-Stull domain. Detrital-zircon analyses suggest a correlation between the siliciclastic rocks of central Sipiwesk Lake and the synorogenic deposits of the Oxford Lake–Knee Lake belt and the Cross Lake group of the Cross Lake greenstone belt. This implies an unconformable relationship between the volcanic assemblage and siliciclastic rocks at Sipiwesk Lake, which is no longer apparent because of deformation and high-grade metamorphism. These correlations suggest a notional potential in the Sipiwesk Lake area for any of the mineral deposit types found in the Oxford-Stull domain, including lode Au, volcanogenic massive sulphide and anorthosite-related Fe-Ti.

Résumé

Une campagne de cartographie du domaine de la granulite de Pikwitonei a été lancée à l'été 2012, lors des travaux dans la région centrale du lac Sipiwesk. L'étude avait pour objectif de refaire les cartes de la région à l'aide de l'interprétation des protolites et de déterminer toute relation entre le domaine de Pikwitonei et les domaines adjacents de la province du lac Supérieur. Dans la région de la carte, les roches de la suite tonalite gneissique dominent, en termes de volume; elles sont constituées d'une unité de tonalite gneissique et d'une unité de trondhjémite gneissique. Un échantillon de trondhjémite gneissique a donné un âge magmatique d'environ 2 784 Ma; cette suite est interprétée de façon provisoire comme le socle sur lequel toutes les autres unités ont été déposées ou dans lesquelles elles ont été mises en place. La suite de gneiss mafique est constituée de gneiss mafique leucocrate et mésocrate interstratifié dans des lits de formation ferrifère locaux. Il est interprété comme un assemblage volcanique mafique indiquant une tendance vers un arc tholéiitique à calco-alcalin. La suite de gneiss mafique est associée localement et interstratifiée dans les roches de la suite de gneiss shoshonitique. La suite de gneiss shoshonitique est constituée de gneiss mafiques et intermédiaires à géochimie shoshonitique qui sont interprétés comme faisant partie du même assemblage volcanique que la suite de gneiss mafique.

Des affleurements de roches silicoclastiques constituées d'arénite arkosique, de wacke arkosique et de mudstone sont associés dans l'espace à l'assemblage volcanique. Les trois variétés de roches silicoclastiques sont généralement interstratifiées. De rares lits de gneiss mafique, interprétés comme du tuf mafique ou du grès, se trouvent à l'intérieur de l'ensemble siliciclastique. De rares occurrences de gneiss aux compositions globales inhabituelles sont présentes, mais elles ne peuvent pas être résolues à l'échelle cartographique. Une des variétés, riche en Al et en Mg, se caractérise par une abondance de cordiérite et d'orthopyroxène, ainsi que de saphirine locale. Il peut s'agir d'un produit d'altération hydrothermale de type

sulfure massif volcanogène (SMV). Un autre gneiss de composition inhabituelle est enrichi en Al et Ca. Il est interprété de façon provisoire comme une épidosite métamorphisée. Les unités précédentes sont pénétrées par des granitoïdes à foliation variable, qui sont présumés être du Précambrien ancien, et un essaim de dykes ultramafiques à mafiques non métamorphisés du Paléoprotérozoïque. La géochimie des dykes mafiques est semblable à celle du basalte contaminé de dorsale médio-océanique et les plus gros dykes ont généralement une direction nord-nord-est, ce qui semble indiquer qu'ils font partie de l'essaim de dykes Molson.

La majorité des roches archéennes sont caractérisées par une gneissosité S_1 qui a été transposée par une foliation S_2. La foliation S_2 est caractérisée par une coïncidence avec le plan axial des plis mineurs F_2. Les associations métamorphiques de leucosome à température ultra-haute (sillimanite-orthopyroxène-quartz±saphirine) sont surimposées par la foliation S_2, ce qui semble indiquer que le D_2 a survécu au métamorphisme intense. On estime que les conditions métamorphiques maximales ont atteint de 1 025 à 1 070 °C et de 8,0 à 9,5 kbar. Les microtextures et les associations minérales rétromorphosées semblent indiquer un cheminement pression-température-temps dans le sens des aiguilles d'une montre, et la décompression à haute température et le D_2 étaient probablement en cours vers environ 2 645 Ma. Les structures fragiles du Paléoprotérozoïque sont constituées de filons et de brèches pseudo-tachylites, qui sont interprétés comme coïncidant avec le magmatisme des dykes mafiques et, plus tard, les zones de fractures bordées de failles.

Les associations lithologiques, la lithogéochimie de la roche entière et la géochimie des isotopes Sm-Nd semblent indiquer une corrélation entre l'assemblage volcanique, qui comprend les suites de gneiss mafique et de gneiss shoshonitique, et le groupe Oxford Lake de la ceinture de roches vertes du lac Oxford-lac Knee du domaine Oxford-Stull adjacent. Des analyses des zircons détritiques semblent indiquer une corrélation entre les roches silicoclastiques de la région centrale du lac Sipiwesk, les dépôts synorogéniques de la ceinture de roches vertes du lac Oxford-lac Knee et le groupe du lac Cross de la ceinture de roches vertes du lac Cross. Cela implique une relation discordante entre l'assemblage volcanique et les roches silicoclastiques du lac Sipiwesk, qui n'est plus apparente en raison de la déformation et du métamorphisme intense. Ces corrélations semblent indiquer l'existence d'un potentiel théorique dans la région du lac Sipiwesk de tous les types de gisements minéraux que l'on trouve dans le domaine Oxford-Stull, y compris le filon aurifère (Au), les sulfures massifs volcanogènes et l'anorthosite de Fe-Ti.

TABLE OF CONTENTS

Page

TABLES

FIGURES

APPENDIX

MAP

Introduction

A mapping campaign in the Pikwitonei granulite domain (PGD) of Manitoba was initiated in the summer of 2012 with work in the central Sipiwesk Lake area. Previous mapping in the area (Hubregtse, 1977, 1978; Hubregtse et al., 1978a) utilized descriptive petrography, and the majority of units were classified as either granofels (sic) or enderbites, which were further separated by the use of mineral-assemblage qualifiers (e.g., garnet-plagioclase-quartz-pyroxene±hornblende granofels and gneiss; Hubregtse et al., 1978a, b). One of the primary goals of the new mapping initiative was to remap the area and add protolith interpretation to define rock units. This was accomplished by integrating field observations with lithogeochemistry, isotope analyses and phase-equilibria modelling. However, interpretation of a protolith was not always possible because of the high metamorphic grade. It is hoped that an understanding of the origins of the gneisses that make up the PGD will lead to a better understanding of the domain and its relationship to adjacent domains and greenstone belts of the Superior province.

Previous work

The earliest geological investigations in the PGD were carried out by the Geological Survey of Canada. Robert Bell completed a track survey of the upper Nelson River, including Sipiwesk Lake and portions of the Grass River via Wintering and Landing lakes (Bell, 1879, 1880). The area was revisited in 1900 by J.B. Tyrrell, who followed a route up the Nelson River from Lake Winnipeg to Sipiwesk Lake and continued to Landing and Wintering lakes before ascending the Burntwood River (Tyrrell, 1903). These early accounts describe the geology of the region as 'Laurentian' or grey gneiss with intrusions of 'trap' or gabbro dikes.

A preliminary map that includes the northern Sipiwesk Lake area was compiled at a scale of 1:253 440 (1 inch to 4 miles) by Harrison (1951). A regional gravity high in the Nelson River area was described by Innes (1960), who interpreted it to represent the roots of a former mountain belt. The structural and metamorphic transition from the PGD rocks of Sipiwesk Lake to retrogressed rocks of the Superior boundary zone (SBZ) in the Wabowden area was the subject of a Ph.D. thesis by Rance (1966), which included a 1:126 720 (one inch to two mile) geological map. Rance was the first to suggest that the nonmetamorphosed mafic and ultramafic dikes of the PGD could be equivalent to the amphibolite dikes of the SBZ. This portion of the PGD and SBZ was also the subject of 1:250 000 scale regional mapping by Bell (1971, 1978) that extended westward to include the Wekusko Lake area. A summary of the PGD geology as it was understood at the time was published by Ermanovics and Davison (1976).

A program to map much of the PGD was initiated by the Manitoba Geological Survey (MGS) in 1976 with mapping by Hubregtse (1977, 1978) in the Sipiwesk, Wintering and Landing lakes areas. The results of this mapping program were synthesized in several publications (Weber and Scoates, 1978; Hubregtse, 1980; Weber, 1983). This was followed by a series of metamorphic petrology studies (Arima and Barnett, 1984; Paktunç and Baer, 1986; Macek, 1989) and collaborative geochronology studies (Krogh et al., 1986), as well as a Ph.D. thesis in the late 1980s that focused on the metamorphic history of the domain (Mezger, 1989; Mezger et al., 1990). A summary of the PGD geology was assembled by Weber and Mezger (1990). The surficial geology of the area was compiled by Matile and Keller (2006), who interpreted much of the Sipiwesk Lake area to be overlain by glaciolacustrine sediments. The most recent work in the area has focused on geochronology and unravelling the complex metamorphic history of the PGD (Kooijman et al., 2010, 2012; Heaman et al., 2011; Smit et al., 2013; Guevara, 2017; Guevara et al., 2020a).

General geology

The PGD is a Neoarchean high-grade metamorphic domain along the northwestern edge of the Superior craton (Figure 1). It is exposed over a length of greater than 200 km and has a maximum width of 75 km (Hubregtse, 1980; Böhm et al., 1999). The southeastern boundary of the domain is marked by a regional orthopyroxene-in isograd that, in part, coincides with the North Kenyon fault and is oblique to the generally east-west fabrics of the Superior province (Hubregtse, 1980; Heaman et al., 2011; Guevara et al., 2020a). The northwestern boundary of the PGD is defined by Paleoproterozoic Hudsonian (ca. 1.80 Ga) deformational fabrics that trend north-northeast and truncate the domain's Neoarchean fabrics (Hubregtse, 1980; Heaman et al., 2011; Kuiper et al., 2011; Couëslan, 2014c, 2016b). The PGD is considered to be part of the Hudson Bay terrane (Percival et al., 2006; Percival et al., 2012). However, recent Sm-Nd isotope results suggest that the orthopyroxene-in isograd crosscuts the boundary between the Hudson Bay and North Caribou terranes (Couëslan, 2014a, 2016a), which amalgamated ca. 2720 Ma through subduction-accretion–style tectonics (Percival et al., 2012). This is in agreement with observations by Hubregtse (1980), who traced metavolcanic rocks from the Cross Lake belt of the North Caribou terrane into the PGD south of Sipiwesk Lake.

The PGD is underlain mainly by orthopyroxene-bearing, felsic to intermediate metaplutonic rocks and mafic granulites (metagabbros, metapyroxenites and metabasalts; Figure 2; Hubregtse, 1978a, 1980; Heaman et al., 2011). Supracrustal rocks were considered to be relatively rare in the PGD and, in the Sipiwesk area, had only been recorded toward the southern end of Bear Island (Hubregtse, 1980). The PGD has experienced two main generations of tectonometamorphism. The D_1-M_1 generation (ca. 2695 Ma) resulted in well-defined, northwest-trending metamorphic layering (S_1) accompanied by isoclinal folding (Hubregtse, 1980). The accompanying M_1 metamorphism is interpreted to have attained amphibolite- to locally hornblende granulite–facies conditions (Hubregtse, 1978a, 1980). The D_2-M_2 generation (ca. 2680 Ma) resulted

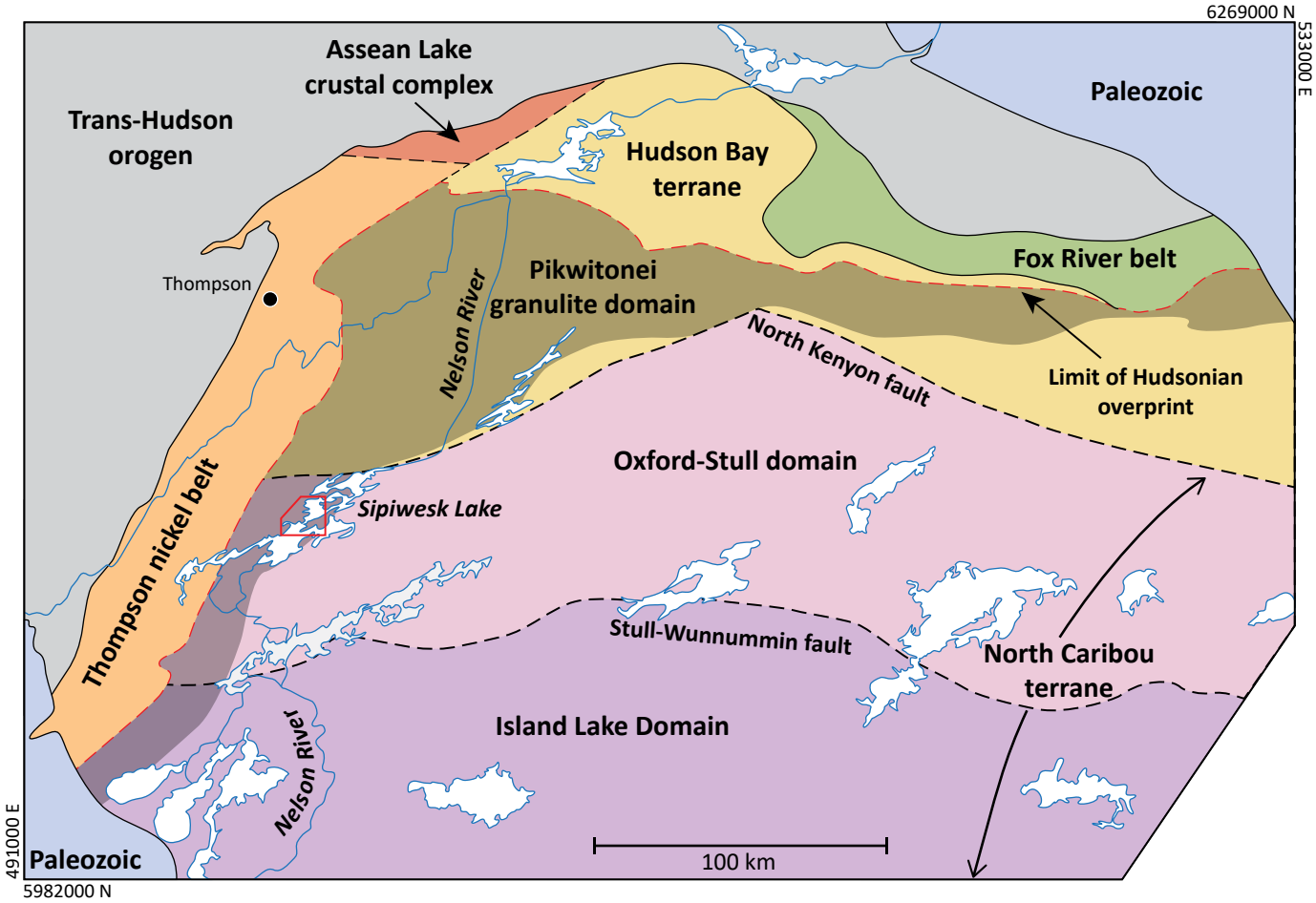

Figure 1: *Geological domains of the northwestern Superior craton of Manitoba (Couëslan, 2016a). Solid red outline indicates approximate location of study area.*

in the development of D_2 fabrics and transposition of S_1 into west-southwest-trending shear folds, accompanied by metamorphism at granulite-facies conditions (Hubregtse, 1980). Heaman et al. (2011) documented isotope dilution–thermal ionization mass spectrometry (ID-TIMS) U-Pb zircon ages of ca. 2716 Ma, ca. 2695 Ma, ca. 2680 Ma and ca. 2642 Ma for samples collected from the Natawahunan, Cauchon and Sipiwesk lakes areas. They attributed the middle two ages to the D_1-M_1 and D_2-M_2 phases of tectonometamorphism. Combined ID-TIMS and laser-ablation split-stream inductively coupled plasma–mass spectrometry (LASS-ICP-MS) U-Pb zircon dating of a sample from Partridge Crop Lake by Guevara et al. (2020a) yielded ages ranging from ca. 2670 to ca. 2650 Ma. These were interpreted as cooling ages after ultrahigh-temperature metamorphism, possibly correlating with the D_2-M_2 event of Heaman et al. (2011). Mezger et al. (1989) reported ID-TIMS U-Pb ages of garnet separates and interpreted ca. 2744–2738 Ma prograde garnet growth in the Natawahunan Lake area; and ca. 2700–2687 Ma prograde garnet growth, ca. 2660–2637 Ma peak-metamorphic garnet growth and ca. 2605–2591 Ma igneous garnet growth (marking the end of high-temperature conditions) in the Cauchon Lake area. Garnet separates dated by Smit et al. (2013) yielded ca. 2724–2680 Ma Lu-Hf ages (interpreted as prograde garnet growth) and ca. 2628–2610 Ma Sm-Nd ages (interpreted as cooling ages).

A variety of peak pressure-temperature conditions have been recorded across the PGD and suggest a metamorphic field gradient ranging from 750–800°C and 6.3–7.0 kbar in the Cauchon Lake area (eastern PGD) to ≥850°C and 6.5–9.0 kbar in the southern and western portions of the PGD (Mezger et al., 1990; Vry and Brown, 1992; Kooijman et al., 2012; Couëslan, 2014b; Guevara et al., 2020a). The PGD has been interpreted as an oblique crustal cross-section (Weber, 1983; Weber and Mezger, 1990), and Mezger et al. (1990) argued for near-isobaric cooling of the PGD and a counter-clockwise pressure-temperature path driven by magmatic underplating. However, Paktunç and Baer (1986) estimated pressures as high as 12 kbar for rocks adjacent to the TNB, which was explained by crustal-thickening processes. Crustal thickening is in agreement with more recent textural observations and phase-equilibrium modelling, which suggest a clockwise pressure-temperature path and near-isothermal decompression (Couëslan, 2013, 2014c; Guevara et al., 2020a).

The northwest Superior craton is intruded by locally abundant mafic to ultramafic dikes that vary from diabasic to gabbroic to peridotitic (Scoates and Macek, 1978). The main

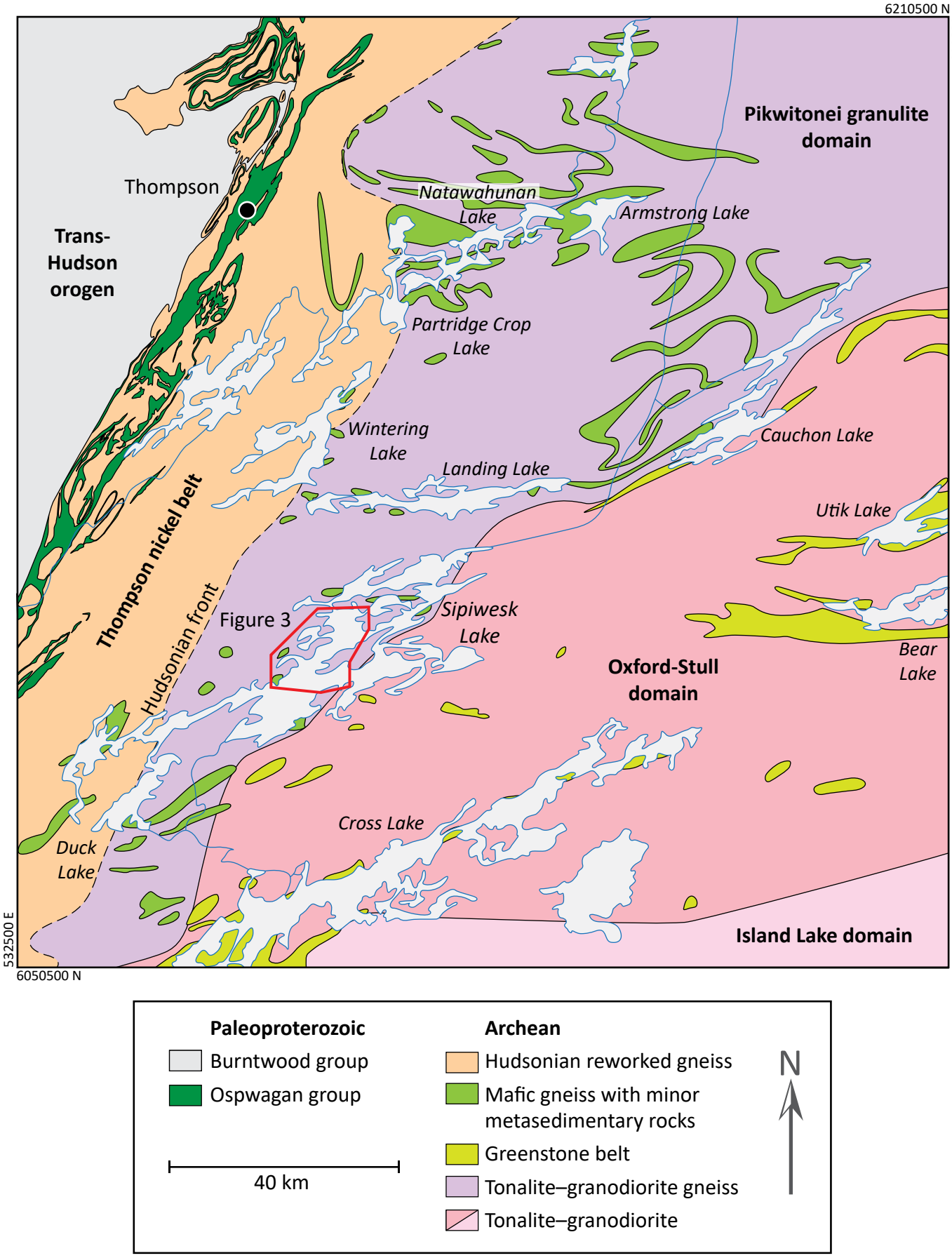

Figure 2: *Simplified geology of the western Pikwitonei granulite domain and adjacent geological domains. Red outline indicates extent of Figure 3 and map area discussed in this report.*

concentration of dikes occurs between the Nelson River and the Superior craton margin, and they likely continue southward beneath Lake Winnipeg and rocks of the Phanerozoic (Scoates and Macek, 1978; Heaman et al., 2009). Intrusion of the dikes occurred during at least two different periods at ca. 2.10 Ga (dominantly east-trending dikes; e.g., Cauchon Lake, Gull Rapids, Birthday Rapids) and ca. 1.88 Ga (Molson dikes; Heaman et al., 1986; Halls and Heaman, 2000; Heaman et al., 2009). The younger, dominantly north-northeast-trending Molson dikes are interpreted to be the more common type in the PGD. Approaching the SBZ, the dikes become metamorphosed and rotated subparallel to the Paleoproterozoic north-northeast-trending foliation (Scoates and Macek, 1978).

Methods and scope

Mapping of the Sipiwesk Lake area was conducted at a scale of 1:20 000, with samples collected for geochemistry and geochronology (Figure 3). The objective was to remap the mafic, intermediate and enderbitic gneiss units, with emphasis on protolith interpretation rather than descriptive petrography (cf. Hubregtse et al., 1978a, b) to assist in assessing the mineral potential of the region and provide further insight into the tectonic significance of the PGD (e.g., Weber and Mezger, 1990). One of the consequences of this approach is the abandonment of the term 'enderbite' in mapping and lithological descriptions. Enderbite is a member of the charnockitic suite, which consists of orthopyroxene-bearing granitic rocks. Charnockite, opdalite and enderbite are equivalent to orthopyroxene-bearing granite, granodiorite and tonalite, respectively (Le Maitre, 2002). These igneous rocks are interpreted to have crystallized from high-temperature anhydrous magmas, which resulted in the formation of igneous orthopyroxene. Because of the high metamorphic grade in the PGD, there are a wide variety of broadly granitoid, orthopyroxene-bearing gneisses that have historically been described as enderbites, opdalites or charnockites (Hubregtse, 1980). However, the orthopyroxene is typically part of a granulite-facies metamorphic assemblage and there is little to no evidence that orthopyroxene occurred as part of a precursor igneous assemblage. These rocks are more properly classified as metagranitoids than as members of the charnockitic suite; as a result, the charnockitic suite nomenclature will not be used in this report.

Migmatite nomenclature

All Archean rocks in the PGD have undergone regional metamorphism, with the vast majority subjected to granulite-facies conditions and partial melting. This report follows the migmatite terminology of Sawyer (2008), which is as follows. A migmatite is a high-grade metamorphic rock that can be heterogeneous at the microscopic to macroscopic scale and is composed of two or more petrographically different parts; one of these parts must have formed by partial melting (anatexis). The neosome is those parts of a migmatite formed by partial melting, which may or may not have resulted in segregation into separate melt and solid fractions. The paleosome is the part of a migmatite not affected by partial melting, where structures older than the partial melting are preserved. The neosome can be composed of several parts. The part of the neosome that is predominantly solid fraction and left after the partial or wholesale extraction of partial melt is referred to as the residuum. The residuum typically forms the melanosome, which is the darker coloured part of the neosome that is typically enriched in mafic minerals. Complementing this is the leucosome, which is the lighter coloured part of the neosome. The leucosome is the part of the migmatite that is derived from segregated partial melt and consists dominantly of feldspar and quartz. Leucosome may be in situ, meaning that it has remained at the site where the melt formed; or in source, meaning that the melt has migrated away from where it formed but is still within the confines of its source layer. Once the melt has migrated out of its source layer and been injected into the surrounding rocks, it is referred to as a vein or dike.

Migmatites can be divided into two main morphological types: metatexites and diatexites. A metatexite is a migmatite that is heterogeneous at the outcrop scale, with coherent pre–partial-melting structures widely preserved in the paleosome, and possibly in the melanosome where the fraction of melt was low. Conversely, a diatexite is neosome dominant with melt pervasively distributed throughout. Pre–partial-melting structures are absent from the neosome and commonly replaced by synanatectic flow structures or by isotropic neosome.

Unit descriptions

Units in the central Sipiwesk Lake area are divided into three main groups:

1) Archean rocks that predate or are synchronous with D_1 deformation: These rocks are characterized by an S_1 gneissosity.
2) Archean rocks that postdate D_1: These rocks are characterized by an S_2 fabric, typically defined by the flattening of quartz-grain aggregates in outcrop.
3) Paleoproterozoic rocks that postdate D_2: These rocks are unaffected by metamorphism or deformation.

Although all Archean rocks have been subjected to intense metamorphism, the 'meta' prefix is omitted to improve readability of the text.

Archean pre- to syn-D_1 gneissic rocks

The rock units within this group are presented in what is tentatively interpreted as geochronological order. See 'Discussion' for details.

Gneissic tonalite suite

Gneissic tonalite and gneissic trondhjemite are the volumetrically dominant rock types in the Sipiwesk Lake area. The two units are locally interbanded. The gneissic tonalite and trondhjemite vary from light grey to pink to white on weath-

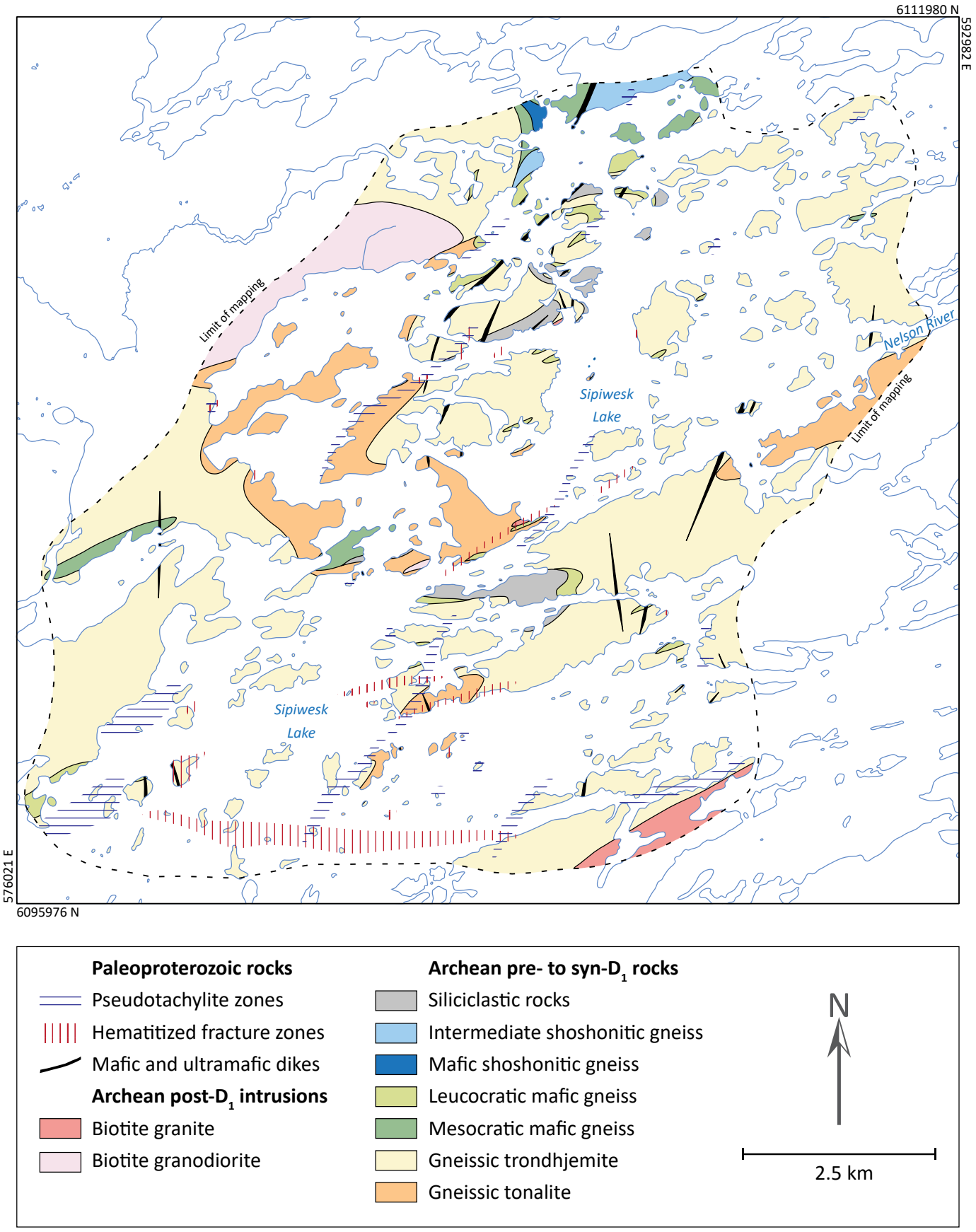

Figure 3: *Geology of the central Sipiwesk Lake area.*

ered surfaces and from honey brown to dark grey-blue on fresh surfaces (Figure 4a). They vary from medium to coarse grained and from nonmagnetic to magnetic. The tonalite contains >10% mafic minerals (Figure 4b), whereas the trondhjemite contains <10%. Mafic minerals consist of varying proportions of clinopyroxene and orthopyroxene, with subordinate magnetite and locally trace biotite. Rare exposures may be orthopyroxene free. Pink feldspar is commonly visible on weathered surfaces, suggesting compositions trending toward granodiorite or granite. While some granodiorite could be present, whole-rock geochemistry and thin-section petrography suggest the pink colouration is most likely from antiperthitic intergrowth in the plagioclase. The tonalite and trondhjemite form metatexites with up to 30% leucosome that is typically transposed but locally forms irregular pods and discordant veins (Figure 4b).

Mafic gneiss suite

Rocks of the mafic gneiss suite are most common in the central and northern portions of the map area. The suite consists dominantly of mafic rocks with sparse ultramafic rocks and banded iron formation, and is locally associated with the shoshonitic gneiss suite. Exposures of the mafic gneiss are typically internally layered and consist of mesocratic and more leucocratic varieties. Although visually different, the two varieties of mafic rock are geochemically similar. Interlayering between the two phases is common and occurs on the scale of centimetres to tens of metres. The proportion of interlayering varies from outcrop to outcrop and can range from entirely one end member to roughly equal proportions of both. The presence of iron formation locally associated with the mafic gneiss suggests that it represents a volcanic assemblage; however, synvolcanic gabbro intrusions are likely present. The rocks typically form a metatexite, but the iron formation may appear as layers of paleosome.

The mesocratic variety of mafic gneiss is dark green to grey, medium to coarse grained and locally strongly magnetic (Figure 5a). It consists dominantly of plagioclase, clinopyroxene, hornblende and orthopyroxene, with subordinate magnetite and rare garnet and biotite. Mafic minerals typically make up more than 40% of the rock. Patches of plagioclase-rich leucosome are common and form up to 20% of a given outcrop. The leucocratic variety of mafic gneiss is light grey-green on weathered surfaces and dark grey to brown-grey on fresh surfaces (Figure 5b). It is medium to coarse grained and varies from nonmagnetic to magnetic. The leucocratic variety is plagioclase rich and contains variable amounts of clinopyroxene and orthopyroxene, with subordinate magnetite and locally minor hornblende and biotite. Quartz is rare but can occur in trace amounts. Mafic minerals typically make up less than 30% of the rock. Patches of coarse-grained leucosome are common and may form up to 30% of the outcrop. Leucosome is typically quartz bearing and plagioclase rich, with minor orthopyroxene and clinopyroxene. Coarse-grained clinopyroxene-rich clots are also common.

A less common garnet-bearing variety of the mafic gneiss can occur adjacent to layers of banded iron formation, as intercalations in arkosic rocks or in rare isolated exposures (Figure 5c). This variety is typically banded on a scale of 1–40 cm, with mafic minerals consisting of varying proportions of garnet, clinopyroxene and orthopyroxene, along with magnetite and local pyrrhotite and biotite. Minor quartz is relatively common. The garnet-bearing rock usually grades into the more typical leucocratic variety, as previously described. There are several possibilities for the paragenesis of the garnet-bearing variety. Weak chloritic alteration could result in the production of garnet during regional metamorphism; however, there is no geochemical evidence of chloritization. It could represent flows of ferrobasalt or be a mixture of volcanogenic and siliciclastic material (see 'Lithogeochemistry and Sm-Nd isotope geochemistry').

Bands and boudins of ultramafic gneiss up to 3 m thick occur within the mafic gneiss suite and rarely in gneissic trondhjemite (Figure 5d). The ultramafic rock is dark brown to black, medium to coarse grained, and magnetic. It is composed of

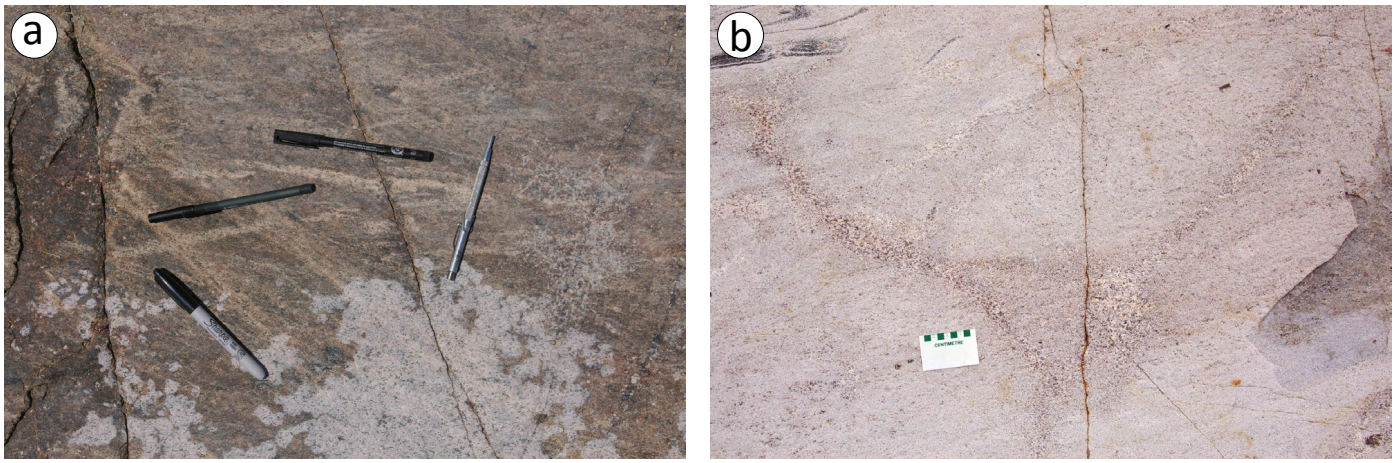

Figure 4: *Outcrop photographs of the gneissic tonalite suite:* ***a)*** *glacially polished gneissic tonalite, the brown colour being a fresh unweathered surface, the lighter patch at the bottom a slightly weathered surface, with pens indicating the orientations of multiple glacial striae and pen magnet indicating north;* ***b)*** *gneissic trondhjemite with pod of in-source leucosome adjacent to scale card.*

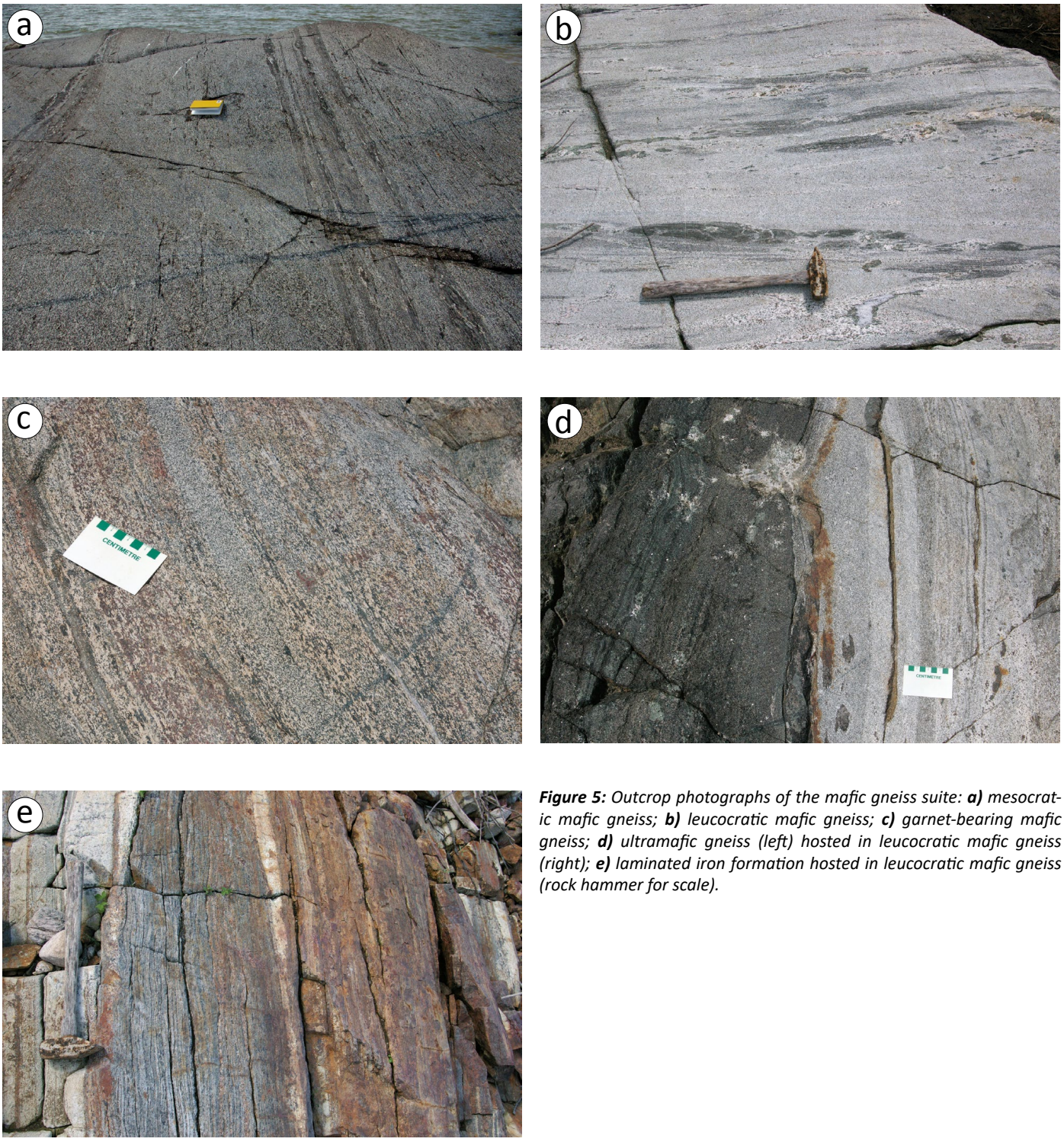

Figure 5: *Outcrop photographs of the mafic gneiss suite:* ***a)*** *mesocratic mafic gneiss;* ***b)*** *leucocratic mafic gneiss;* ***c)*** *garnet-bearing mafic gneiss;* ***d)*** *ultramafic gneiss (left) hosted in leucocratic mafic gneiss (right);* ***e)*** *laminated iron formation hosted in leucocratic mafic gneiss (rock hammer for scale).*

clinopyroxene and orthopyroxene, with subordinate hornblende, minor plagioclase and magnetite, and rare biotite. The ultramafic rock could represent metamorphosed pyroxenite dikes, pyroxenitic layers in gabbro or ultramafic volcanic rocks.

Banded iron formation typically occurs as gossan-stained bands up to 1.5 m thick associated with mafic gneiss suite (Figure 5e). The iron formations are typically medium grained, strongly magnetic and characterized by chert laminations. They are rich in quartz, green orthopyroxene and magnetite, with variable amounts of pyrrhotite and garnet.

Shoshonitic gneiss suite

Two varieties of shoshonitic gneiss (intermediate and mafic) are present in the north-central portion of the map area. The intermediate variety is volumetrically dominant and is locally interbanded with the mesocratic mafic gneiss. The intermediate gneiss is light pink to pinkish grey on weathered surfaces and dark grey on fresh surfaces (Figure 6a). It varies from well layered to relatively homogeneous and typically forms a metatexite. It is medium to coarse grained and magnetic. Mafic minerals typically make up 10–20% of the rock

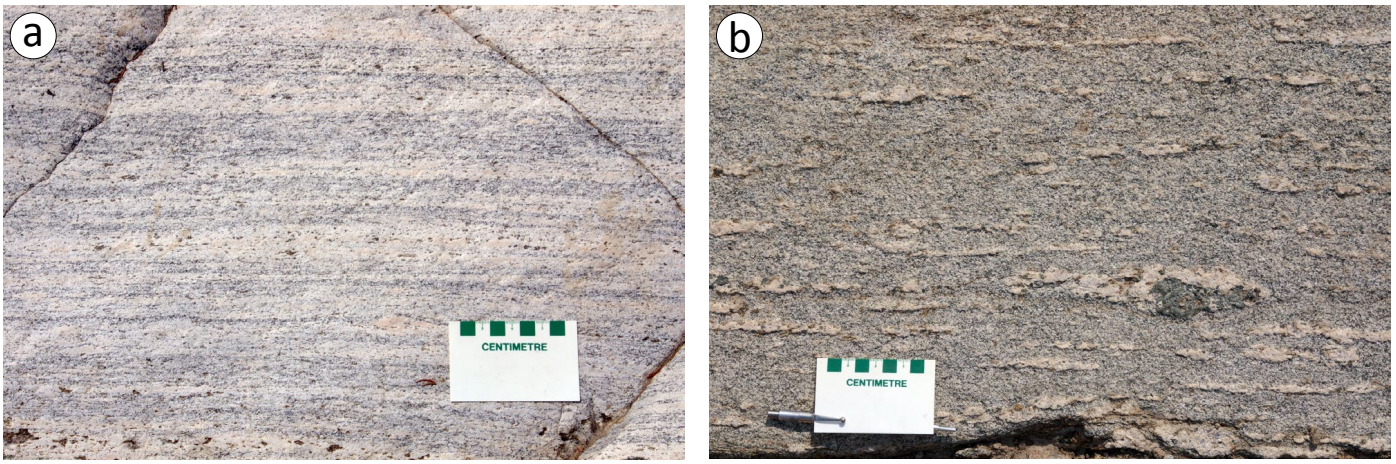

Figure 6: *Outcrop photographs of the shoshonitic gneiss suite:* ***a)*** *intermediate shoshonitic gneiss;* ***b)*** *mafic shoshonitic gneiss.*

and comprise varying proportions of clinopyroxene, orthopyroxene, hornblende and biotite, with subordinate magnetite. Exposures locally contain up to 10% quartz. There is typically an antithetic relationship between the amount of hornblende and the amount of clinopyroxene present, which may vary across a single outcrop. A greater proportion of pyroxenes is locally correlated to more leucocratic bands, suggesting that the incongruent breakdown of hornblende and biotite to feldspar may play a role. Well-layered, pyroxene-rich exposures of this subunit can appear similar to the leucocratic variety of mafic gneiss. The similar appearance to, as well as the local interleaving with, the mafic gneiss suite suggest it may be part of the same assemblage.

The mafic shoshonitic gneiss is a grey-brown, medium- to coarse-grained and strongly magnetic metatexite. It is typically biotite rich with subordinate clinopyroxene and magnetite, but the proportions of biotite and clinopyroxene are locally variable. The relatively high biotite content results in a strongly foliated rock that is characterized by ubiquitous transposed leucosome (Figure 6b). Quartz typically makes up <5% of the rock. The leucosome is clinopyroxene bearing and commonly cored by coarse-grained K-feldspar augen.

Siliciclastic rocks

Exposures of siliciclastic rocks are most common in the central and north-central portions of the map area. These rocks are typically recognized based on the presence of aluminous minerals such as garnet, cordierite, sillimanite and/or the presence of very quartz-rich layers. The rocks are typically well banded, and interlayering between the mudstone, arkosic arenite and arkosic wacke is common. Local layers of mafic rock are present in exposures of the supracrustal rocks and may be common in the wacke. The mafic layers could represent an influx of volcaniclastic material and/or intrusion of mafic dikes.

Mudstone

The mudstone forms diatexites that vary from pinkish orange to light grey and locally have a gossanous brown weathered surface. They are typically medium to coarse grained and nonmagnetic. The composition of these rocks is somewhat variable, but they typically contain quartz, plagioclase and K-feldspar, with varying proportions of pink garnet, biotite, orthopyroxene, sillimanite and rutile, with or without cordierite and rare sapphirine (Figure 7a). Garnet±cordierite–bearing leucosome is ubiquitous. Layering in these rocks is typically gradational and partially obscured by high strain and intense partial melting. Mudstone layers may be greater than 20 m thick and are commonly interlayered with, and compositionally gradational into, arkosic rocks.

Arkosic rocks

Arkosic rocks in the Sipiwesk Lake area vary from arkosic arenite to arkosic wacke. The arenite is white to light pink on weathered surfaces and dark grey on fresh surfaces (Figure 7b). It varies from fine to coarse grained and from nonmagnetic to magnetic. Exposures are quartz and plagioclase rich, with variable proportions of pink garnet, biotite, orthopyroxene and magnetite. Mafic minerals make up less than 10% of the rock. Centimetre-scale gradational layering is common, and the unit is locally interlayered with arkosic wacke and mudstone. The arkosic arenite forms metatexite to diatexite, with the latter characterized by discontinuous, quartz-rich bands of paleosome/residuum in a matrix of leucosome.

The arkosic wacke is light grey to brown, fine to coarse grained, banded on a centimetre scale and locally magnetic (Figure 7c). Layers are typically plagioclase rich, with variable proportions of quartz, orthopyroxene, clinopyroxene, garnet, biotite, sillimanite and magnetite. Mafic minerals make up >10% of the rock. The wacke can occur as metatexite or diatexite. Orthopyroxene-bearing leucosome, with or without garnet, is common and can form up to 40% of exposures. The arkosic wacke is commonly interbanded with arkosic arenite and mudstone layers. Although tentatively interpreted as wacke, these rocks could alternatively represent a sandstone with a higher lithic-clast content. At one location, the arkosic wacke and arenite occur interbedded with mafic layers (Figure

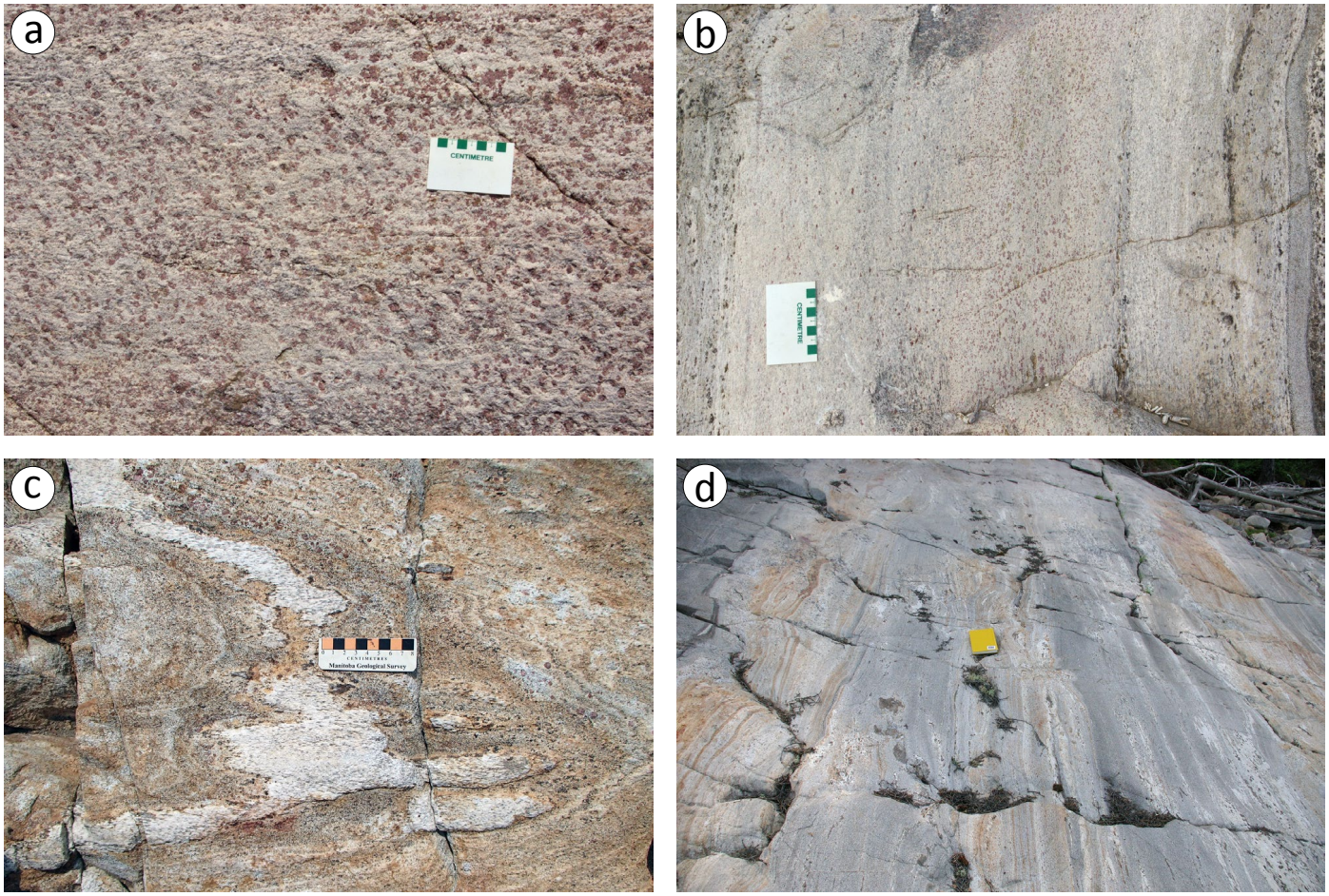

Figure 7: *Outcrop photographs of siliciclastic rocks:* ***a)*** *mudstone occurs as garnet- and sillimanite-rich diatexite;* ***b)*** *arkosic arenite;* ***c)*** *arkosic wacke;* ***d)*** *gradationally interlayered arkosic wacke and mafic gneiss, the mafic gneiss interpreted as either mafic tuff or mafic sandstone.*

7d). Gradational contacts between the arkosic and mafic layers suggest contemporaneous deposition. This implies that the mafic rocks likely represent mafic tuff or mafic sandstone.

Gneissic rocks of unusual bulk composition

Two suites of rocks with unusual bulk compositions are present in the Sipiwesk Lake area. One suite, enriched in Al and Mg, occurs in the central portions of the map area. The second suite, enriched in Al and Ca, is present in the southeastern part of the map area. Neither suite occurs at map scale. The age of these rocks relative to other pre- to syn-D_1 units is unknown; however, it is likely to be contemporaneous with the mafic gneiss suite and/or siliciclastic rocks.

Al-Mg gneiss suite

Exposures of the Al-Mg gneiss suite are yellow-grey to brown, medium to very coarse grained and nonmagnetic (Figure 8a). This unit is typically cordierite rich, with variable proportions of orthopyroxene, sapphirine and quartz, and local sillimanite, spinel, rutile, phlogopite, K-feldspar and plagioclase (Figure 8b, c). It typically occurs as layers <2.5 m thick, which are gradationally banded. Occurrences of Al-Mg gneiss are spatially associated with siliceous rocks similar to the arkosic arenite, and with bands of mafic gneiss. The close association of the Al-Mg suite with probable supracrustal rocks suggests a supracrustal protolith; however, the paragenesis of this suite is uncertain (see 'Discussion').

Al-Ca gneiss suite

Rocks of the Al-Ca gneiss suite occur as 40–100 cm thick bands spatially associated with mafic granulite and typically hosted in gneissic trondhjemite (Figure 8d). The bands are typically pale greenish yellow, fine to medium grained and nonmagnetic. This unit is plagioclase and garnet rich, with subordinate deep green clinopyroxene. Blue-grey, Ca-rich scapolite is locally present and quartz can be present in major or minor amounts. The texture of the rocks varies according to quartz content. Quartz-poor layers are characterized by interstitial garnet, which gives the rock a mottled appearance (Figure 8e). The mottled layers are locally boudinaged, suggesting they behaved competently during deformation. Quartz-rich layers are typically strongly foliated (Figure 8f). The paragenesis of this rock is uncertain; however, it could be the product of intense epidotization prior to high-grade metamorphism (see 'Discussion').

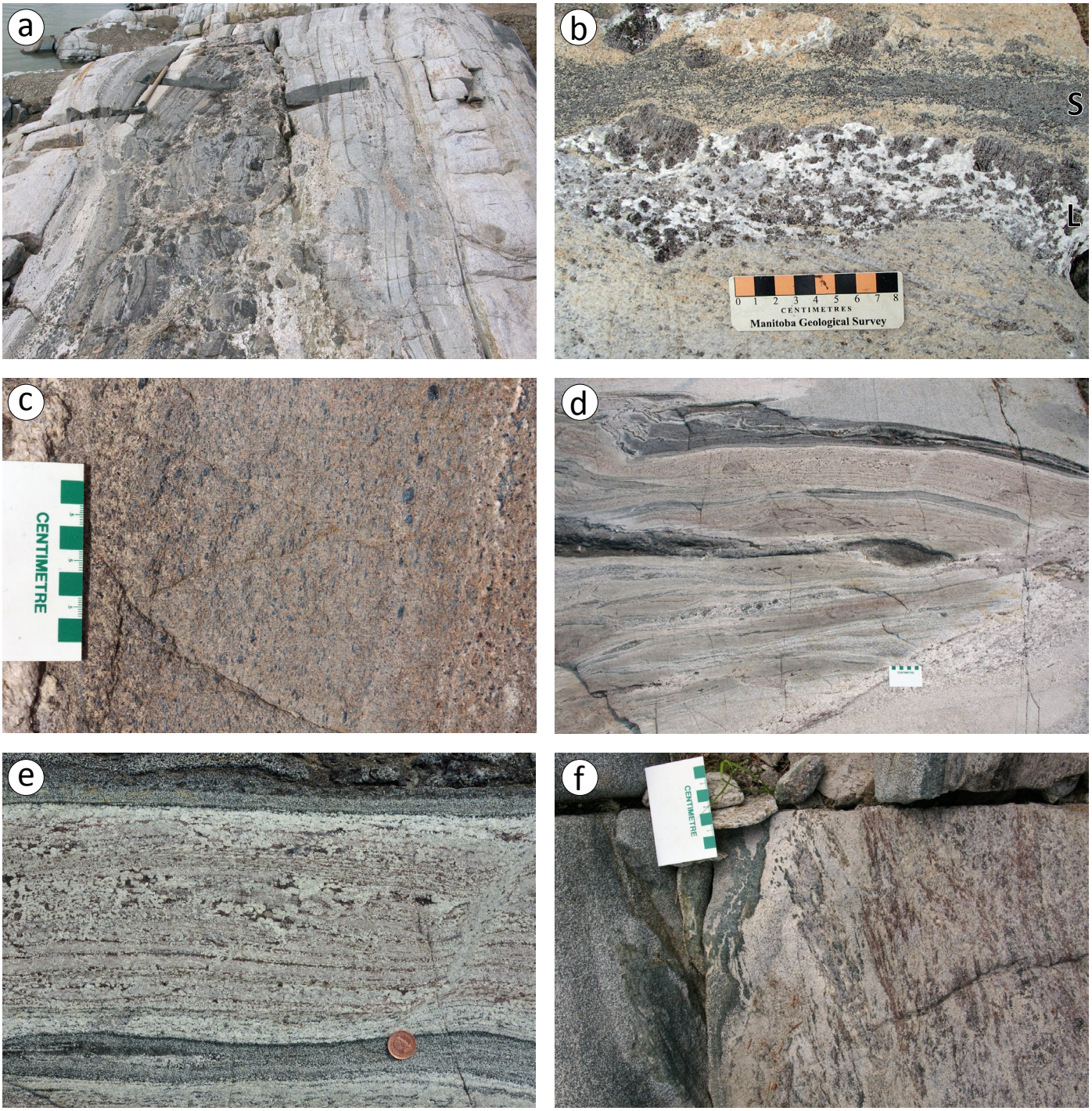

Figure 8: *Outcrop photographs of gneissic rocks of unusual composition:* ***a)*** *Al-Mg gneiss suite (sledgehammer for scale);* ***b)*** *Al-Mg gneiss rich in yellow cordierite, 'L' representing a pod of orthopyroxene-rich leucosome and 'S' representing a layer enriched in sapphirine and orthopyroxene;* ***c)*** *Al-Mg gneiss with dark blue sapphirine in a cordierite- and orthopyroxene-rich groundmass;* ***d)*** *Al-Ca gneiss suite;* ***e)*** *quartz-poor Al-Ca gneiss consisting of anorthite-rich plagioclase with interstitial garnet and subordinate clinopyroxene, scapolite and titanite;* ***f)*** *quartz-rich Al-Ca gneiss (right of scale card) displaying higher strain than the rock in (e).*

Archean post-D_1 rocks

Intrusions of moderately to strongly foliated, pyroxene-free granitoid rocks flank the northwest and southeast margins of the map area. Rare exposures of these potentially large intrusive bodies are relatively homogeneous and lack S_1 metamorphic banding and M_2 mobilizate, suggesting that they formed after the peak of the M_2 phase of metamorphism. An intrusion of foliated biotite granite is present along the southeast margin of the map area. A locally augen-textured, strongly foliated, biotite±hornblende granodiorite occurs adjacent to orthopyroxene-bearing rocks along the northwest margin of the map area. Strongly foliated, augen-textured granitoids elsewhere along the eastern margin of the PGD are interpreted to be overprinted by Hudsonian retrogression and deformation (Couëslan, 2016b). This could suggest that Archean structures and peak-metamorphic mineral assemblages in the granodio-

rite are obscured and that the relative age of the intrusion is unconstrained.

Small granitic pegmatite and aplite dikes (typically <3 m) are locally present throughout the map area but are volumetrically minor. The dikes are typically massive, although a weak S_2 foliation is locally present. They are mineralogically simple and commonly contain minor magnetite and allanite (Figure 9a). Rare garnet-bearing dikes appear to be spatially related to exposures of supracrustal rocks. No systematic orientation of granitic dikes was noted. Rare intrusions of medium- to coarse-grained granite were observed in the central portion of the map area. The granite is pink and biotite bearing, and forms bodies 8–50 m wide.

Paleoproterozoic, post-D_2 rocks

Mafic–ultramafic dikes

Unmetamorphosed mafic to ultramafic dikes are relatively common in the map area and range from <1 cm to >50 m in width. Chilled margins are relatively common for smaller diabasic dikes and rare examples of rhythmic banding may indicate composite diking. Dendritic plagioclase is locally present along the margins of larger dikes (Figure 9b). Igneous layering is common in larger gabbroic and ultramafic dikes, as are gabbroic pegmatite segregations (Figure 9c). The segregations are typically amphibole bearing and locally contain biotite and minor quartz. Ultramafic dikes typically consist of hornblende peridotite. Although smaller dikes may be rather random in orientation, larger dikes are consistently oriented in a north-northeasterly direction with subvertical dips, which is the prevalent orientation of the ca. 1880 Ma Molson dike swarm (Scoates and Macek, 1978; Heaman et al., 2009).

Lithogeochemistry and Sm-Nd isotope geochemistry

Representative samples of most of the principal map units were collected for lithogeochemical analysis. In addition, Sm-Nd isotope geochemistry was obtained for samples of siliciclastic rocks, gneissic trondhjemite and rocks of the shoshonitic and Al-Mg gneiss suites. Results of the lithogeochemical and Sm-Nd isotope analyses are provided in Appendix 1, Tables 1 and 3.

Sampling and analytical methods

A representative suite of 42 samples was collected during bedrock mapping. Due to the high metamorphic grade of rocks in the Sipiwesk Lake area, many of the units were subjected to varying intensities of anatexis. In rock types that underwent minimal partial melting, care was taken to sample material with minimal leucosome. In rock types subjected

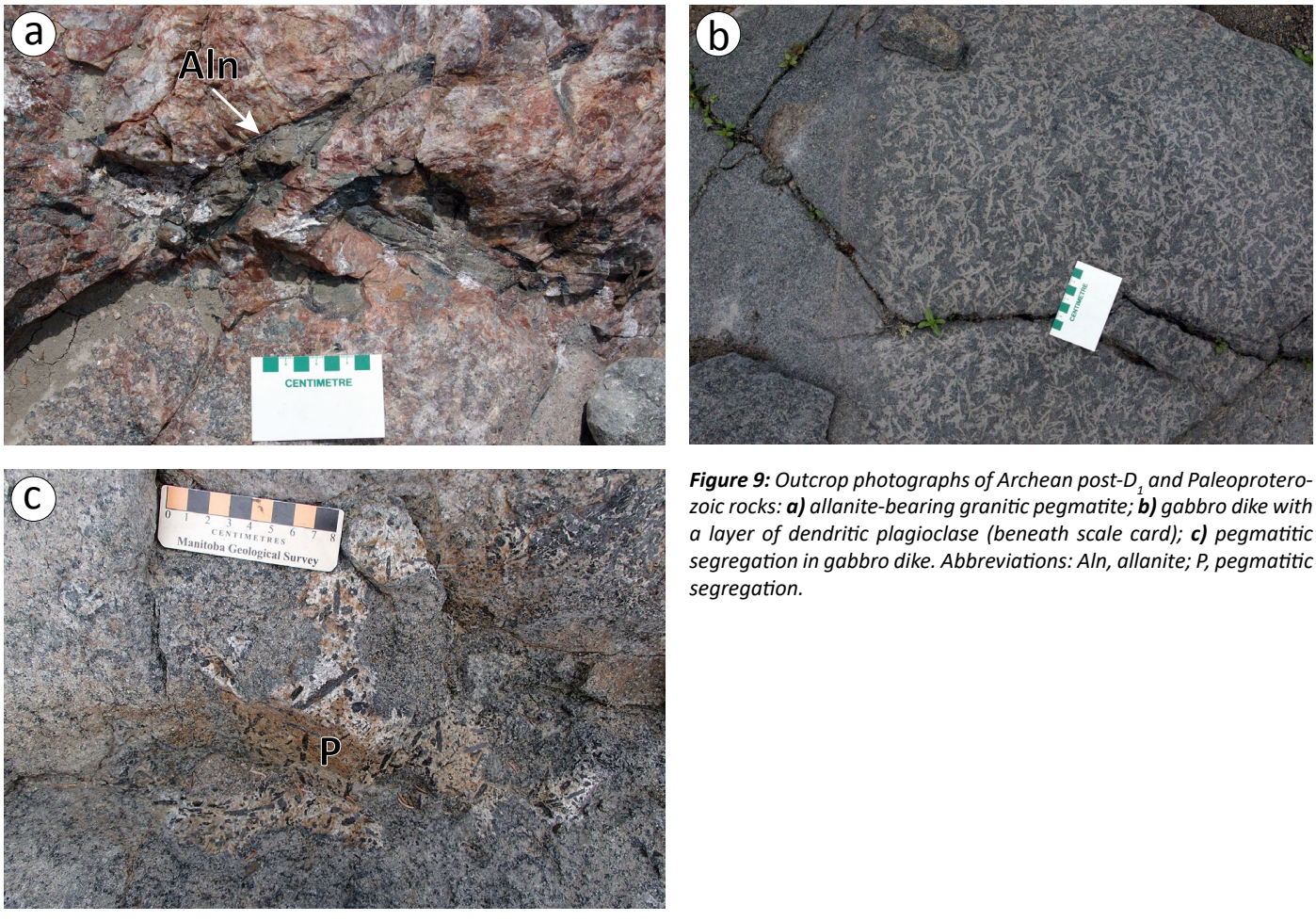

Figure 9: *Outcrop photographs of Archean post-D_1 and Paleoproterozoic rocks:* ***a)*** *allanite-bearing granitic pegmatite;* ***b)*** *gabbro dike with a layer of dendritic plagioclase (beneath scale card);* ***c)*** *pegmatitic segregation in gabbro dike. Abbreviations: Aln, allanite; P, pegmatitic segregation.*

to more intense partial melting, samples were selected that appear to be representative of the bulk composition in terms of proportion of leucosome to melanosome or residuum, and care was taken to avoid what appeared to be injected leucosome in favour of material that appeared to consist of in-situ or in-source leucosome. Weathered surfaces were removed at the time of sampling or cut off with a saw at the MGS Midland Sample and Core Library prior to crushing. Samples were crushed to <5 mm using a steel jaw crusher. Pulps were produced in a steel swing mill and were homogenized by rolling and then splitting to approximately 55 g of analytical material. A minimum of one internal standard and one blind duplicate was inserted for every 20 samples submitted for analysis.

Samples were analyzed at Activation Laboratories Ltd. (Ancaster, Ontario) using the '4Litho' analytical package, which employs a lithium metaborate/tetraborate fusion technique, followed by nitric-acid digestion and analysis by inductively coupled plasma–emission spectrometry (ICP-ES) for the major elements and selected trace elements (Sc, Be, V, Sr, Y, Zr, Ba), and inductively coupled plasma–mass spectrometry (ICP-MS) for the remainder of the trace elements and the rare-earth elements (REE). Selected samples of siliciclastic rock and iron formation, and gneisses of unusual bulk composition, were analyzed by total-digestion ICP-ES for selected trace elements (Cu, Cd, Ni, Zn, Ag, Pb) and sulphur contained within sulphides, and for ferrous iron by titration.

Three samples of siliciclastic rock, one sample of gneissic trondhjemite, one sample from the shoshonitic gneiss suite and one sample from the Al-Mg gneiss suite were submitted for Sm-Nd isotope geochemical analysis to the University of Alberta Radiogenic Isotope Facility (Edmonton, Alberta). The rock-sampling and initial-processing procedures followed were the same as outlined for the lithogeochemistry samples. The samples were processed and analyzed for Sm-Nd isotopes following the chromatographic and mass-spectrometry methods outlined by Unterschutz et al. (2002) and Schmidberger et al. (2007). Samarium and neodymium isotopic compositions were determined by multicollector (MC)-ICP-MS, for which an in-house Nd-isotope standard was used (Schmidberger et al., 2007). Chemical-processing blanks were <200 pg for Nd and Sm. The Nd data are presented relative to a $^{143}Nd/^{144}Nd$ value of 0.511850 for the La Jolla standard, and crustal residence model ages (T_{CR}) were calculated based on the model of Goldstein et al. (1984), which assumes a linear evolution of isotopic ratios in the depleted mantle, using present-day depleted-mantle values of $^{143}Nd/^{144}Nd = 0.513160$ and $^{147}Sm/^{144}Nd = 0.2141$.

Gneissic tonalite suite

Two samples of gneissic tonalite and five samples of gneissic trondhjemite were submitted for lithogeochemistry. The tonalite samples are intermediate, based on SiO_2 content (59–62 wt. %), while the trondhjemite samples are acid (65–72 wt. % SiO_2). Magnesium-number (Mg# = Mg/Mg+Fe) values for the tonalite range from 0.46 to 0.48, while the trondhjemite samples are typically lower (0.34–0.41); however, one sample of trondhjemite yielded an Mg# of 0.52. Both samples of tonalite plot as metaluminous on the alumina saturation–index diagram, while the trondhjemite samples are marginally metaluminous, with one sample plotting as peraluminous (Figure 10a).

Chondrite-normalized REE profiles of the tonalite are characterized by smooth, relatively shallow negative slopes ($[La/Yb]_{CN}$ = 6.3–6.9; Figure 10b). The REE profiles of the trondhjemite are steeper ($[La/Yb]_{CN}$ = 32–139), with some samples displaying small positive anomalies at Eu (Figure 10c). Primitive mantle–normalized trace-element profiles for the tonalite are characterized by negative anomalies at Nb, Ti and, in one sample, Zr (Figure 10d). The trace-element profiles of the trondhjemite are also characterized by negative anomalies at Nb and Ti, and positive anomalies at Zr for two samples (Figure 10e). The negative anomalies at Nb and Ti are suggestive of a magmatic-arc environment for these intrusions or of partial melting of arc-affinity rocks. An initial ε_{Nd} value of +0.3 for trondhjemite sample 108-12-1183 (at 2.78 Ga; Table 1) suggests derivation from a slightly juvenile source or contamination of a juvenile magma by evolved crust.

Mafic gneiss suite

A diagram for differentiating metasedimentary from metaigneous rocks using relatively immobile elements was devised by Winchester et al. (1980) and modified by Couëslan (2018). The diagram plots Ni, which should be elevated in mafic igneous rocks and the fine-grained and heavy-mineral component of clastic sedimentary rocks, against Zr/TiO_2, which should be elevated in felsic igneous rocks and clastic sedimentary rocks. Several limitations to the diagram should be recognized. It is unable to distinguish felsic igneous rocks from psammitic sedimentary rocks, both of which tend to plot along the y-axis with elevated Zr/TiO_2 values (typically >100). Primitive alkaline rocks typically plot within the sedimentary rocks field because they contain elevated Ni and Zr. In general, igneous rocks of intermediate composition are more likely to be misclassified than felsic or mafic compositions.

With these considerations in mind, both mesocratic and leucocratic varieties of the mafic gneiss plot within the igneous rocks field on the Ni vs. Zr/TiO_2 diagram (Figure 11a) and within the basalt fields of Pearce (1996; Figure 11b) and Jensen and Pyke (1982; Figure 11c). One sample of the mesocratic phase (108-12-1099A) plots within the komatiite field of Jensen and Pyke (1982); however, it contains only 12.24 wt. % MgO and is more properly categorized as a picrite (Le Maitre, 2002). Most Mg# values range from 0.52 to 0.42, with two outliers of 0.66 (108-12-1099A) and 0.36 (108-15-1202). Thorium is commonly below detection limit in the mafic gneiss suite. Although Th is considered to be a relatively immobile element, it is also considered to be an incompatible element that will preferentially partition into silicate melts (Jenner, 1996; Hollings and Wyman, 2005). Leucosome is ubiquitous within the mafic

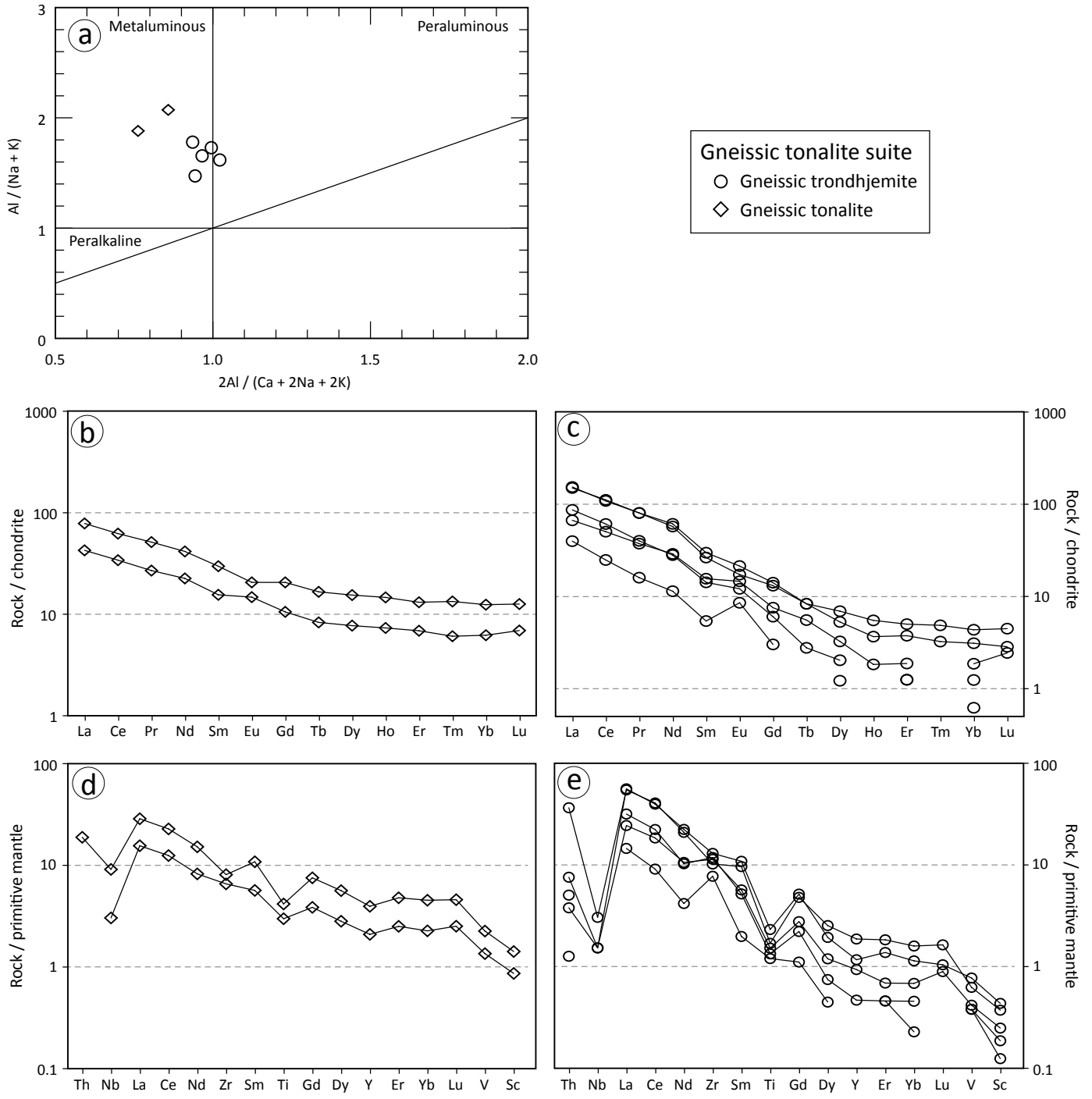

Figure 10: *Geochemical diagrams for the gneissic tonalite suite:* ***a)*** *alumina saturation–index diagram of Maniar and Piccoli (1989);* ***b)*** *chondrite-normalized rare-earth element (REE) profiles of the gneissic tonalite;* ***c)*** *chondrite-normalized REE profiles of the gneissic trondhjemite;* ***d)*** *primitive mantle–normalized trace-element profiles of the gneissic tonalite;* ***e)*** *primitive mantle–normalized trace-element profiles of the gneissic trondhjemite. Normalizing values for chondrite and primitive mantle from McDonough and Sun (1995).*

gneiss, indicating that partial melting has occurred. Since Th concentrations are generally low in mafic rocks, partial melting and the partitioning of Th into the silicate melt and subsequent removal or segregation of the melt could result in depletion of Th within the remainder of the rock.

Chondrite-normalized REE profiles for the mafic gneiss generally display moderate negative slopes that are slightly concave upward in the heavy rare-earth–element (HREE) portion (Figure 12a); samples 108-12-1023A and 108-15-1202 are the exception and will be discussed below. Although the sample size is small, the mesocratic rocks are characterized by slightly steeper slopes ($[La/Yb]_N$ = 2.3–4.3) than the leucocratic variety ($[La/Yb]_N$ = 2.0–2.4). Normal mid-ocean–ridge basalt (N-MORB)–normalized trace-element profiles generally have negative slopes with slight to moderate negative anomalies at Nb, Zr and Ti, and slight enrichment of V and Sc (Figure 12b). The negative anomalies at Zr and Ti are less pronounced for the leucocratic gneiss than for the mesocratic gneiss. Both REE

Table 1: Summary of Sm-Nd isotopic data for selected rock samples from the central Sipiwesk Lake area.

Sample number	Rock type	Sm (ppm)	Nd (ppm)	$^{147}Sm/^{144}Nd$[1]	$^{143}Nd/^{144}Nd$[2]	ε_{Nd}[3]	T_{CR}[4] (Ga)
97-12-055	Arkosic wacke	2.69	18.85	0.086	0.510595 (7)	-1.2	3.05
108-12-1064C	Mudstone	3.12	20.33	0.093	0.510541 (9)	-4.5	3.28
108-12-1084B	Al-Mg gneiss	1.79	14.43	0.075	0.510370 (7)	-1.6	3.05
108-12-1146A	Mudstone	14.18	93.70	0.091	0.510743 (5)	-0.1	3.00
108-12-1183	Trondhjemite gneiss	2.00	13.1	0.093	0.510745 (8)	0.3	3.03
108-12-1209	Mafic shoshonitic gneiss	5.83	32.50	0.108	0.511060 (8)	0.1	3.02

[1] Estimated error better than 0.5%
[2] Presented relative to $^{143}Nd/^{144}Nd = 0.511850$ for La Jolla standard; numbers in parathesis are 2σ uncertainties x 10^{-6}
[3] ε_{Nd} values at 2.72 Ga (2.78 Ga for 108-12-1183) calculated using present-day chondritic ratios of $^{143}Nd/^{144}Nd = 0.512638$ and $^{147}Sm/^{144}Nd = 0.1967$
[4] Crustal residence Nd model ages (T_{CR}) calculated according to linear model of Goldstein et al. (1984)

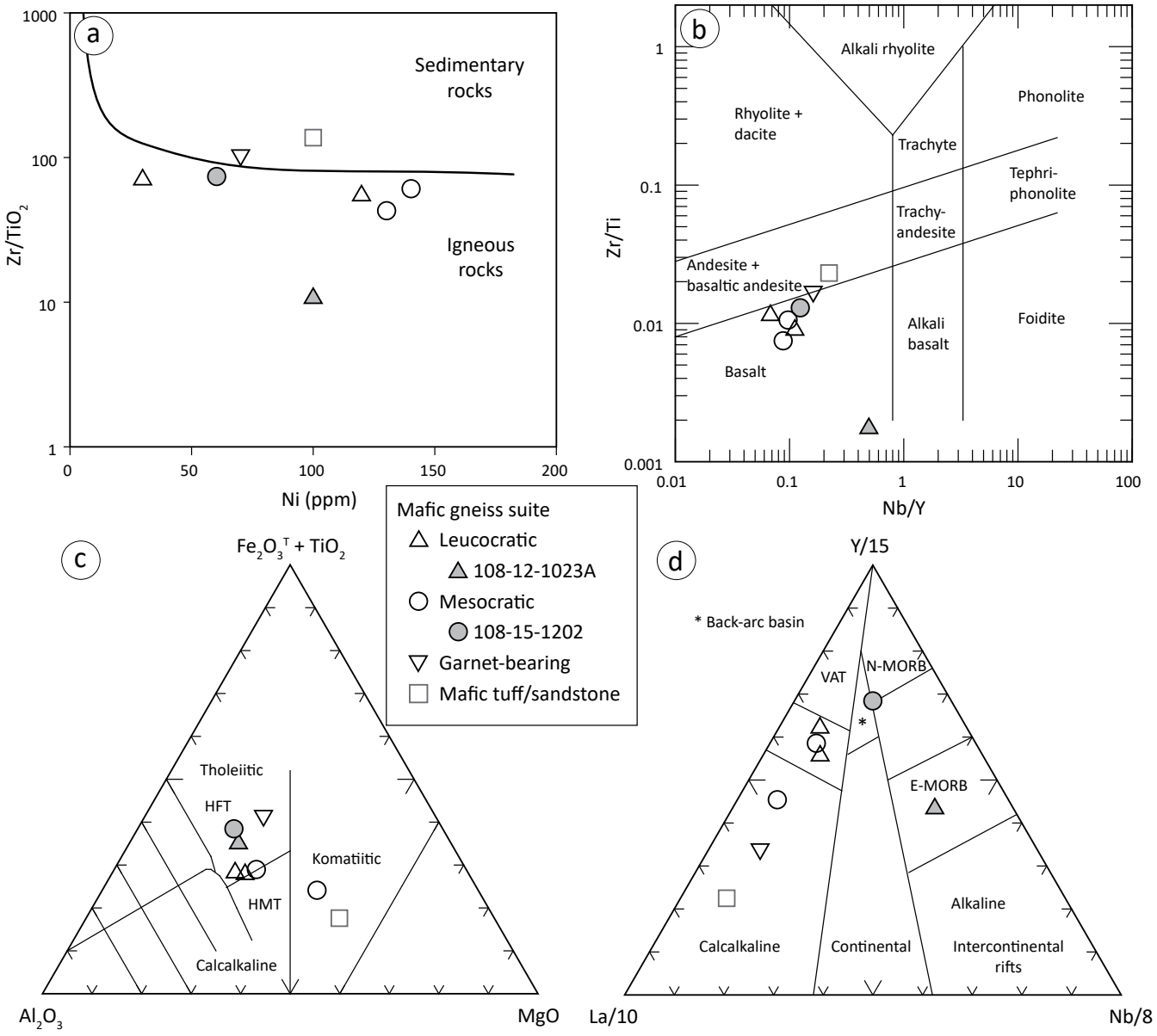

***Figure 11**: Geochemical diagrams for the mafic gneiss suite: **a)** Zr/TiO_2–Ni diagram of Couëslan (2018; modified after Winchester et al., 1980); **b)** Zr/Ti–Nb/Y diagram of Pearce (1996); **c)** Al_2O_3–$Fe_2O_3^T$+TiO_2–MgO diagram of Jensen and Pyke (1982); **d)** La–Y–Nb diagram of Cabanis and Lecolle (1989). Abbreviations: E-MORB, enriched mid-ocean–ridge basalt; HFT, high-Fe tholeiite; HMT, high-Mg tholeiite; N-MORB, normal mid-ocean–ridge basalt; VAT, volcanic-arc tholeiite.*

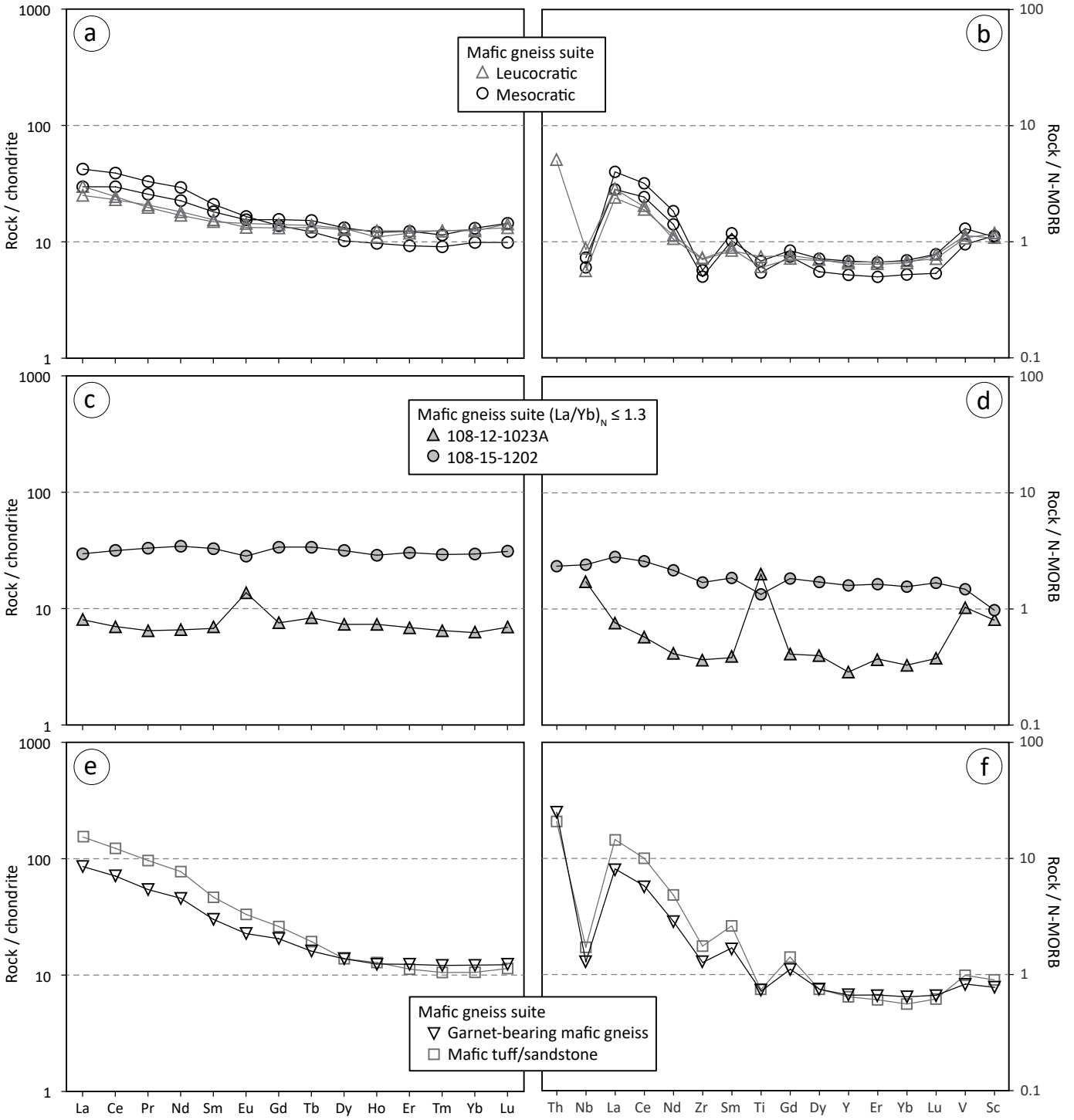

Figure 12: *Chondrite-normalized rare-earth–element profiles (left column) and N-MORB–normalized trace-element profiles (N-MORB; right column) for the mafic gneiss suite. Normalizing values for chondrite from McDonough and Sun (1995) and those for N-MORB from Sun and McDonough (1989).*

and trace-element profiles are suggestive of arc-affinity rocks, which is in agreement with the La/10–Y/15–Nb/8 diagram of Cabanis and Lecolle (1989; Figure 11d). The leucocratic rocks plot in the transitional field between volcanic-arc tholeiite and calcalkaline basalt, while the mesocratic gneiss plots within the transitional field and the calcalkaline field.

Sample 108-12-1023A is a leucocratic mafic gneiss. It has a chondrite-normalized REE profile that is relatively flat ([La/Yb]$_N$ = 1.3) with a positive Eu anomaly (Eu/Eu* = 1.9; Figure 12c). The N-MORB-normalized trace-element profile is slightly enriched in light rare-earth elements (LREE), has positive anomalies at Nb, Ti, V and Sc, and Th is below detection limit (Figure 12d). The positive anomalies for chondrite-normalized Eu and MORB-normalized Nb, Ti, V and Sc could indicate that the sample represents a cumulate rock; however, the low Th content could also suggest a rock that has been affected by the

generation and removal of partial melts. Fine-grained, interstitial K-feldspar observed in thin section could represent crystallized melt films or 'melt pseudomorphs' (Holness and Sawyer, 2008; Holness et al., 2011), which would indicate the former presence of melt. Sample 108-15-1202 occurs as a discontinuous band associated with rocks of the Al-Ca gneiss suite and is hosted in gneissic trondhjemite. It has a relatively flat chondrite-normalized REE profile ($[La/Yb]_N$ = 1.0) and flat N-MORB-normalized trace-element profile with values close to 1 (Figure 12c, d). The relatively flat REE and trace-element profiles of this sample suggest a MORB affinity; however, it is unclear if the rock represents a dike intruding the gneissic trondhjemite or a xenolith of mafic rock.

Garnet-bearing mafic gneiss (sample 108-12-1111D) was collected from a layer that grades into typical leucocratic mafic gneiss and is associated with banded iron formation. It is characterized by a lower Mg# (0.37) than typical for the mafic rocks, which could indicate a ferrobasaltic composition. The chondrite- and N-MORB–normalized profiles of the sample are similar to most other rocks of the mafic gneiss suite; however, they are characterized by a greater enrichment in Th and LREE ($[La/Yb]_N$ = 7.0; Figure 12e, f). This could indicate that the rock represents a more fractionated flow, was sourced from slightly more enriched material or was contaminated by crustal material. The relatively higher Fe content could indicate contamination by material from the same source as the adjacent iron formation; however, the iron formation contains Th and LREE concentrations similar to those of typical mafic gneiss. Sample 108-12-1146B was collected from a mafic gneiss layer intercalated with arkosic arenite and wacke. It is tentatively interpreted as a mafic tuff or sandstone and has a trace-element profile similar to that of sample 108-12-1111D (Figure 12e, f). Both of these samples plot within the sedimentary rocks field on the Ni vs. Zr/TiO_2 diagram (Figure 11a), which supports the presence of clastic material.

Shoshonitic gneiss suite

Three samples of intermediate and one sample of mafic shoshonitic gneiss were analyzed for lithogeochemistry. The intermediate variety contains 55–60% SiO_2, while the mafic variety contains 51% SiO_2. The rocks are relatively enriched in K_2O (4.1–5.6 wt. %; K_2O/Na_2O = 1.0–1.6) and plot within the shoshonite-series field on the K_2O vs. SiO_2 diagram of Peccerillo and Taylor (1976; Figure 13a). Both intermediate and

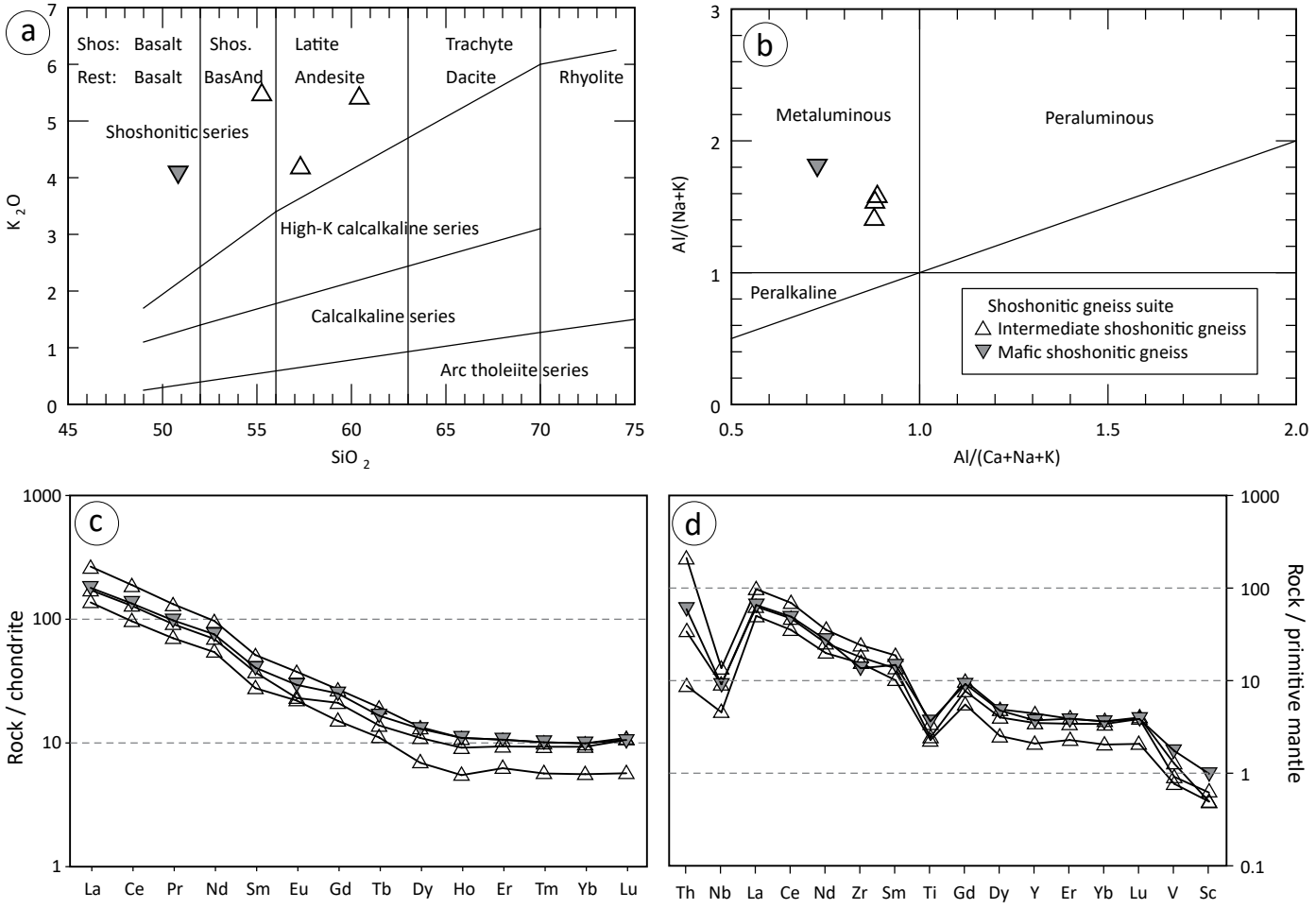

Figure 13: *Geochemical diagrams for the shoshonitic gneiss suite:* ***a)*** *K_2O–SiO_2 diagram of Peccerillo and Taylor (1976);* ***b)*** *alumina-saturation–index diagram of Maniar and Piccoli (1989);* ***c)*** *chondrite-normalized rare-earth element profiles;* ***d)*** *primitive mantle–normalized trace-element profiles. Normalizing values for chondrite and primitive mantle from McDonough and Sun (1995).*

mafic varieties plot as metaluminous on the alumina-saturation–index diagram (Figure 13b). Magnesium-number values for the intermediate gneiss vary from 0.35 to 0.45, and the mafic gneiss yielded an Mg# of 0.46. Although these rocks bear certain similarities to sanukitoids of the Superior province (Stern et al., 1989), they are not as primitive in terms of Mg, Ni and Cr content.

Chondrite-normalized REE profiles are similar for both the intermediate and mafic shoshonitic gneiss with steep negative slopes ($[La/Yb]_{CN}$ = 18–27) and relatively flat HREE portions (Figure 13c). Primitive mantle–normalized trace-element profiles are enriched in large-ion lithophile elements (LILE), have variable Th values and display negative anomalies for Nb and Ti (Figure 13d). The mafic shoshonite yielded an initial ε_{Nd} value of +0.1 (at ca. 2.72 Ga; Table 1).

Siliciclastic rocks

Mudstone

The two samples of mudstone that were analyzed plot within the sedimentary field of the Zr/TiO_2 vs. Ni diagram (Figure 14a). Alumina-saturation index (ASI, molar Al_2O_3/

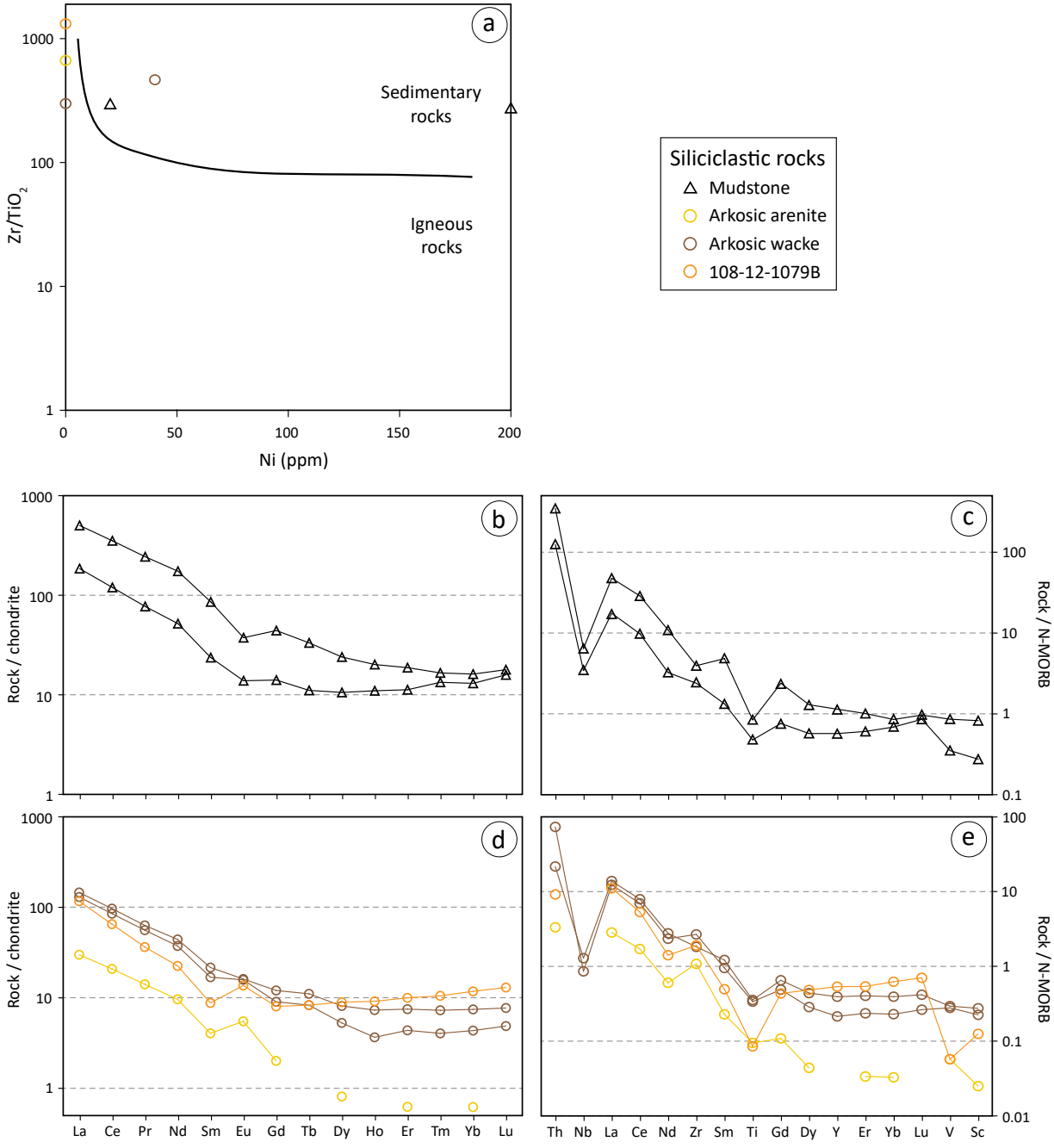

Figure 14: *Geochemical diagrams for the siliciclastic rocks:* ***a)*** *Zr/TiO_2–Ni diagram of Couëslan (2018; modified after Winchester et al., 1980);* ***b)*** *chondrite-normalized rare-earth–element profiles for mudstone;* ***c)*** *N-MORB–normalized trace-element profiles for mudstone;* ***d)*** *chondrite-normalized rare-earth–element profiles for arkosic rocks;* ***e)*** *N-MORB-normalized trace-element profiles for arkosic rocks. Normalizing values for chondrite from McDonough and Sun (1995) and those for N-MORB values from Sun and McDonough (1989).*

[$CaO+Na_2O+K_2O$]) values range from 1.37 to 2.06, and Mg# values range from 0.51 to 0.65. Chondrite-normalized REE profiles are characterized by moderate negative slopes ($[La/Yb]_N$ = 14–31) with concave-upward HREE portions (Figure 14b). Europium anomalies are weakly negative (Eu/Eu* = 0.58–0.73). The N-MORB–normalized trace-element profiles are generally enriched in Th and LREE, with negative anomalies at Nb and Ti (Figure 14c). The mudstone samples yielded Sm-Nd model ages of ca. 3.00–3.28 Ga (Table 1).

Arkosic rocks

Two samples each of arkosic arenite and arkosic wacke were analyzed for lithogeochemistry. One sample of arkosic arenite (108-12-1079B) will be discussed separately. Most samples plot along the y-axis on the Zr/TiO_2 vs. Ni diagram, where psammitic and felsic volcanic rocks are expected to plot, with one sample of arkosic wacke plotting within the sedimentary field (Figure 14a). Although most of the arkosic rocks cannot be distinguished from felsic volcanic rocks in Figure 14a, U-Pb isotope analyses of zircon from one sample yielded a polymodal population of grains, which suggests a clastic sedimentary protolith (see 'Zircon U-Pb geochronology', sample 97-12-055). However, it may be that some of the rocks mapped and interpreted as arkose are volcanic in origin (dacitic or rhyolitic rocks).

The arkosic wacke is characterized by ASI values of 1.11 and 1.23, and Mg# values of 0.39 and 0.43. The arenite has a slightly lower ASI value of 1.08 and a higher Mg# value of 0.58. Chondrite-normalized REE profiles of the wacke have moderate negative slopes ($[La/Yb]_N$ = 20–30) with flat to slightly concave-upward HREE profiles (Figure 14d). Weak Eu anomalies vary from slightly negative to positive (Eu/Eu* = 0.96–1.22). Chondrite-normalized REE profiles of the arenite are similar but with a steeper negative slope ($[La/Yb]_N$ = 48), HREE concentrations at or below detection limit and a more pronounced positive Eu anomaly (Eu/Eu* = 1.82). The N-MORB–normalized trace-element profiles of the arkosic rocks are distinctly arc like, with enrichment in Th and LREE, and depletions of Nb and Ti (Figure 14e). The samples also display slight to moderate enrichment of Zr. One sample of arkosic wacke yielded a Sm-Nd model age of ca. 3.05 Ga (Table 1).

Arkosic arenite sample 108-12-1079B occurs in direct contact with rocks of the Al-Mg gneiss suite. It plots along the y-axis of the Zr/TiO_2 vs. Ni diagram (Figure 14a) and has an ASI value of 1.2 and an Mg# value of 0.51. Chondrite-normalized REE profiles are similar to those of arkosic wacke but with a distinct concave-upward shape ($[La/Yb]_{CN}$ = 9.9) and positive Eu anomaly (Eu/Eu* = 1.6; Figure 14d). The N-MORB–normalized trace-element profile is also similar to that of arkosic wacke but with more pronounced negative Nb, Ti and V anomalies (Figure 14e). The normalized REE and trace-element profiles of 108-12-1079B are distinct from those of the other arkosic arenite sample (97-12-020A01).

Gneissic rocks of unusual bulk composition

Al-Mg gneiss suite

The Al-Mg gneiss suite is characterized by high to very high ASI values (1.8–52) and high Mg# values (0.65–0.83). These rocks are typically low in alkalis, with generally <1.5% each of CaO, Na_2O and K_2O. Samples plot along the y-axis of the Zr/TiO_2 vs. Ni diagram, where psammitic and felsic igneous rocks are expected to plot (Figure 15a). Chondrite-normalized REE profiles are variable but appear to indicate two broad groups (Figure 15b, c). One group has moderate negative slopes ($[La/Yb]_{CN}$ = 18–23) with variable Eu anomalies (Eu/Eu* = 0.26–1.6). The second group is characterized by concave-upward REE profiles ($[La/Yb]_{CN}$ = 1.5–6.2) and both positive and negative Eu anomalies. The N-MORB–normalized trace-element profiles are also variable (Figure 15d, e). The higher $[La/Yb]_{CN}$ group is characterized by negative slopes and negative anomalies at Nb and Ti. The other group is characterized by overall concave-upward profiles, positive anomalies at Th and Zr, and variable enrichment or depletion of Nb and Ti. Both groups are depleted in V and Sc. Sample 108-12-1084B yielded a Sm-Nd model age of 3.05 Ga (Table 1).

A comparison of arkosic arenite 108-12-1079B with rocks of the Al-Mg gneiss suite is warranted because of their close association. The arkosic arenite plots along the y-axis of the Zr/TiO_2 vs. Ni diagram with rocks of the Al-Mg gneiss suite (Figure 15a). The ASI (1.2) and Mg# (0.51) values are lower than typical for the Al-Mg gneiss suite. Normalized REE profiles for the arkose are similar to the concave-upward profiles of the lower $[La/Yb]_{CN}$ group of Al-Mg gneiss (Figure 15c). The trace-element profile of the arkose also shares similarities with the lower $[La/Yb]_{CN}$ group but with more pronounced negative anomalies at Nb, Ti and V (Figure 15e).

Al-Ca gneiss suite

Rocks of the Al-Ca gneiss suite are characterized by very low Na_2O (<0.68 wt. %), K_2O (<0.21 wt. %), MgO (<0.27 wt. %) and Mg# (0.06–0.10); are rich in Al_2O_3 (18–22 wt. %) and CaO (13–20 wt. %); and contain variable amounts of SiO_2 (49–63 wt. %). Analysis of ferrous iron in two of the samples reveals relatively high ratios of $Fe^{3+}/Fe^{2+}+Fe^{3+}$ (0.54–0.55). Samples plot along the y-axis of the Zr/TiO_2 vs. Ni diagram, where psammitic and felsic igneous rocks are expected to plot (Figure 16a). Chondrite-normalized REE profiles have negative slopes for LREE and middle rare-earth elements (MREE) and slight positive slopes for HREE (Figure 16b; $[La/Yb]_{CN}$ = 5–17). Anomalies at Eu range from slightly negative to slightly positive (Eu/Eu* = 0.8–1.5). The N-MORB–normalized profiles are enriched in Th and LREE, with depletions in Nb, Ti, V and Sc (Figure 16c).

Mafic–ultramafic dikes

Two samples of diabase, two samples of gabbro and one sample of peridotite were analyzed. The dikes are considered

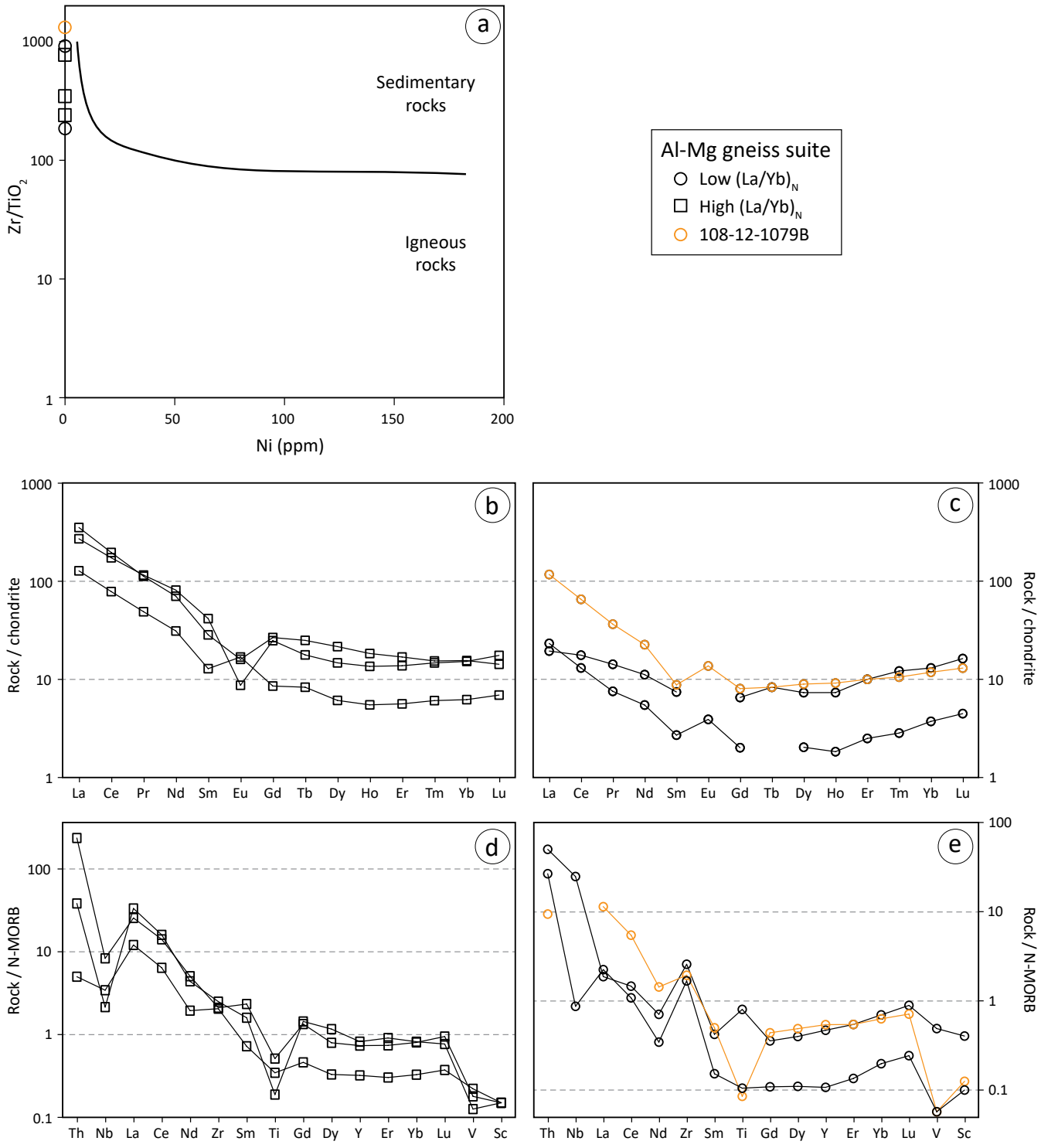

Figure 15: *Geochemical diagrams for the Al-Mg gneiss suite:* ***a)*** *Zr/TiO_2–Ni diagram of Couëslan (2018; modified after Winchester et al., 1980);* ***b)*** *chondrite-normalized rare-earth element profiles of Al-Mg gneiss with higher La/Yb;* ***c)*** *chondrite-normalized rare-earth element profiles of Al-Mg gneiss with lower La/Yb;* ***d)*** *N-MORB–normalized trace-element profiles of Al-Mg gneiss with higher (La/Yb);* ***e)*** *N-MORB–normalized multi-element profiles of Al-Mg gneiss with lower (La/Yb). Normalizing values for chondrite from McDonough and Sun (1995) and for N-MORB from Sun and McDonough (1989).*

basic, with SiO_2 contents of 46–51 wt. %. The MgO contents vary from approximately 8 wt. % in the diabase samples (Mg# 0.52–0.56) to 11.4–16.4 wt. % in the gabbro (Mg# 0.65–0.72) and to 22.9% in the peridotite (Mg# 0.79). Chromium values are >300 ppm in all samples, and up to 1530 ppm in the gabbro and 2280 ppm in the peridotite. Chondrite-normalized REE profiles are relatively flat, with the diabase slightly more enriched in LREE ($[La/Yb]_{CN}$ = 1.6–1.8) than the gabbro and peridotite ($[La/Yb]_{CN}$ = 0.73–1.2; Figure 17a). There is little to no Eu anomaly (Eu/Eu* = 0.99–1.1). The N-MORB–normalized multi-element profiles are relatively flat to slightly negative sloping, with the diabase being somewhat enriched in Th, Nb

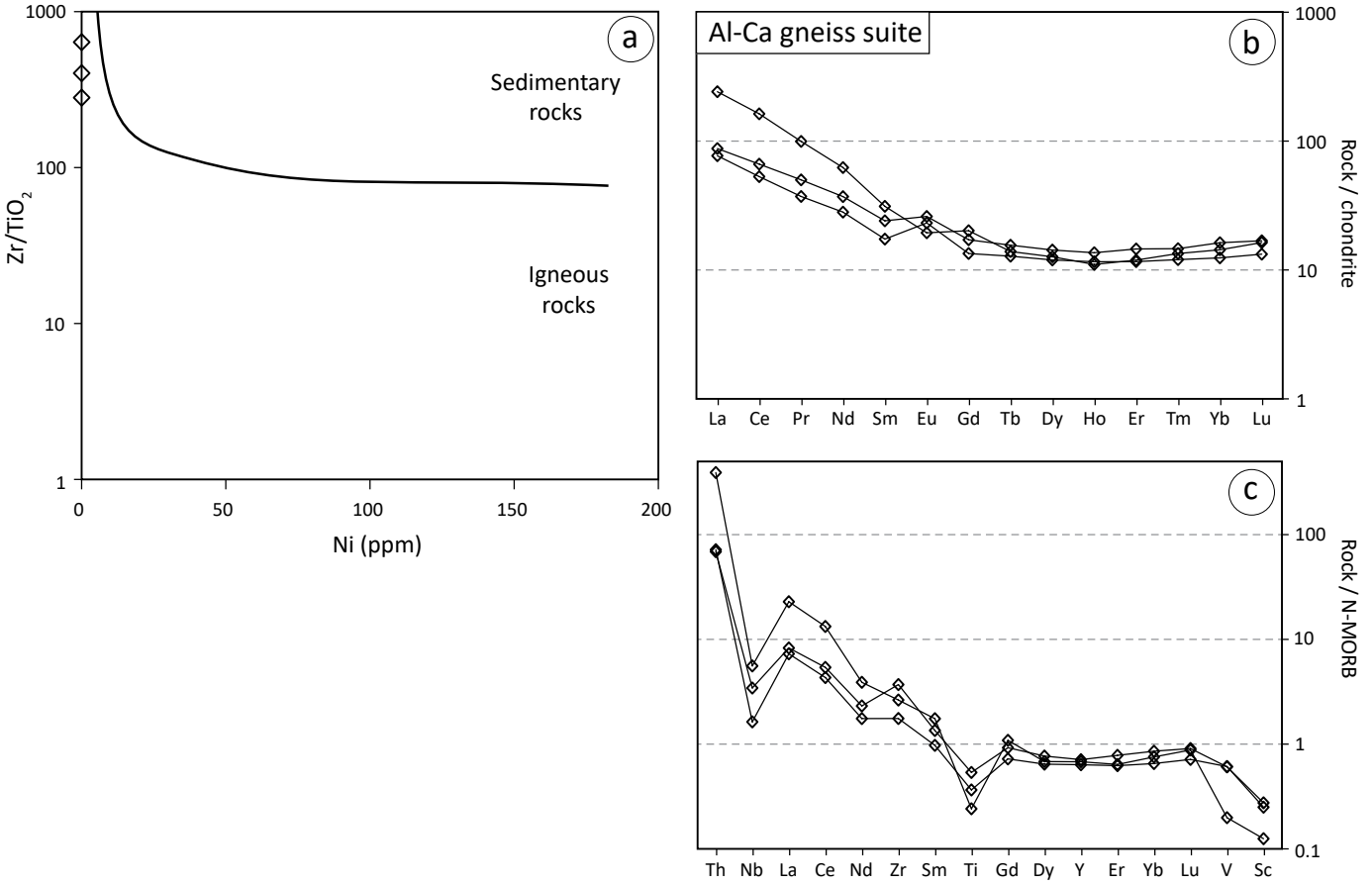

Figure 16: *Geochemical diagrams for the Al-Ca gneiss suite:* ***a)*** *Zr/TiO_2–Ni diagram of Couëslan (2018; modified after Winchester et al., 1980);* ***b)*** *chondrite-normalized rare-earth–element profiles;* ***c)*** *N-MORB–normalized multi-element profiles. Normalizing values for chondrite from McDonough and Sun (1995) and N-MORB values from Sun and McDonough (1989).*

and LREE compared to the gabbro and peridotite. The profiles of the mafic dikes are similar to slightly contaminated N-MORB. This is supported by the samples plotting in the N-MORB and back-arc basin fields in discrimination diagrams (Figure 17c, d).

Structure and metamorphism

Structures

Exposures throughout the map area are characterized by relatively high-strain features. The S_1 gneissosity is present in the gneissic tonalite suite, mafic gneiss suite, shoshonitic gneiss suite, siliciclastic rocks and gneissic rocks of unusual composition. Where primary compositional layering (S_0) is present, such as in the siliciclastic rocks, it is transposed parallel to S_1. Leucosome typically subparallels and locally crosscuts the S_1 gneissosity, suggesting a period of high-grade metamorphism that either outlasted or postdated D_1. The leucosome typically displays a well-developed S_2 foliation, which implies that the metamorphic event either predated or was outlasted by D_2. The S_2 foliation is most apparent as aligned quartz aggregates (Figure 18a). The S_1 gneissosity is transposed by the S_2 foliation, which commonly strikes 240–260° and dips steeply toward the north (typically >70°). The S_2 foliation is axial planar to minor folds (F_2; Figure 7c, Figure 18b), which are interpreted to be parasitic to regional similar folds. Rootless parasitic folds are locally observed. Lineations (L_2) typically parallel minor fold axes and trend 050–080°, with a relatively moderate plunge of 30–60°.

Paleoproterozoic brittle structures are locally abundant in the map area. Zones of pseudotachylite veining up to 5 m wide are present in localized north-northeast-trending zones throughout the map area. The intervening blocks enclosed by veins of pseudotachylite locally form a chaotic juxtaposition (breccia) of various locally derived rock types. Some exposures reveal the presence of multiple crosscutting generations of pseudotachylite (Figure 18c). Pseudotachylite veins cut, and are cut by, the unmetamorphosed mafic dikes (Figure 18d, e). This could suggest brittle faulting was contemporaneous with mafic magmatism, although there is no spatial relationship between the pseudotachylyte zones and dike abundance.

Brittle fault zones occur as zones of pervasive fracturing and hematization up to 10 m wide. The fractures are commonly lined with chlorite and locally filled with vuggy carbonate. The fracture zones are locally cored by discrete faults lined with chloritic/clay–rich fault gouge (Figure 18f). Fault grooves and slickenlines indicate both sinistral and dextral senses of displacement. Brittle faults were observed cutting both pseudotachylite veins and mafic dikes, and typically trend north-

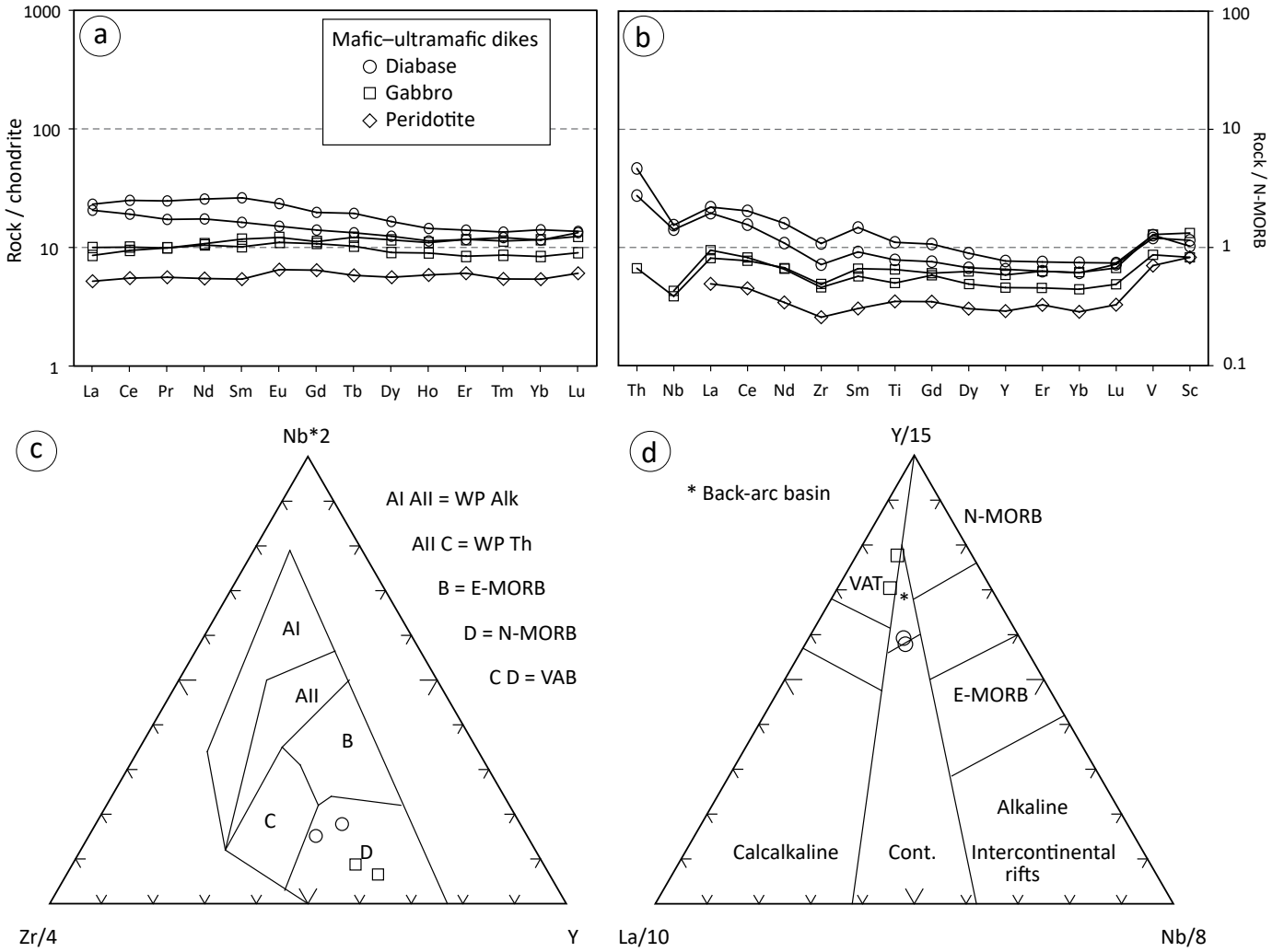

Figure 17: *Geochemical diagrams for mafic-ultramafic dikes:* ***a)*** *chondrite-normalized rare-earth element profiles;* ***b)*** *N-MORB–normalized multi-element profiles;* ***c)*** *Zr–Nb–Y diagram of Meschede (1986);* ***d)*** *La–Y–Nb diagram of Cabanis and Lecolle (1989). Normalizing values for chondrite from McDonough and Sun (1995) and for N-MORB from Sun and McDonough (1989). Abbreviations: Cont., continental basalt; E-MORB, enriched mid-ocean–ridge basalt; N-MORB, normal mid-ocean–ridge basalt; VAB, volcanic-arc basalt; VAT, volcanic-arc tholeiite; WP Alk, within-plate alkali basalt; WP Th, within-plate tholeiite.*

east with relatively steep dips. The brittle fault zones are most common in the southern portion of the map area and tend to coincide with prevalent pseudotachylite zones.

Metamorphic mineral assemblages

Several samples were studied in thin section for metamorphic mineral assemblages; however, discussion will be limited to three of these samples: two samples from the Al-Mg gneiss suite (108-12-1079C and 108-12-1080A) and one sample of mudstone (108-12-1064C). These samples were selected because of their aluminous bulk compositions and diverse mineral assemblages, good correspondence with calculated phase-equilibrium models (see 'Discussion') and relatively well constrained metamorphic conditions provided by the models.

Aluminum-magnesium gneiss sample 108-12-1079C contains the mineral assemblage quartz–cordierite–orthopyroxene–K-feldspar–sillimanite–biotite–rutile; zircon is present as an accessory phase. Quartz forms the groundmass as grains that are typically elongate parallel to the foliation and rutilated. Local orthopyroxene grains are rutilated and rutile also occurs as discrete fine-grained prisms in the groundmass. Textural relationships between cordierite, sillimanite and orthopyroxene are complex. Cordierite occurs as elongate grains or lenses that parallel the foliation. Cordierite and orthopyroxene are commonly intergrown and appear to have formed at equilibrium, and lenses of cordierite locally contain cores of prismatic sillimanite (Figure 19a). In turn, cordierite often appears overprinted by intergrowths of prismatic sillimanite-quartz and/or orthopyroxene, skeletal sillimanite-quartz and skeletal sillimanite-orthopyroxene (Figure 19b). Both prismatic and skeletal sillimanite grains are oriented and define a lineation (L_2) within the foliation. Potassium feldspar is generally mesoperthitic and occurs as sparse fine grains within the quartz-rich groundmass and more commonly as elongate, medium- to coarse-grained, polycrystalline lenses.

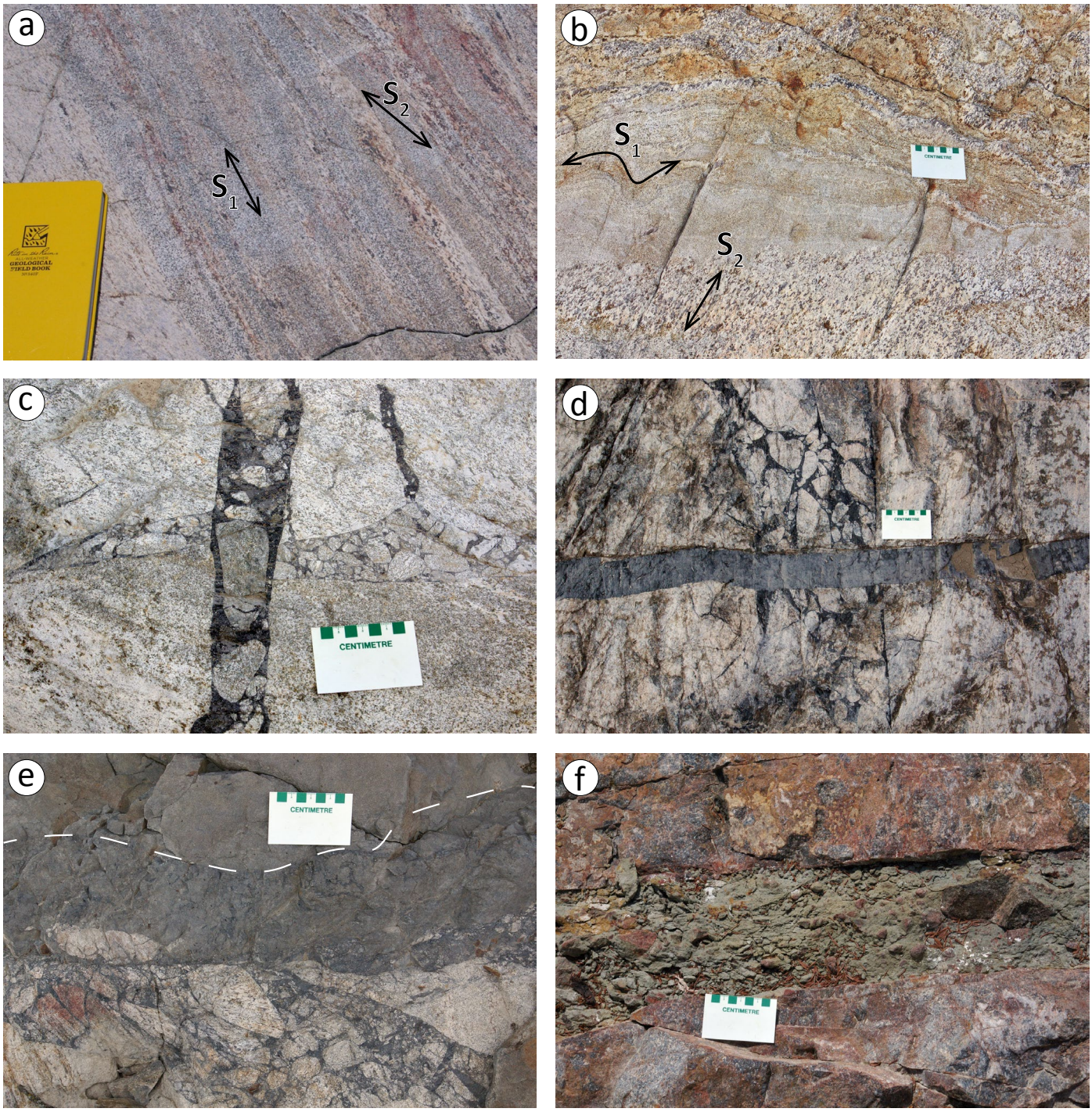

Figure 18: *Outcrop images of structures from the central Sipiwesk Lake area:* ***a)*** *relationship of S_1 gneissosity and S_2 quartz fabric in leucocratic mafic gneiss;* ***b)*** *F_2 minor folds with axial-planar S_2 quartz fabric;* ***c)*** *two generations of pseudotachylite veins in leucocratic mafic gneiss;* ***d)*** *diabase dike crosscutting pseudotachylite breccia;* ***e)*** *pseudotachylite breccia cutting diabase dike, the broken line indicating the margin of pseudotachylite breccia;* ***f)*** *fault gouge in hematized fracture zone.*

A close spatial association between the K-feldspar lenses and aggregates of sillimanite, cordierite and/or orthopyroxene may suggest the two are related as K-feldspar–rich leucosome associated with mafic-rich melanosome. The K-feldspar is locally replaced by skeletal sillimanite-quartz intergrowths. Biotite occurs as pseudomorphic replacements of cordierite (Figure 19c) and orthopyroxene, and more commonly as symplectic intergrowths with quartz as a replacement of cordierite, orthopyroxene and K-feldspar. Discrete grains of biotite without obvious replacement textures are extremely rare, suggesting biotite is present only as a retrograde phase. The replacement of cordierite and K-feldspar by symplectic intergrowths is also indicative of retrograde reactions, likely occurring under subsolidus conditions (Waters, 2001). The peak metamorphic assemblage of this rock is therefore interpreted as quartz-cordierite-orthopyroxene-sillimanite-rutile-melt, which is considered to be an ultrahigh-temperature assemblage (Harley, 1998; Kelsey, 2008; Kelsey and Hand, 2015).

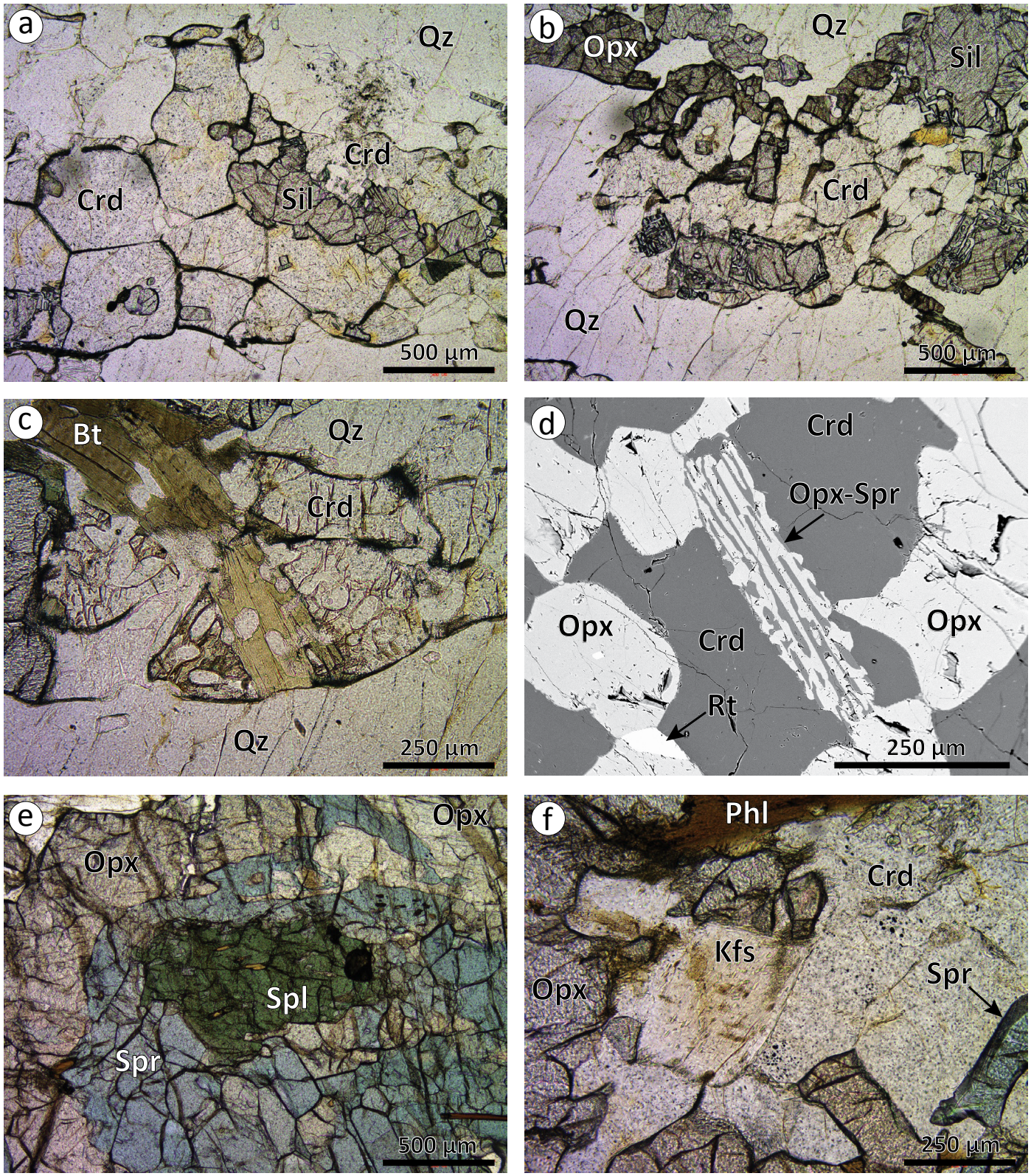

Figure 19: *Photo- and electron-micrographs of metamorphic assemblages from rocks of the Al-Mg gneiss suite:* ***a)*** *cordierite with a core of prismatic sillimanite (sample 108-12-1079C; plane-polarized light [PPL]);* ***b)*** *cordierite rimmed and partially replaced by orthopyroxene, sillimanite and skeletal quartz-sillimanite intergrowth (sample 108-12-1079C; PPL);* ***c)*** *cordierite pseudomorphously replaced by biotite (sample 108-12-1079C; PPL);* ***d)*** *orthopyroxene-sapphirine symplectite, intergrowth appearing to be pseudomorphous after an unknown tabular or prismatic mineral (sample 108-12-1080A; back-scattered electron);* ***e)*** *spinel armoured by sapphirine (sample 108-12-1080A; PPL);* ***f)*** *discrete grain of K-feldspar (sample 108-12-1080A; PPL). Abbreviations: Bt, biotite; Crd, cordierite; Kfs, K-feldspar; Opx, orthopyroxene; Phl, phlogopite; Qz, quartz; Rt, rutile; Sil, sillimanite; Spl, spinel; Spr, sapphirine.*

Aluminum-magnesium gneiss sample 108-12-1080A is coarse grained and granoblastic, and contains the mineral assemblage orthopyroxene–cordierite–sapphirine–phlogopite–rutile±spinel±K-feldspar. Zircon and monazite occur as accessory phases. Orthopyroxene, cordierite and phlogopite are typically rutilated. Symplectic intergrowth of orthopyroxene and sapphirine is relatively common. It typically occurs at the margins of orthopyroxene or sapphirine grains; however, it can also form discrete pseudomorphs (Figure 19d). The pseudomorphs appear to be elongate tabular or prismatic. The precursor phase of the pseudomorph is uncertain. Rare spinel occurs as dark green grains that are completely enclosed by sapphirine (Figure 19e). Rare feldspar is typically fine grained and interstitial to cordierite, orthopyroxene and sapphirine. The fine interstitial texture makes identification of the feldspar species difficult; however, rare discrete equant grains appear to consist of perthitic K-feldspar (Figure 19f). The interstitial texture of the feldspar suggests it could represent pseudomorphs of a melt phase (Holness and Sawyer, 2008; Holness et al., 2011).

Mudstone sample 108-12-1064C is medium grained with an assemblage of quartz–K-feldspar–garnet–plagioclase–biotite–sillimanite–orthopyroxene–rutile±sapphirine. Zircon and monazite occur as accessory phases. Garnet typically occurs as xenomorphic poikiloblasts that are elongate parallel to the foliation; however, sparse idiomorphic to subidiomorphic grains that are largely free of inclusions are also present. This suggests at least two generations of garnet growth. Orthopyroxene occurs intergrown with prismatic sillimanite (Figure 20a). The intergrowths appear as elongate xenomorphic poikiloblasts of orthopyroxene with discrete inclusions of prismatic sillimanite. The orthopyroxene-sillimanite intergrowth is interpreted as a pseudomorphic texture. The pseudomorphs are strongly associated with, and similar in habit to, the xenomorphic garnet. The prismatic sillimanite defines a strong lineation within the foliation. The sillimanite grains locally contain high relief, isotropic cores that could be garnet (Figure 20b). Idiomorphic and subidiomorphic garnet grains are locally observed in direct contact with the orthopyroxene-sillimanite pseudomorphs (Figure 20c, d). Sillimanite also occurs in the groundmass along sillimanite-rich laminations. Coarse-grained segregations of quartz and K-feldspar likely represent pods or lenses of leucosome. The K-feldspar is commonly mesoperthitic, while plagioclase is locally antiperthitic. Rare grains of sapphirine are present in the rock as fine rounded inclusions in K-feldspar and subidiomorphic garnet (Figure 20d). Fine-grained biotite occurs throughout the rock, aligned with the foliation. Symplectic intergrowths of quartz and biotite are common and appear to overprint orthopyroxene (Figure 20e). This suggests that some or all of the biotite is a retrograde phase. Rare skeletal intergrowths of sillimanite and quartz are also present.

In situ U-Pb monazite geochronology

Two samples used for metamorphic studies, mudstone 108-12-1064C and Al-Mg gneiss 108-12-1080A, were selected for in situ monazite dating in order to constrain the timing of metamorphism in the Sipiwesk Lake area.

Methodology

Thin sections approximately 60 µm thick were made from samples 108-12-1064C and 108-12-1080A. Monazite grains were located by scanning the thin sections with a CAMECA SX100 electron microprobe using the back-scattered electron (BSE) detector at the University of Manitoba, Department of Geological Sciences Microbeam Laboratory. Individual monazite grains were imaged with the BSE detector. Element-distribution maps of selected grains were generated using wavelength-dispersive spectroscopy (WDS) for Ce, Pb, Th and Y. The thin sections and monazite images were sent to the University of New Brunswick (Fredericton, New Brunswick) laser-ablation inductively coupled plasma–mass spectrometry (LA-ICP-MS) laboratory for U-Pb analysis.

The monazite grains were analyzed in situ using an ASI S-155-LR 193 nm excimer laser-ablation system coupled to an Agilent 7700x quadrupole ICP-MS. Instrument parameters and measurement protocols are outlined in Mohammadi et al. (2019). Corrections for laser-induced element fractionation and instrument drift/bias were achieved by replicate analysis (minimum of 15) of external monazite standard GSC 8153 (507 Ma; reference values from R. Stern, pers. comm., 2015) distributed throughout the ablation sequence; approximate U and Th concentrations were also calculated using 8153 monazite assuming a stoichiometric wt. % P (12.3) in monazite. Veracity of fractionation and drift corrections were checked using 425 Ma 44069 monazite (Aleinikoff et al., 2006) and 1766 Ma Thompson Mine monazite (reference values from I. Williams, pers. comm., 2015). Reference glass NIST610 was used to tune the instrument for low oxide production and high sensitivity. A beam diameter of 13 µm was used for all samples. The U-Pb data can be found in Appendix 1, Tables 4 and 5, with all errors reported at 2σ.

Reflected light photomicrographs were taken after analysis so that ablation pits could be accurately located on BSE images. Analyses that sampled matrix material, cracks in monazite grains and potentially portions of multiple age domains were eliminated. Concordia diagrams, binned histograms, probability-density distribution curves and $^{207}Pb/^{206}Pb$ ages were calculated using Isoplot™ v4.15 (Ludwig, 2003), with error ellipses and ages reported at 2σ. Analyses that were more than ±5% discordant were not considered.

Mudstone

Mudstone sample 108-12-1064C contains monazite grains that range from 40 to 500 µm. The grains are xenomorphic, range from equant to elongate, and occur in both felsic and

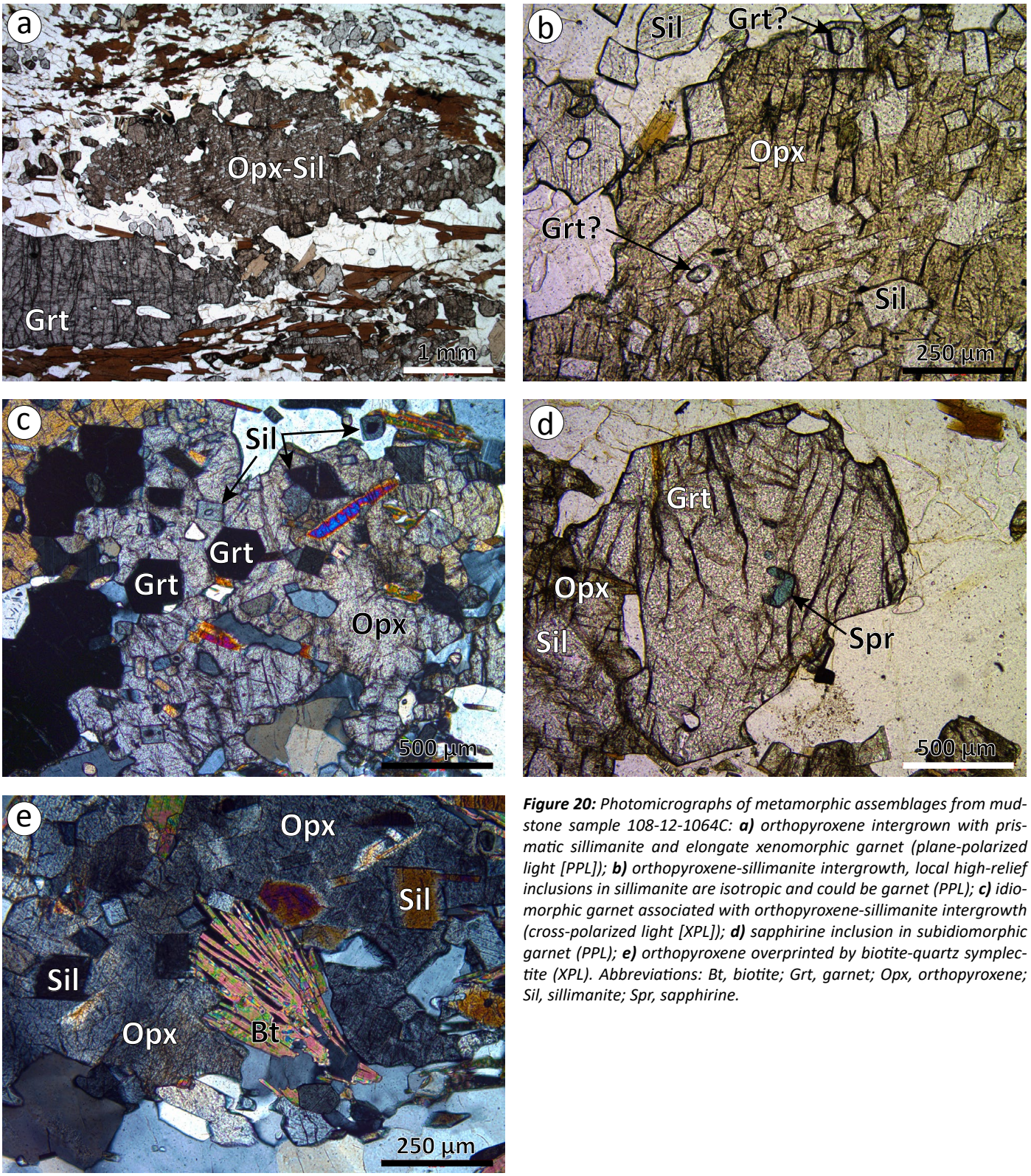

Figure 20: *Photomicrographs of metamorphic assemblages from mudstone sample 108-12-1064C:* ***a)*** *orthopyroxene intergrown with prismatic sillimanite and elongate xenomorphic garnet (plane-polarized light [PPL]);* ***b)*** *orthopyroxene-sillimanite intergrowth, local high-relief inclusions in sillimanite are isotropic and could be garnet (PPL);* ***c)*** *idiomorphic garnet associated with orthopyroxene-sillimanite intergrowth (cross-polarized light [XPL]);* ***d)*** *sapphirine inclusion in subidiomorphic garnet (PPL);* ***e)*** *orthopyroxene overprinted by biotite-quartz symplectite (XPL). Abbreviations: Bt, biotite; Grt, garnet; Opx, orthopyroxene; Sil, sillimanite; Spr, sapphirine.*

mafic domains of the matrix and as inclusions in garnet and orthopyroxene-sillimanite intergrowths. However, no correlation exists between monazite ages and the textural settings of monazite grains. A $^{207}Pb/^{206}Pb$ age-probability curve of 36 analyses indicates one dominant peak at ca. 2644 Ma, a smaller peak at ca. 2596 Ma and a shoulder at ca. 2567 Ma (Figure 21a). The prominent peak (age node 2) corresponds to 25 analyses of relatively darker, homogeneous to diffusely zoned cores of larger monazite grains (Figure 21b). The average Th/U ratio is relatively high (Th/U = 119). This population yielded largely discordant results with a weighted-mean $^{207}Pb/^{206}Pb$ age of 2644 ±5 Ma (MSWD = 2.1; Figure 21c). A $^{207}Pb/^{206}Pb$ age-probability curve of the remaining 11 analyses yields a broad peak at ca. 2595 Ma (age node 1; Figure 21d). These analyses correspond to smaller, homogeneous to mottled monazite grains and brighter margins of larger grains (e.g., analysis 8-2; Figure

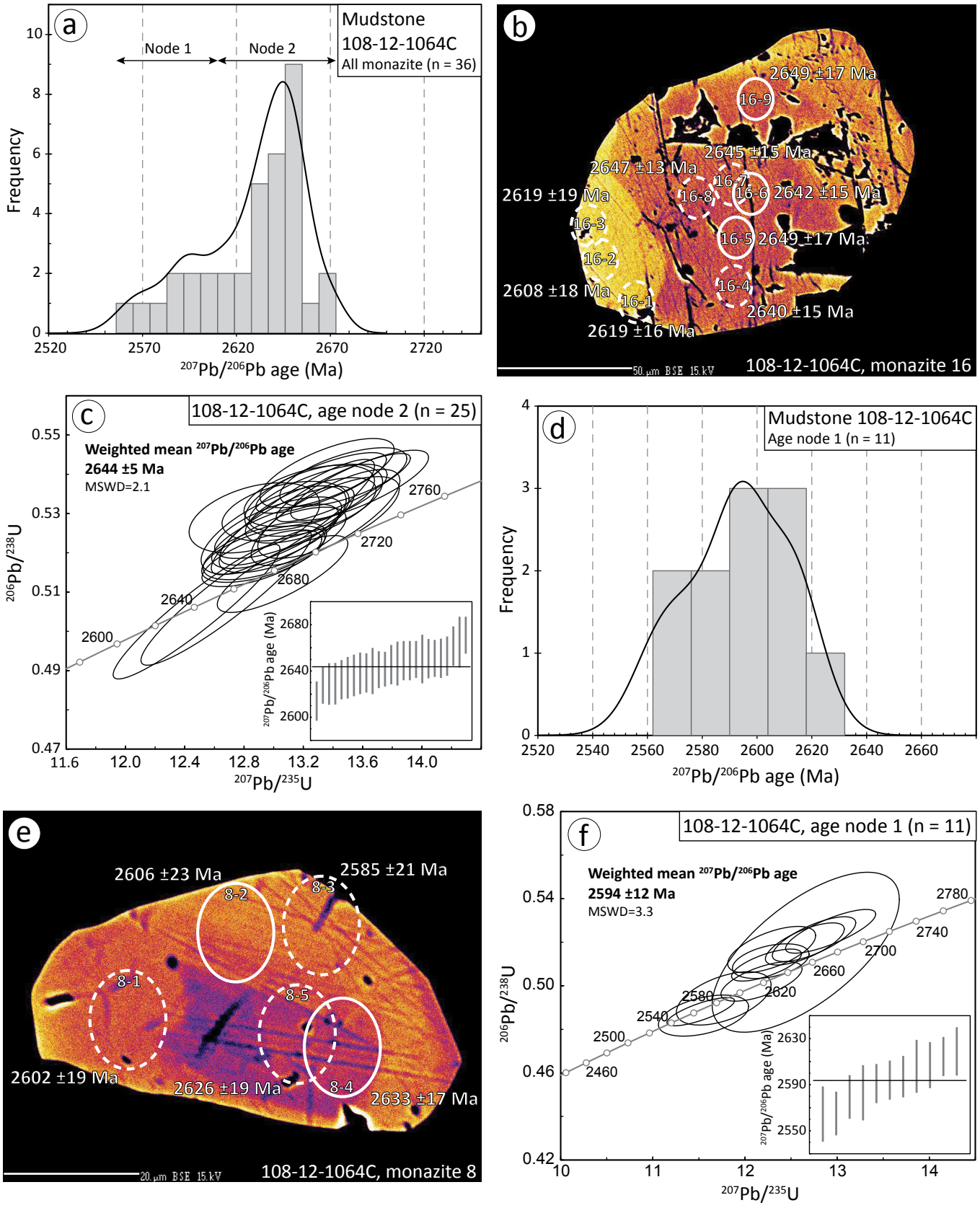

Figure 21: *Results of in situ U-Pb dating of monazite in mudstone 108-12-1064C:* ***a)*** *combined frequency histogram and probability-density distribution (PDD) curve of $^{207}Pb/^{206}Pb$ ages (Ma) for filtered metamorphic monazite;* ***b)*** *location of ablation pits with $^{207}Pb/^{206}Pb$ calculated ages on a backscattered-electron image of monazite 16, the darker core material yielding node 2 ages;* ***c)*** *U-Pb concordia diagram with inset $^{207}Pb/^{206}Pb$ mean-age diagram for the node 2 ages in (a);* ***d)*** *combined frequency histogram and PDD curve of $^{207}Pb/^{206}Pb$ ages that constitute node 1 in (a);* ***e)*** *location of ablation pits with calculated $^{207}Pb/^{206}Pb$ ages on a backscattered-electron image of monazite 8, the brighter rim yielding node 1 ages;* ***f)*** *U-Pb concordia diagram with inset $^{207}Pb/^{206}Pb$ mean-age diagram for the analyses of node 1 in (a). Dashed outlines in (b) and (e) indicate omitted analyses (see text for details).*

21e). The average Th/U ratio of this population is also relatively high (Th/U = 197). The analyses yielded an array of concordant to slightly discordant results with a weighted-mean $^{207}Pb/^{206}Pb$ age of 2594 ±12 Ma (MSWD = 3.3; Figure 21f).

Al-Mg gneiss

Sample 108-12-1080A contains monazite grains that range from 40 to 500 µm. The grains are xenomorphic and vary from equant to elongate and irregular. The monazite occurs in the matrix and as inclusions in cordierite, orthopyroxene, sapphirine and orthopyroxene-sapphirine symplectite; however, no correlation exists between monazite ages and the textural settings of monazite grains. A $^{207}Pb/^{206}Pb$ age-probability curve of 62 analyses indicates two prominent peaks at ca. 2648 Ma and ca. 2606 Ma, and smaller peaks at ca. 2569 Ma, ca. 2598 Ma, ca. 2620 Ma, ca. 2626 Ma and ca. 2639 Ma, with a shoulder at ca. 2666 Ma (Figure 22a). The multiple small age populations can be attributed to very small 2σ errors associated with a subset of the $^{207}Pb/^{206}Pb$ age data. However, it is common for multiple analyses of a single compositional zone (as observed in a BSE image) in a single monazite grain to yield ages from two or more of these closely spaced age populations (Figure 22b). The fact that adjacent analyses from what appears to be the same compositional zone can yield ages belonging to different closely spaced age populations indicates that they belong to one single broader population, or that there are compositional or age domains that are not resolvable in BSE images. Assuming the former, the $^{207}Pb/^{206}Pb$ age-probability curve likely defines three broader age nodes at ca. 2569 Ma, ca. 2606 Ma and ca. 2648 Ma.

The youngest age node (age node 1; ca. 2569 Ma) corresponds to four analyses, including darker rims and embayments on larger monazite grains and portions of homogeneous grains (Figure 22c). The average Th/U ratio is 9. The four analyses yielded concordant to discordant results with a weighted-mean $^{207}Pb/^{206}Pb$ age of 2569 ±5 Ma (MSWD = 0.25; Figure 22d). Age node 2 (ca. 2606 Ma) corresponds to 23 analyses of darker to moderate intensity rims and annuli on larger monazite grains, and portions of homogeneous grains (Figure 22c). Average Th/U ratio for this group is 11. The analyses yielded an array of concordant to nearly concordant results that do not define a weighted-mean concordant age. Because of the precision of each analysis, a Tukey's biweight mean was used to calculate a $^{207}Pb/^{206}Pb$ age of 2608 ±4 Ma (Figure 22e). Age node 3 corresponds to 35 analyses consisting of complexly zoned and moderate to bright cores of larger monazite grains (Figure 22c). Average Th/U ratio is 14. The analyses yielded an array of concordant to slightly discordant results that do not define a weighted-mean concordant age, but define a Tukey's biweight mean $^{207}Pb/^{206}Pb$ age of 2645 ±4 Ma (Figure 22f). Alternatively, the array of analyses that constitute nodes 2 and 3 could represent a continuum of monazite ages that range from ca. 2672 to 2595 Ma.

U-Pb zircon geochronology

Two clastic sedimentary rocks and one gneissic trondhjemite sample were collected for U-Pb zircon geochronology to constrain the timing of sedimentation and magmatic crystallization, respectively. Because of the complex and high-grade metamorphic history of the area and the potential for a complex zircon-growth history, it was decided to analyze both detrital and magmatic zircon by laser-ablation, multicollector, inductively coupled plasma–mass spectrometry (LA-MC-ICP-MS). One hundred and five grains were analyzed per sample. The U-Pb zircon data can be found in Appendix 1, Tables 6–8.

Methodology

Each sample consisted of 3–5 kg of representative rock, which was collected by hammer from outcrop and manually trimmed in the field to remove weathering and altered fractures. Because of the high metamorphic grade, leucosome is ubiquitous and can form a significant proportion of a sample (especially of the siliciclastic rocks); however, care was taken to include only material that appeared to be in source or in situ, and to reject material that appeared to be injected. The sampled material was then bagged and sealed in a clean plastic rock pail and shipped to the University of Alberta Radiogenic Isotope Facility (Edmonton, Alberta) for mineral separation, processing and analysis.

The mineral separation techniques followed those outlined in Heaman et al. (2002), and the resulting zircons were hand picked, mounted in epoxy and polished to half-section thickness for analysis. All analyses were performed on a Nu Plasma MC-ICP-MS coupled to a New Wave Research UP213 Nd:YAG laser-ablation system. Ion-counting detectors were used to measure ^{207}Pb, ^{206}Pb and ^{204}Pb, whereas U was measured on Faraday collectors. Instrumental parameters and measurement protocols are outlined in Simonetti et al. (2005). Corrections for laser-induced element fractionation and instrument drift/bias were achieved by analysis of an external zircon standard (OG1) after the analysis of every 10–12 unknowns. A beam diameter of 30 µm was used for all samples. All errors are reported at 2σ and are a quadratic combination of the standard internal measurement error and external reproducibility of the zircon standard. For the purposes of interpretation, the results were filtered to include only the most concordant (95–105%) and precise (2σ analytical errors ≤30 Ma) $^{207}Pb/^{206}Pb$ ages. Concordia ages and diagrams, binned histograms and probability-density distribution curves, and $^{207}Pb/^{206}Pb$ ages were calculated using the Isoplot version 3.0 application of Ludwig (2003), with error ellipses shown at 2σ.

Gneissic trondhjemite

Sample 108-12-1183 consists of gneissic trondhjemite from the southeastern portion of the map area (Figure 23a). The trondhjemite is light pink and medium grained, with 5–7% biotite and 1–2% each of orthopyroxene, clinopyroxene and

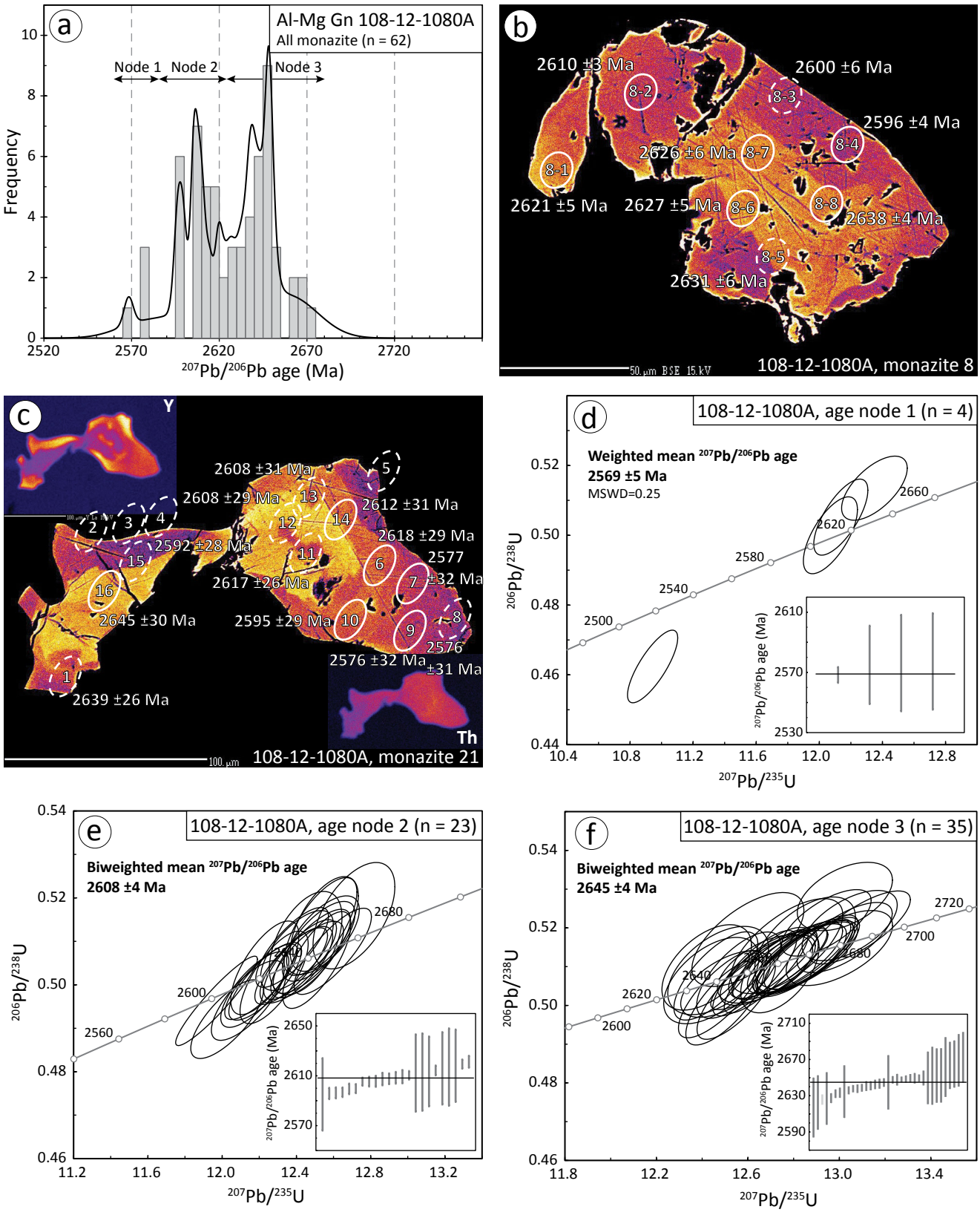

Figure 22: *Results of in situ U-Pb dating of monazite in Al-Mg gneiss 108-12-1080A:* ***a)*** *combined frequency histogram and probability-density distribution (PDD) curve of $^{207}Pb/^{206}Pb$ ages (Ma) of metamorphic monazite;* ***b)*** *location of ablation pits with $^{207}Pb/^{206}Pb$ calculated ages on a backscattered-electron image of monazite 8;* ***c)*** *location of ablation pits with calculated $^{207}Pb/^{206}Pb$ ages on a backscattered-electron image of monazite 21, the brighter core material yielding node 3 ages, the moderate annulus yielding node 2 ages and the darker rim material yielding node 1 ages, and inset maps showing relative concentrations of Y and Th;* ***d)*** *U-Pb concordia diagram with inset $^{207}Pb/^{206}Pb$ mean-age diagram for the analyses of node 1 in (a);* ***e)*** *U-Pb concordia diagram with inset $^{207}Pb/^{206}Pb$ mean-age diagram for the analyses of node 2 in (a);* ***f)*** *U-Pb concordia diagram with inset $^{207}Pb/^{206}Pb$ mean-age diagram for the analyses of node 3 in (a). Dashed outlines in (b) and (c) indicate eliminated analyses (see text for details). Abbreviation: gn, gneiss.*

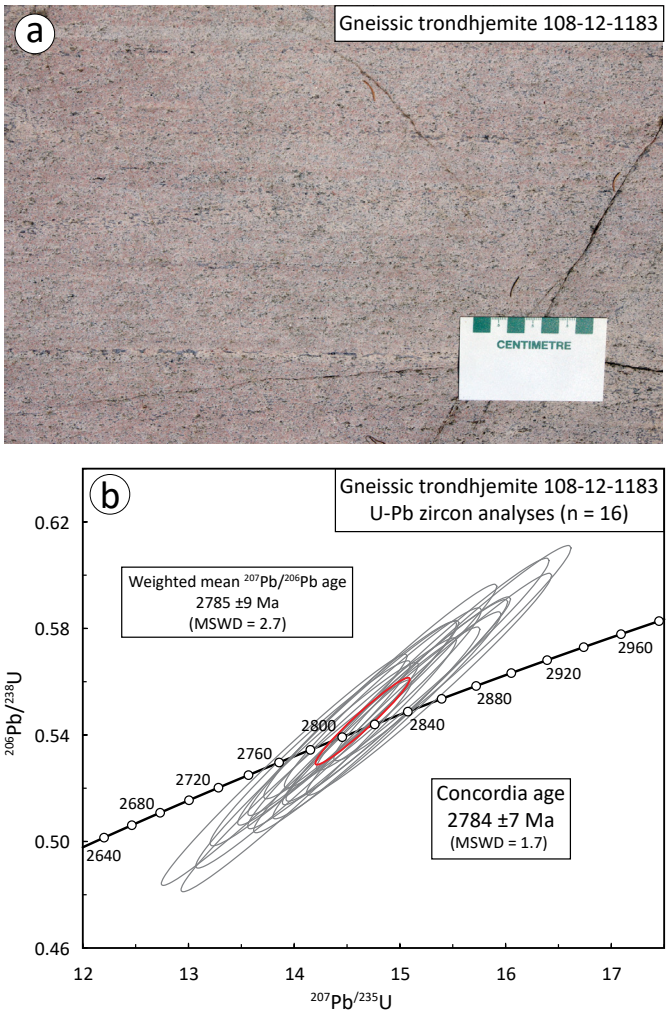

Figure 23: *Images and diagrams for U-Pb zircon analyses of gneissic trondhjemite 108-12-1183:* ***a)*** *outcrop image of sample location;* ***b)*** *U-Pb concordia diagram for zircon analyses.*

ilmenite. The outcrop contains 10–20% attenuated leucosome pods and minor mafic schlieren <5 cm thick. The recovered zircons are variable in size, dominantly tabular and euhedral to subhedral. Sixty analyzed zircons yielded results that are <5% discordant. A cathodoluminescence (CL) image of the grain mount was used to select analyses that appeared to ablate only the central domains of zircon but not adjoining rims or overgrowths. This reduced the dataset to 23 analyses. Of these analyses, a subset of 16 analyses consisted of domains characterized by relatively dark, oscillatory zoning with euhedral outlines, which are characteristic of magmatic zircon (Hoskin and Schaltegger, 2003). This subset yielded a weighted-mean $^{207}Pb/^{206}Pb$ age of 2785 ±9 Ma and a concordant U-Pb age of 2784 ±7 Ma, which is considered the best estimate for the crystallization age of the trondhjemite (Figure 23b).

Siliciclastic rocks

Sample 97-12-055 consists of layered to laminated arkosic wacke collected from the central portion of the map area (Figure 24a). The 105 recovered zircons are variable in size and range from equant to tabular and euhedral to rounded. Dark overgrowths are common in a CL image of the grain mount and cores are locally embayed. Thirty-two of the analyzed zircons yielded results that were <5% discordant. Four of these analyses are younger than 2700 Ma and are interpreted as metamorphic zircon. Three analyses yielded a weighted-mean $^{207}Pb/^{206}Pb$ age of 2660 ±7 Ma, and a single analysis yielded a $^{207}Pb/^{206}Pb$ age of 2682 ±11 Ma (Figure 24b). The remaining analyses are interpreted to represent detrital zircon and define multiple age-populations with a dominant mode at 2902 ±4 Ma, several minor populations from ca. 2740 to ca. 2944 Ma and a single zircon analysis yielding an age of ca. 2979 Ma. A maximum age for the arkosic rock is interpreted to be ca. 2740 Ma. A minimum age is bracketed by the oldest metamorphic zircon at ca. 2682 Ma.

Sample 108-12-1146A consists of mudstone–wacke from the north-central portion of the map area. The outcrop consists of a sequence of arkosic wacke with local mudstone layers, interbedded with and grading into arkosic arenite over approximately 20 m (Figure 24c). The centre of the interval contains horizons of mafic rock <1.5 m thick that likely represents mafic tuff or sandstone. Of the 105 zircon grains analyzed, 85 yielded results <5% discordant. The results define multiple age populations with a dominant mode at 2711 ±8 Ma, additional local maxima at ca. 2790, 2895 and 2953 Ma, and single zircon analyses yielding ages of ca. 3017 Ma and ca. 3478 Ma (Figure 24d). The significance of the dominant mode is difficult to interpret, as it consists of a continuum of ages from younger, likely metamorphic zircon at ca. 2656 Ma to older, likely detrital zircon at ca. 2766 Ma.

Discussion

This discussion is subdivided into three subsections. The first provides an outline and interpretation of the metamorphic geology of the central Sipiwesk Lake area. This is followed by a comparison of rocks in the area to rocks from the adjacent domains of the Superior province. The final subsection discusses possible origins for the gneissic rocks of unusual bulk composition.

Metamorphic geology

Phase-equilibrium diagrams were calculated for the three samples selected for metamorphic study (mudstone 108-12-1064C and Al-Mg gneiss 108-12-1079C and 108-12-1080A). The phase-equilibrium diagrams allow for the comparison of observed metamorphic assemblages with assemblages predicted through forward modelling. This, combined with the in situ monazite dating, provides some insight into the metamorphic history of the Sipiwesk Lake area.

Phase-equilibrium modelling

Phase-equilibrium diagrams were calculated using the Theriak-Domino software package (de Capitani and Brown, 1987; de Capitani and Petrakakis, 2010) and the updated

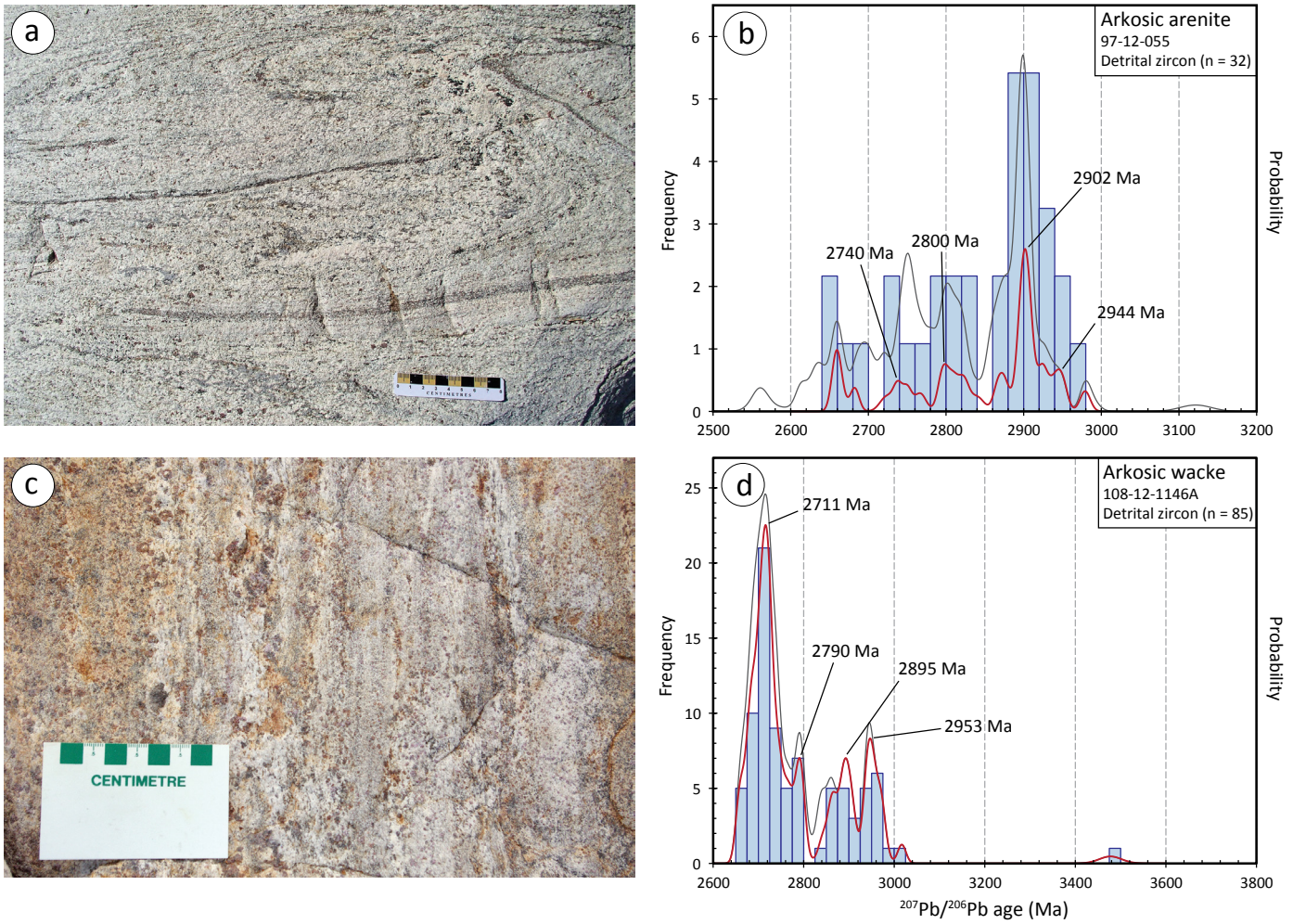

Figure 24: *Images and diagrams for detrital U-Pb zircon analyses of siliciclastic rocks:* ***a)*** *outcrop image for arkosic wacke 97-12-055;* ***b)*** *combined frequency histogram and probability-density distribution (PDD) curve of $^{207}Pb/^{206}Pb$ ages (Ma) of detrital zircon from 97-12-055;* ***c)*** *outcrop image for mudstone–wacke 108-12-1146A;* ***d)*** *combined frequency histogram and PDD curve of $^{207}Pb/^{206}Pb$ ages (Ma) of detrital zircon from 108-12-1146A. Dark grey PPD curve in (b) and (d) is for all analyzed data; red PPD curve is for data within ±5% of concordia.*

ds5.5 thermodynamic dataset of Holland and Powell (1998). The activity models used are those outlined in Tinkham and Ghent (2005) and Pattison and Tinkham (2009), with the following exceptions: 1) the monoclinic amphibole model is that of Diener et al. (2007); 2) the biotite model is that of White et al. (2007); 3) the garnet model is that of White et al. (2007), with the Margules parameters of almandine–grossular and pyrope–grossular following THERMOCALC v.3.31 data files; 4) the spinel model is that of White et al. (2002); 5) the sapphirine model is that of Kelsey et al. (2004); and 6) the liquid model is that of White et al. (2007), with the enthalpies of forsterite and fayalite liquid adjusted by –10 kJ/mol and –9 kJ/mol, respectively, following THERMOCALC v.3.31 data files. Samples were modelled in the chemical system NCKFMASHT (Na_2O-CaO-K_2O-FeO-MgO-Al_2O_3-SiO_2-H_2O-TiO_2). The water content of the system is assumed to equal the loss-on-ignition (LOI) value for each sample. Because the samples are granulites containing retrograde biotite, and minor amounts of other volatiles such as CO_2 could be present, this likely represents a maximum value for the amount of H_2O in the system during peak metamorphism.

Petrographic thin sections of the samples were examined and modal abundances were calculated based on >780 point counts for each thin section (point-count results available in Appendix 1, Table 9). Electron microprobe data of selected minerals was collected for samples 108-1064C and 108-1080A, and is available in Appendix 1, Tables 10–15. Observed modal abundances and mineral compositions were later compared to the predicted values to ensure a close fit with the models.

The peak metamorphic mineral assemblage for Al-Mg gneiss sample 108-12-1079C is interpreted as quartz-cordierite-orthopyroxene-sillimanite-rutile-melt. The calculated phase-diagram section suggests pressure-temperature conditions of approximately 8–9.5 kbar and 915–1070°C for this assemblage (assemblage 1, Figure 25a), which is consistent with ultrahigh-temperature metamorphism (Harley, 1998; Kelsey, 2008; Kelsey and Hand, 2015).

The observed mineral assemblage in Al-Mg gneiss 108-12-1080A is orthopyroxene-cordierite-sapphirine-phlogopite-rutile-feldspar-spinel±melt, which suggests a rather limited

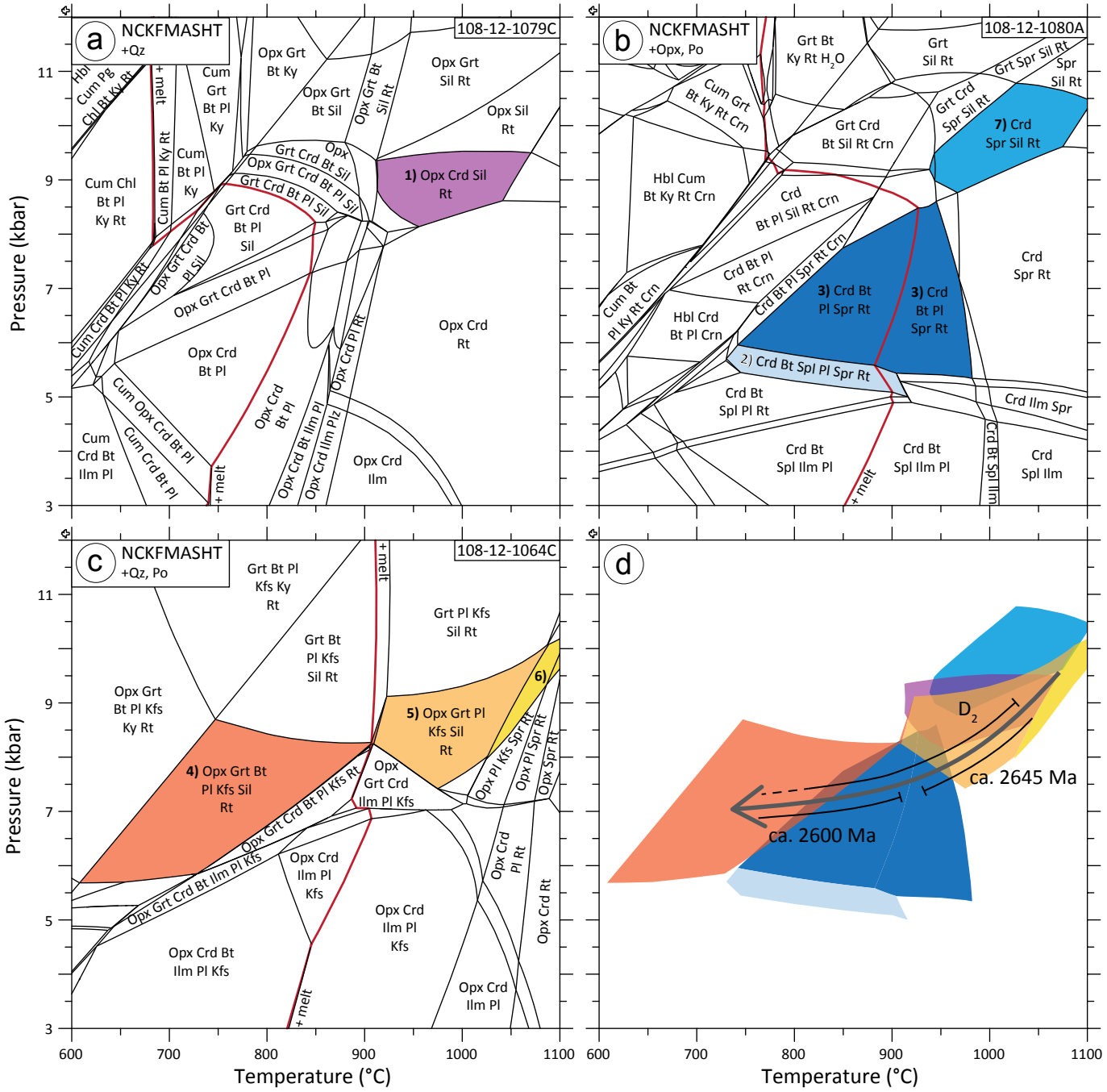

Figure 25: *Phase-equilibrium diagrams in NCKFMASHT:* ***a)*** *Al-Mg gneiss sample 108-12-1079C;* ***b)*** *Al-Mg gneiss sample 108-12-1080A;* ***c)*** *mudstone sample 108-12-1064C;* ***d)*** *overlay of assemblage fields from (a), (b) and (c). Red lines indicate the solidus in each diagram. Numbered assemblages are discussed in the text. Abbreviations: Bt, biotite; Chl, chlorite; Crd, cordierite; Crn, corundum; Cum, cummingtonite; Grt, garnet; H_2O, water; Hbl, hornblende; Ilm, ilmenite; Kfs, K-feldspar; Ky, kyanite; Opx, orthopyroxene; Pg, paragonite; Pl, plagioclase; Po, pyrrhotite; Qz, quartz; Rt, rutile; Sil, sillimanite; Spl, spinel; Spr, sapphirine.*

pressure-temperature range of 5–6 kbar and 725–900°C (assemblage 2, Figure 25b). Rare grains of spinel occur enclosed by sapphirine, which suggests that the spinel is metastable. The model predicts spinel to be stable at relatively low pressures (<6 kbar) and, as temperature increases, the pressure at which spinel is stable decreases. This implies that spinel was part of a prograde assemblage, likely under subsolidus conditions, which remained metastable during peak metamorphism and along the subsequent retrograde path. However, it is highly unlikely that a subsolidus prograde phase would remain metastable at such high metamorphic grades. Because spinel is relatively rare in the observed mineral assemblage, there may be inhomogeneous distribution of spinel within the sample used for geochemical analysis. This could result in discrepancies between the predicted and observed mineral assemblages. Removing spinel from the predicted mineral assemblages results in a broader pressure-temperature range of 5.5–8.5 kbar and 750–1000°C (assemblage 3), which is more consistent with the phase-equilibrium models of the other samples.

Mudstone sample 108-12-1064C contains the mineral assemblage quartz–K-feldspar–garnet–plagioclase–biotite–sillimanite–orthopyroxene–rutile±sapphirine. Excluding sapphirine, this assemblage indicates pressure-temperature conditions of approximately 5.5–8.5 kbar and 600–900°C (assemblage 4, Figure 25c). Assuming that the biotite is retrograde and the coarse-grained segregations of quartz and K-feldspar represent leucosome, the pressure-temperature conditions outlined by the diagram are increased to approximately 7.5–10 kbar and 900–1100°C (assemblage 5). The presence of rare sapphirine inclusions in plagioclase and garnet are indicative of higher peak temperatures. Sapphirine-garnet is not predicted to become part of a stable assemblage until approximately 1025°C (assemblage 6).

Interpretation of metamorphic conditions

The observed mineral assemblages outlined in the previous section were all affected by varying degrees of retrograde metamorphism during cooling. This is supported by the various pseudomorphic and symplectic/skeletal intergrowths observed in each of the samples (Figure 19b–d; Figure 20). As a result, the various observed assemblages represent different regions in P-T-t space. The mineral assemblage quartz-cordierite-orthopyroxene-sillimanite-rutile-melt in sample 108-12-1079C defines ultrahigh-temperature metamorphic conditions of approximately 8–9.5 kbar and 915–1070°C (assemblage 1, Figure 25a). The presence of sapphirine as inclusions in garnet in mudstone 108-12-1064C suggests that peak temperature was likely greater than 1025°C (assemblage 6, Figure 25c). It is likely that the orthopyroxene-sapphirine symplectite present in sample 108-12-1080A is pseudomorphous after a higher temperature phase. One possibility suggested by the elongate prismatic shape of the pseudomorph is sillimanite, which would imply the retrograde reaction:

orthopyroxene + hydrous cordierite + Al-sapphirine + sillimanite → Al-orthopyroxene + anhydrous cordierite + sapphirine + melt

This would also imply a peak metamorphic assemblage of orthopyroxene-cordierite-sapphirine-sillimanite-rutile-melt for the sample (8.8–10.8 kbar and 950–1100°C; assemblage 7, Figure 25b) and necessitates that the observed phlogopite be a retrograde phase.

Sillimanite as part of the peak metamorphic assemblage in Al-Mg gneiss 108-12-1080A would require decompression during cooling and a clockwise P-T path to attain the observed metamorphic assemblage of orthopyroxene-cordierite-sapphirine-phlogopite-rutile-feldspar (assemblage 3, Figure 25b). In mudstone 108-12-1064C, the orthopyroxene-sillimanite intergrowth is closely associated with, and has a habit similar to, the xenomorphic garnet. This suggests that the orthopyroxene-sillimanite intergrowth could be pseudomorphous after the xenomorphic garnet. Possible garnet inclusions in the sillimanite could be further evidence for this reaction (Figure 20b). The breakdown of garnet to form orthopyroxene and sillimanite would indicate high-temperature decompression via the reaction:

garnet ($Mg_3Al_2Si_3O_{12}$) + quartz (SiO_2) → orthopyroxene ($3MgSiO_3$) + sillimanite (Al_2SiO_5)

The strong lineation defined by the sillimanite suggests that high-temperature decompression was concurrent with D_2 (Figure 25d). The presence of idiomorphic garnet in close association with, and often impinging on (Figure 20c, d), the orthopyroxene-sillimanite intergrowth suggests that it likely represents a second generation of garnet growth that postdates the orthopyroxene-sillimanite pseudomorphs. The second generation of garnet growth could be the product of anhydrous retrogression of orthopyroxene under amphibolite-facies metamorphic conditions.

Monazite geochronology

The lack of correlation between monazite ages and textural setting of monazite grains, combined with the lack of mineral-chemistry data, makes meaningful interpretation of the in situ monazite geochronology exceedingly difficult. The monazite ages from this study are generally younger than the metamorphic zircon ages obtained from arkose sample 97-12-055 (2660 ±7 Ma and 2682 ±11 Ma) and younger than the majority of U-Pb zircon ages recorded for the PGD (Heaman et al., 2011; Guevara et al., 2020a). The youngest zircon ages (ca. 2649 Ma) reported by Guevara et al. (2020a) at Partridge Crop Lake were interpreted to record melt crystallization following ultrahigh-temperature metamorphism. Heaman et al. (2011) reported ages of ca. 2644 Ma for metamorphic zircon growth in tonalitic gneiss and ca. 2640 Ma for metamorphic zircon growth in amphibolite at Cauchon Lake. The latter age was interpreted to record an amphibolite-facies metamorphic event. Guevara et al. (2020b) recorded zircon as young as ca. 2640 Ma, which was ascribed to latest melt accumulation and crystallization in a locally derived leucogranite. Mezger et al. (1989) reported U-Pb garnet ages of 2660–2637 Ma from Cauchon Lake, which were interpreted to record granulite-facies metamorphism. They also reported U-Pb igneous garnet ages of 2605–2591 Ma and a U-Pb igneous zircon age of ca. 2598 Ma, which were interpreted to record granitoid magmatism under amphibolite-facies metamorphic conditions.

Monazite cores from mudstone sample 108-12-1064C and Al-Mg gneiss sample 108-12-1080A yielded nearly identical mean $^{207}Pb/^{206}Pb$ ages of 2644 ±5 Ma and 2645 ±4 Ma, respectively. Average Th/U ratios of the monazite cores from the mudstone (108-12-1064C) are high (Th/U = 119) and could indicate crystallization in the presence of a melt phase. Relatively higher Y content is suggested by the lower intensity (darker) appearance of the cores in BSE images and is supported by element mapping of a limited number of monazite grains. Higher Y could indicate monazite crystallization during a period of garnet resorption and could record the pseudomorphous replacement of garnet by the orthopyroxene-sillimanite

intergrowth during D_2. Together, the Th/U ratio and relative Y content could indicate decompression under suprasolidus conditions (>900°C) at ca. 2645 Ma (Figure 25d).

Moderate-intensity monazite rims and annuli from the Al-Mg gneiss yielded a $^{207}Pb/^{206}Pb$ age of 2608 ±4 Ma. This is slightly older than, but within error of, the youngest monazite from the mudstone at 2594 ±12 Ma. The ca. 2594 Ma monazite from the mudstone sample is also characterized by a high Th/U ratio (Th/U = 197), which could be indicative of crystallization in the presence of a melt phase. This would require a new cycle of heating and cooling, or suggest that temperatures remained above the solidus (approximately 900°C) during a 50 m.y. time period. Alternatively, the fractional crystallization of melt in isolated pods could result in crystallization temperatures significantly lower than the predicted solidus (Koblinger and Pattison, 2017), and could allow for slow cooling during this time period (Figure 25d). The S_2 quartz fabric present in leucosome implies that D_2 continued as the rocks attained subsolidus conditions.

There is an alternative interpretation for the two older monazite populations in the Al-Mg gneiss. These monazites could represent a continuum of ages from ca. 2672 Ma to ca. 2595 Ma. The continuous crystallization of monazite during approximately 80 Ma could record slow cooling of the rock at relatively high metamorphic grade. This alternative interpretation can still be in agreement with the previously outlined scenario; however, the initial monazite growth in sample 108-12-1080A could have started as early as ca. 2672 Ma. As the rock continued to cool, likely in the presence of a melt phase, additional monazite would continue to crystallize until ca. 2595 Ma. This alternative also results in greater overlap with the findings of Guevara et al. (2020a), which reported post–ultrahigh-temperature decompression and zircon crystallization in the Partridge Crop Lake area from ca. 2673 to ca. 2649 Ma.

The youngest monazite from the Al-Mg gneiss yielded a mean $^{207}Pb/^{206}Pb$ age of 2569 ±5 Ma (Figure 22d). The significance of this age is unknown but is assumed to be related to cooling/retrograde reactions.

Metamorphic-geology synthesis

In summary, peak metamorphism is best constrained by the assemblage in sample 108-12-1079C (assemblage 1, Figure 25a) and the presence of sapphirine in sample 108-12-1064C (assemblage 6, Figure 25c), which indicate ultrahigh-temperature metamorphic conditions of 8–9.5 kbar and 1025–1070°C. The rocks were then subjected to decompression during cooling, resulting in the observed assemblages and retrograde textures in samples 108-12-1080A (assemblage 3, Figure 25b) and 108-12-1064C (assemblage 4, Figure 25c). Cooling and decompression were contemporaneous with D_2 and likely underway by ca. 2645 Ma (or possibly as early as 2672 Ma); however, relatively high temperatures may have remained until at least ca. 2600 Ma, accompanied by continued D_2 deformation (Figure 25d).

These ages are considerably younger than the ca. 2680 Ma age interpreted by Heaman et al. (2011) for the M_2-D_2 event. However, it should be noted that there is no evidence that prograde and peak M_2 metamorphism were synchronous with D_2. The M_2 leucosome is commonly subparallel to S_1 and is deformed by F_2 minor folds, and the S_2 fabrics are preserved in the crystallized leucosome and microtextures of the post–peak M_2 metamorphic assemblages. A significant portion of the monazite ages obtained in this study are also younger than the zircon ages obtained by Guevara et al. (2020a) for post–ultrahigh-temperature decompression in the Partridge Crop Lake area from 2673 to 2649 Ma. This could indicate diachronous decompression and cooling, or differences in the rate of decompression and cooling, across the PGD. The clockwise pressure-temperature-time path and prolonged history of (high-grade) metamorphism are both characteristic of a collisional orogen. Therefore, the PGD likely represents the core of a collisional orogenic belt.

Correlations with rocks of the adjacent northwest Superior province

The PGD has generally been considered a part of the Hudson Bay terrane (Percival et al., 2006; Stott et al., 2010), which is characterized by crustal-residence Nd-model ages for granitoid and sedimentary rocks ranging from ca. 2.97 Ga to ca. 4.15 Ga but typically consisting of Paleoarchean to Eoarchean ages (Figure 26; Böhm et al., 2000, 2003, unpublished data, 2005; Skulski et al., 2000; Rayner and Stott, 2005; Corkery, unpublished data, 2007). Crustal-residence Nd-model ages of granitoid and sedimentary rocks from the Sipiwesk Lake area range from 3.28 to 3.00 Ga, which overlap with but are younger than typical Hudson Bay terrane rocks. The Nd-model ages of Sipiwesk area rocks are more similar to ages obtained for the North Caribou terrane (T_{CR} = 3.32–2.97 Ga; Böhm, unpublished data, 1997; Skulski et al., 2000; Beaumont-Smith, unpublished data, 2004; Corkery, unpublished data, 2004, 2007; Rayner and Stott, 2005; Anderson and Martins, 2019b; Böhm et al., 2021). This suggests a lithological affinity with the Oxford-Stull domain of the North Caribou terrane, which lies immediately east of the Sipiwesk Lake area. This affinity is in agreement with Hubregtse (1980), who suggested that the PGD is structurally continuous with the lower grade greenstone and tonalite terranes of the northwestern Superior province. The two closest greenstone belts within the Oxford-Stull domain are the Oxford Lake–Knee Lake greenstone belt and the Cross Lake greenstone belt.

Traditionally, supracrustal rocks of the Oxford Lake–Knee Lake belt have been divided into two groups: the 2.84–2.83 Ga Hayes River group (Corkery et al., 2000; Anderson, 2017b) and the ca. 2.73–2.71 Ga Oxford Lake group (Corkery et al., 2000; Lin et al., 2006). Work by Syme et al. (1997) and Anderson et al. (2013) suggests that this stratigraphic scheme is likely over-

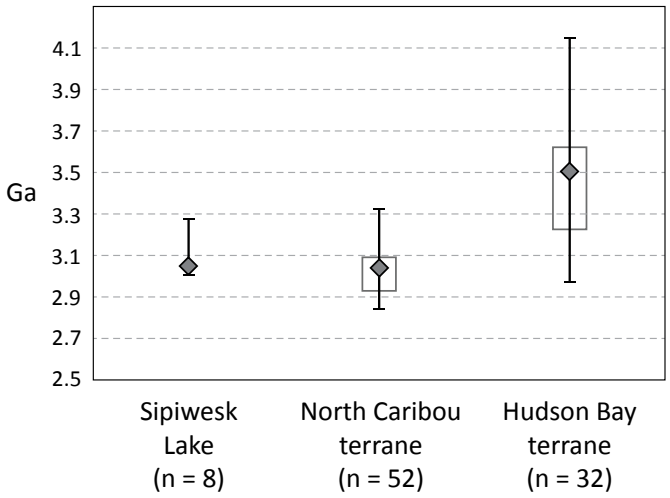

Figure 26: *Range of crustal-residence Nd-model ages for granitoid and sedimentary rocks of the Sipiwesk Lake area and adjacent terranes of the northwestern Superior craton. Diamonds indicate median values and rectangles indicate the interquartile range (middle 50% of the data). Data for the Sipiwesk Lake area are from this report and Böhm (unpublished data, 1997). Data for the North Caribou terrane are from Böhm (unpublished data, 1997), Skulski et al. (2000), Beaumont-Smith (unpublished data, 2004), Corkery (unpublished data, 2004, 2007), Rayner and Stott (2005), Anderson and Martins (2019b) and Böhm et al. (2021). Data for the Hudson Bay terrane are from Böhm et al. (2000, 2003, unpublished data, 2005), Skulski et al. (2000), Rayner and Stott (2005) and Corkery (unpublished data, 2007). Crustal-residence ages from Skulski et al. (2000) and Rayner and Stott (2005) were recalculated using the model of Goldstein et al. (1984).*

simplified; however, it is retained here so that correlations can be made with previous reports. The Hayes River group consists dominantly of pillowed and massive basalt flows and related gabbro, with minor felsic and intermediate volcanic rocks, volcaniclastic and turbiditic sedimentary rocks, and iron formation (Syme et al., 1997; Anderson et al., 2013; Anderson, 2017a). Geochemistry of the Hayes River group is suggestive of a back-arc–basin setting (Anderson, 2017b). The Oxford Lake group unconformably overlies the Hayes River group. It consists of marine volcanic, volcaniclastic and derived sedimentary rocks, which were traditionally subdivided into a lower subgroup dominated by volcanic rocks and an upper subgroup dominated by sedimentary rocks; however, subsequent work suggests the stratigraphy is considerably more complex (Anderson, 2017a). The volcanic subgroup includes high-K calcalkaline to shoshonitic-affinity volcanic rocks that range in composition from basalt to rhyolite and are intercalated with locally derived, coarse epiclastic rocks. The more extensive sedimentary subgroup consists of a thick succession of submarine-fan conglomerate, sandstone, greywacke-mudstone turbidite and iron formation, with minor basalt flows (Anderson et al., 2013; Anderson, 2017a). Recent work by Anderson (2016b) at Knee Lake suggests that fluvial-alluvial sandstone and conglomerate, which were previously identified as part of the Oxford Lake group, are part of a younger sequence. This fluvial-alluvial sequence was deposited unconformably on the Hayes River and Oxford Lake groups. Abundant granitoid and vein-quartz clasts in the conglomerate suggest regional uplift and erosion (Anderson, 2017b) and deposition in synorogenic basins. Detrital zircon from the synorogenic deposits yielded a maximum depositional age of ca. 2.71 Ga (Corkery et al., 2000; Anderson, 2017a, b).

Supracrustal rocks of the Cross Lake belt are divided into three groups: the ca. 2.76 Ga Pipestone Lake group, the ca. 2.73 Ga Gunpoint group and the <2.71 Ga Cross Lake group (Corkery et al., 1992). The Pipestone Lake group consists dominantly of pillowed basalt with subordinate massive flows, minor mudstone and mafic wacke, and rare iron formation. The volcanic rocks are intruded by layered ultramafic to anorthositic rocks, which are interpreted to be contemporaneous. Two samples of anorthositic rock yielded ages of ca. 2760 Ma, implying a similar age for the volcanic rocks of the Pipestone Lake group (Corkery et al., 1992); however, mafic sills of similar age are also found in the older Hayes River group at Knee Lake (S. Anderson, pers. comm., 2020). Similarities in stratigraphy and geochemistry suggest that the Pipestone Lake group could be correlative with the ca. 2.83 Ga Hayes River group. The Gunpoint group unconformably overlies the Pipestone Lake group and comprises felsic volcaniclastic rocks, conglomerate, sandstone, and subordinate siltstone and mudstone interbedded with iron formation (Corkery et al., 1992). The Cross Lake group unconformably overlies rocks of the Pipestone Lake and Gunpoint groups. It consists of a fluvial-alluvial sequence of coarse clastic rocks with subordinate shoshonitic basalt and reworked volcaniclastic rocks, and is locally overlain by marine sedimentary rocks. The Gunpoint and Cross Lake groups are likely correlative with the Oxford Lake group and the synorogenic deposits of the Oxford Lake–Knee Lake belt, respectively. A lithogeochemistry dataset of more than 400 samples from the Oxford Lake–Knee Lake belt was recently released by the Manitoba Geological Survey (Anderson and Martins, 2019a). This dataset, combined with unpublished data from the Cross Lake belt (T. Corkery, unpublished data, 2001), allows for comparison with Sipiwesk Lake rocks.

Mafic gneiss

Local layers of iron formation within the mafic gneiss at Sipiwesk Lake suggest that the gneiss is part of a supracrustal package and is derived, at least in part, from mafic volcanic rocks. The leucocratic mafic gneiss is the least enriched variety of mafic gneiss (Figure 27a). Normalized trace-element profiles are most similar to those of mafic rocks of the Bleak Island assemblage, 'unit B' of the Hayes River group of the Oxford Lake–Knee Lake belt (Figure 27b, c) and the Pipestone Lake group of the Cross Lake belt (Figure 27d). The normalized profiles of the mesocratic mafic gneiss are characterized by more prominent negative anomalies at Zr and Ti, which makes them more similar to the mafic rocks of the Gunpoint group of the Cross Lake belt (Figure 27e). The mafic tuff/sandstone and garnet-bearing mafic gneiss are the most enriched variet-

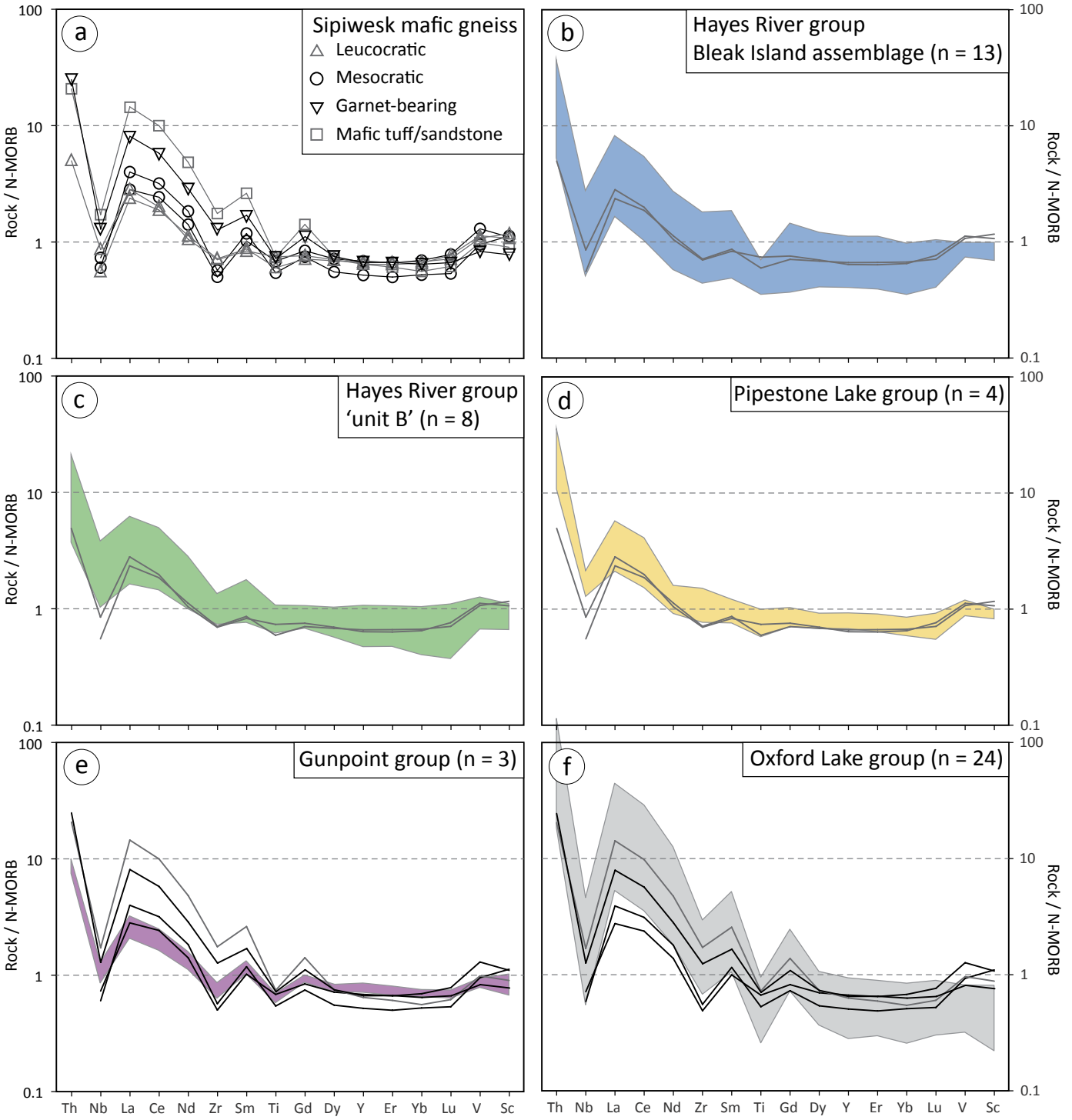

Figure 27: *N-MORB–normalized multi-element profiles comparing the mafic gneiss suite and mafic volcanic rocks from the Oxford Lake–Knee Lake and Cross Lake belts. Normalizing values for N-MORB from Sun and McDonough (1989).*

ies of mafic gneiss and have normalized trace-element profiles similar to those of Oxford Lake group rocks from the Oxford Lake–Knee Lake belt (Figure 27f).

Shoshonitic gneiss suite

Local exposures of the intermediate shoshonitic gneiss are well layered and can appear similar to the leucocratic mafic gneiss. The intermediate shoshonite can also be found interlayered with the mesocratic mafic gneiss. This could indicate that at least some occurrences of the shoshonitic gneiss are derived from volcanic rocks. The geochemistry of the suite suggests a shoshonitic affinity (Figure 13a, Figure 28a). Shoshonitic rocks are present in both the Oxford Lake and Cross Lake groups. Discrimination plots and normalized trace-element profiles of the shoshonitic gneiss are similar to those of the Oxford Lake shoshonites, which are more enriched than the Cross Lake shoshonitic rocks (Figure 28). Two shoshonite samples from Oxford Lake yielded initial ε_{Nd} values of +0.2 and +0.3

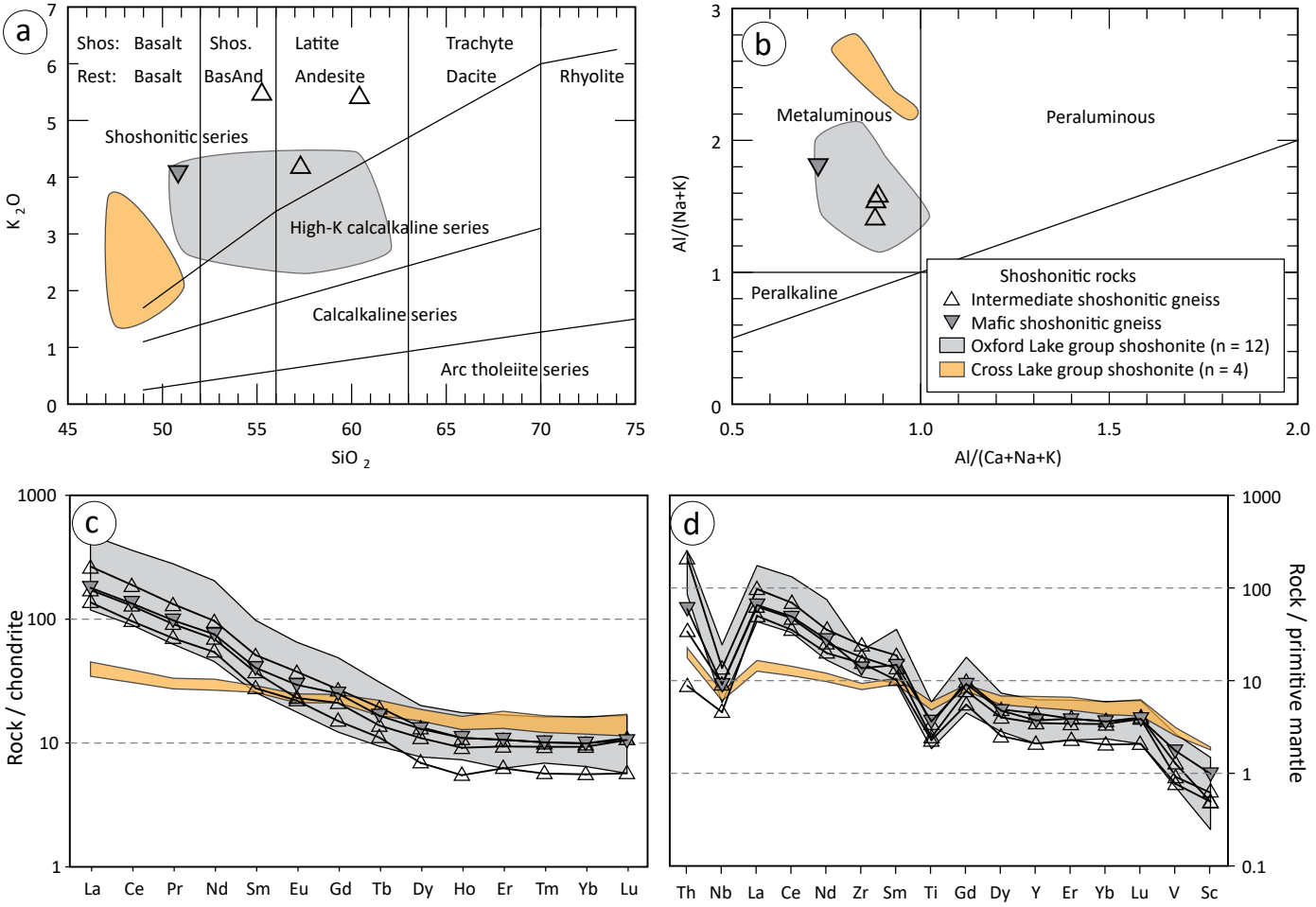

Figure 28: *Geochemical diagrams comparing the shoshonitic gneiss suite with shoshonitic rocks of the Oxford Lake–Knee Lake and Cross Lake belts:* ***a)*** *K_2O–SiO_2 diagram of Peccerillo and Taylor (1976);* ***b)*** *alumina saturation–index diagram of Maniar and Piccoli (1989);* ***c)*** *chondrite-normalized rare-earth–element profiles;* ***d)*** *primitive mantle–normalized multi-element profiles. Normalizing values for chondrite and primitive mantle from McDonough and Sun (1995). Abbreviations: BasAnd, Basaltic andesite; Shos., Shoshonite.*

(calculated at 2720 Ma; Anderson and Martins, 2019b). These are similar to the initial ε_{Nd} value of +0.1 obtained for the mafic shoshonitic gneiss.

Geochronology

Detrital zircon recovered from sedimentary rocks associated with the Hayes River and Oxford Lake groups commonly yields unimodal populations that mirror their largely volcanogenic source (ca. 2.83 and ca. 2.72 Ga, respectively; Corkery et al., 2000; Anderson, unpublished data, 2012). Conversely, detrital zircon recovered from the synorogenic deposits and the Cross Lake group commonly yields complex age-population distributions that include rare Paleoarchean zircon, which reflects multiple sources of detritus and marks the cratonization of the northwestern Superior province (Corkery et al., 1992, 2000; Skulski et al., 2000; Böhm, unpublished data, 2008; Syme, unpublished data, 2008; Anderson, 2016b, unpublished data, 2012).

Detrital zircon from both arkosic wacke sample 97-12-055 and mudstone–wacke sample 108-12-1146A yielded polymodal age distributions, with populations similar to those of the synorogenic deposits and Cross Lake group (Figure 29). In addition, rare Paleoarchean zircon has been recovered from these younger sequences (Corkery et al., 1992, 2000), just as a Paleoarchean zircon was recovered from arkosic wacke 108-12-1146A. It is noted that one greywacke sample from Cross Lake, tentatively identified as Gunpoint group (36-05-05-1H), yielded more complex detrital populations and included a Paleoarchean zircon (Corkery, unpublished data, 2005). The Gunpoint group sample contains detrital-zircon populations similar to that of the arkosic-wacke sample from Sipiwesk Lake (97-12-055).

Granitoid intrusions associated with the Oxford Lake–Knee Lake belt can be subdivided into four broad groups: pre–Hayes River group (ca. 2880–2845 Ma); post–Hayes River group, pre–Oxford Lake group (ca. 2815–2780 Ma); syn–Oxford Lake group (ca. 2735–2705 Ma); and post–Oxford Lake group (ca. 2670 Ma; Anderson, 2017b). The post–Hayes River group pre–Oxford Lake group intrusions were traditionally grouped into the Bayly Lake complex. The Sipiwesk Lake gneissic trondhjemite (108-12-1183) is of a similar age at ca. 2784 Ma.

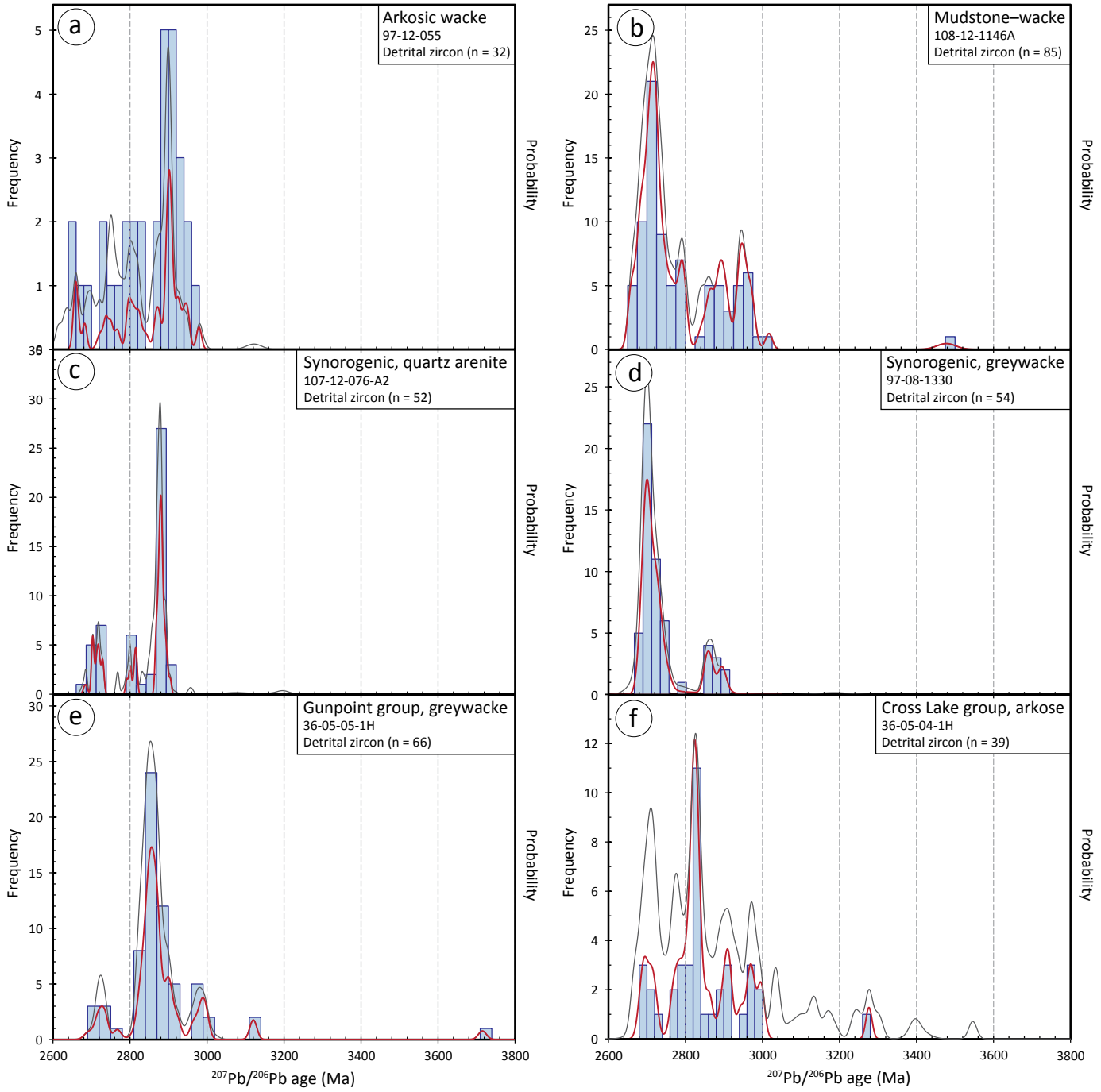

Figure 29: *Combined frequency histogram and probability-density–distribution (PDD) curve diagrams for detrital zircon from Sipiwesk Lake siliciclastic rocks* ***(a, b)*** *and selected siliciclastic rocks from the Oxford Lake–Knee Lake belt* ***(c, d)*** *and Cross Lake belt* ***(e, f)****. Data for Oxford Lake–Knee Lake belt samples from Syme et al. (unpublished data, 2008) and Anderson et al. (unpublished data, 2012); data for Cross Lake belt samples from Corkery (unpublished data, 2005). Grey PDD curves indicate all $^{207}Pb/^{206}Pb$ zircon data from a sample, and red PDD curves indicate data within ±5% of concordia.*

Synthesis of unit correlations and tectonostratigraphic implications

The lithogeochemistry of the leucocratic mafic gneiss suggests an affinity with the Hayes River and Pipestone Lake groups, whereas the mesocratic mafic gneiss is geochemically more similar to the Oxford Lake and Gunpoint groups. The lithogeochemistry of the shoshonitic gneiss is indistinguishable from shoshonitic rocks of the Oxford Lake group. The interbanding of the mafic gneiss suite and locally the shoshonitic gneiss suite suggests either contemporaneous emplacement or tectonic interleaving on a small scale. Therefore the mafic gneiss suite and shoshonitic gneiss suite are part of a single assemblage with Oxford Lake group affinities or consist of Oxford Lake group–like rocks tectonically interleaved with rocks that resemble the Hayes River group and Pipestone Lake group. Complex tectonic interleaving of Hayes River group and Oxford Lake group rocks occurs in central and southern Knee Lake, suggesting the latter is possible (Anderson, 2017a);

however, the interbanding of the mafic gneiss suite occurs at a much smaller scale (centimetres to metres), which would require considerable attenuation. The preferred interpretation is that the mafic gneiss suite and shoshonitic gneiss suite represent a single assemblage with affinity to the Oxford Lake group, but the alternative remains viable. Both the Hayes River group and the Oxford Lake and Gunpoint groups include felsic volcanic rocks, which were not recognized in the Sipiwesk Lake area. It is therefore quite likely that felsic volcanic rocks are present but have been misidentified as either felsic intrusive rocks or arkosic rocks. Complex detrital-zircon distributions of the siliciclastic rocks are similar to those of sedimentary rocks of the Cross Lake group and Oxford Lake–Knee Lake belt synorogenic deposits. If the siliciclastic rocks are correlative with these sequences and the mafic and shoshonitic gneiss suites are correlative with the Oxford Lake group, it implies an unconformable relationship between the volcanic and sedimentary packages at Sipiwesk Lake. This unconformable relationship is no longer apparent because of high-grade metamorphism and deformation.

Only one U-Pb zircon age was obtained for the gneissic tonalite suite, from a sample of gneissic trondhjemite (ca. 2784 Ma). This age is considered, as mentioned above, to be post Hayes River group and pre Oxford Lake group. This implies the gneissic tonalite suite could represent the basement upon which the mafic and shoshonitic gneiss suites and the siliciclastic rocks were deposited. Alternatively, the gneissic tonalite suite could be in faulted contact with the younger rocks. It should be noted that the gneissic tonalite suite is the most voluminous unit in the central Sipiwesk Lake area and additional sampling would likely result in a range of magmatic ages.

Whole-rock Sm-Nd isotope geochemistry suggests that the PGD transects the boundary between the Hudson Bay and North Caribou terranes (Couëslan, 2014a, 2016a). The PGD is also characterized by a prolonged period of metamorphism and a clockwise pressure-temperature-time path, both indicative of collisional orogenic zones. This suggests that the PGD represents an orogenic zone that postdates the accretion of the Hudson Bay and North Caribou terranes, and marks a collision between the northwestern Superior province and an unidentified cratonic mass (Couëslan, 2016a). The oldest period of metamorphic zircon growth reported for the PGD is ca. 2715 Ma (Heaman et al., 2011). Metamorphism in the PGD therefore overlaps the interpreted timing of synorogenic deposition in the Oxford Lake–Knee Lake belt and Cross Lake belt (i.e., less than ca. 2710 Ma; Corkery et al, 1992, 2000). The synorogenic deposits are interpreted to be derived from the eroding highlands that mark the collision of the Hudson Bay and North Caribou terranes; however, it is also possible that the deposits were being fed by detritus from an emerging Pikwitonei orogenic belt. This is underscored by the dominant zircon population of ca. 2711 Ma in mudstone–wacke sample 108-12-1146A, which may represent a continuum of zircon ages ranging from ca. 2766 Ma detrital zircon to ca. 2656 Ma metamorphic zircon.

Possible protolith of the gneissic rocks of unusual bulk composition

Al-Mg gneiss suite

The extreme enrichment of Mg and Al and depletion of alkalis in this unit limits the potential protoliths for this rock. Two possible protoliths are high-Mg mudstones, like those associated with evaporitic deposits (Reinhardt, 1987; Kadir et al., 2016), or hydrothermally altered rocks, such as those found associated with volcanogenic massive sulphide (VMS) deposits. Chondrite- and primitive mantle–normalized element profiles of the Al-Mg gneiss suite are broadly more similar to the metasedimentary rocks than rocks of the mafic gneiss suite. This could suggest a sedimentary origin for the Al-Mg gneiss suite. In addition, U-Pb dating of zircon from a sample of Al-Mg gneiss by Heaman et al. (2011; TK84-13) yielded a complex age-probability distribution, which could be interpreted as a detrital signature.

Mudstones associated with evaporitic sequences are rich in Mg and poor in alkalis. Metamorphosed equivalents of these rocks can form cordierite-orthoamphibole assemblages similar to rocks associated with VMS deposits (Reinhardt, 1987). Plotting cordierite-orthoamphibole rocks on an AFM diagram reveals that VMS-related rocks typically have intermediate FeO/MgO ratios, whereas Mg-rich evaporitic mudstones plot toward the MgO side of the diagram (Figure 30a; Reinhardt, 1987). The Sipiwesk Al-Mg gneiss suite plots within the field of evaporitic mudstones on the AFM diagram; however, evaporitic mudstone compositions from Reinhardt (1987) and claystones from a saline-lacustrine environment from Kadir et al. (2016) plot as typical fine-grained clastic rocks on the Ni vs. Zr/TiO_2 diagram (Figure 30b). This contrasts with the Al-Mg gneiss suite, which plots in the field of psammitic and felsic igneous rocks. In addition, evaporite deposits are typically associated with abundant carbonate rocks. To date, calcareous rocks have not been found in association with the Al-Mg gneiss suite.

Chlorite-rich rocks associated with VMS deposits in the Kristineberg area of Sweden (Hannington et al., 2003; Barrett et al., 2005) commonly plot within the evaporitic mudstone field of the AFM diagram, suggesting that the FeO/MgO ratio is not diagnostic (Figure 30a). Therefore, the Al-Mg gneiss suite could be derived from rocks that underwent seafloor-style hydrothermal alteration. Chlorite-rich rocks associated with VMS systems are characterized by high ASI values and may be enriched in Mg. Alteration indices calculated with NORMAT (Piché and Jébrak, 2004) suggest intense alteration of the rocks (IFRAIS = 0–36) and dominantly chlorite alteration for most of the samples (ICHLO = 46–96; Table 2; Appendix 1, Table 16). Although seafloor-style alteration usually affects volcanic rocks, the normalized element profiles of the Al-Mg gneiss suite do not coincide with those of the mafic gneiss suite. In

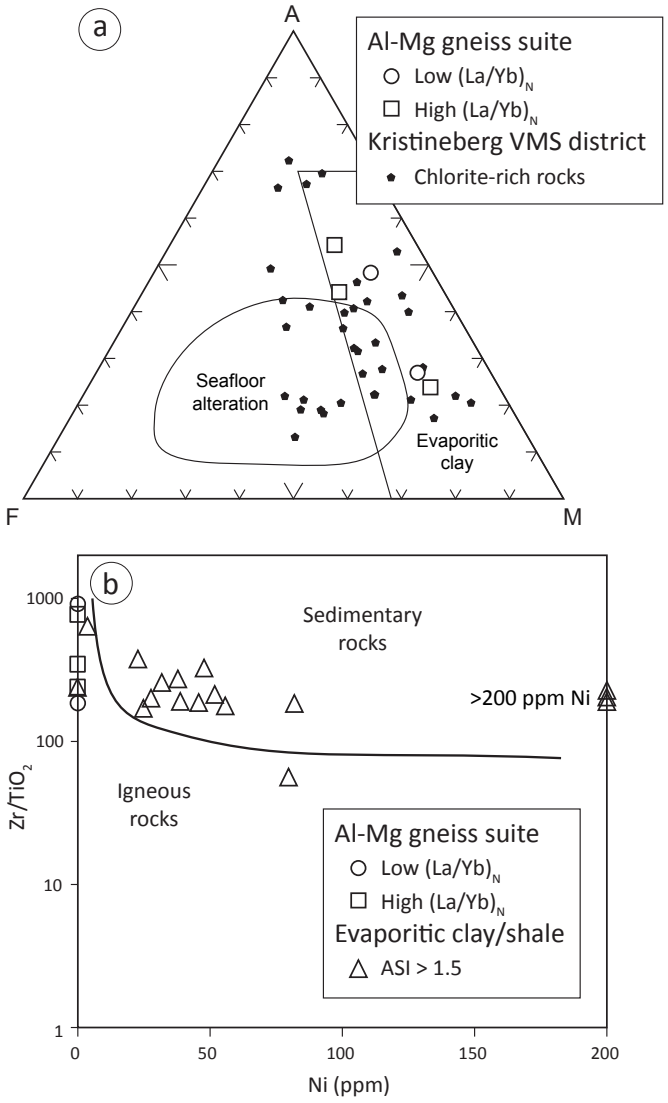

Figure 30: *Geochemical diagrams for Al- and Mg-rich rocks:* ***a)*** *AFM diagram of Reinhardt (1987) projected from biotite and plagioclase ($A = Al_2O_3 – [CaO + Na_2O + K_2O]$; $F = FeO – 6 \times [1 – Mg\#] \times K_2O$; $M = MgO – 6 \times Mg\# \times K_2O$);* ***b)*** *$Zr/TiO_2$–Ni diagram of Couëslan (2018; modified after Winchester et al., 1980). Data for Kristineberg district rocks from Hannington et al. (2003) and Barrett et al. (2005); data for evaporitic clay/shale from Reinhardt (1987) and Kadir et al. (2016).*

addition, negative anomalies at Sc and V, and no detectable Cr, would argue against a mafic precursor.

Chromium is typically considered to be immobile, even within water-dominated systems, and the low concentration of Cr in these rocks could indicate an intermediate or felsic volcanic precursor. Felsic volcanic rocks have not been recognized in the Sipiwesk Lake area; however, differentiating between felsic volcanic rocks and arkosic sedimentary and felsic intrusive rocks can be exceedingly difficult in granulite-facies rocks. Mafic and felsic volcanic rocks occur in both the Hayes River and Oxford Lake groups of the adjacent Superior province (Anderson et al., 2013; Anderson, 2017b) and VMS-related hydrothermal alteration is recognized at Oxford and Utik lakes (Böhm et al., 2007; Anderson et al., 2012). If the Al-Mg gneiss suite is derived from hydrothermally altered felsic rocks, a possible least-altered equivalent could be the spatially associated arkosic arenite (sample 108-12-1079B). The trace-element profiles for this arenite sample are distinctly different from the other arenite (97-12-020; Figure 14d, e), and similarities exist between 108-12-1079B and some members of the Al-Mg gneiss suite (Figure 15c, e). Additional sampling of arkosic arenite and Al-Mg gneiss suite rocks would be required to further evaluate this possibility.

It is possible that the trace-element geochemistry of the Al-Mg gneiss suite has been significantly modified. A number of studies have reported variable mobility of Ni, Cr, Nb, Y, LREE, Eu and Th in strongly altered rocks associated with VMS deposits (Finlow-Bates and Stumpfl, 1981; Jenner, 1996; Gemmell and Fulton, 2001; Hollings and Wyman, 2005). Microtextures (such as melt pseudomorphs; Holness and Sawyer, 2008; Holness et al., 2011) in the rocks provide evidence for the former presence of melt. The formation and loss of one or more generations of partial melt could result in a residuum depleted in LILE (including Th and LREE) and enriched in high-field-strength elements (HFSE). This could partly explain the compositional variability within the gneiss suite. The protolith of the high Al-Mg gneiss suite remains enigmatic. It is tentatively identified as a product of intense hydrothermal alteration; however, its precursor remains unidentified.

Al-Ca gneiss suite

The abundances of CaO, Al_2O_3 and SiO_2 in rocks of the Al-Ca gneiss suite could indicate that they were derived from the decarbonation of marl; however, low concentrations of MgO, Na_2O and K_2O are unusual for typical marl. The major-element geochemistry and mineralogy of rocks of the Al-Ca gneiss suite is broadly similar to anorthositic gabbro; however, anorthositic gabbro and gabbro samples collected from both Duck Lake and Cauchon Lake elsewhere in the PGD contain higher concentrations of Na_2O (>1.16 wt. %), Cr (>80 ppm) and MgO (>2.59 wt. %), and have significantly higher Mg# values (>0.54) than the Al-Ca gneiss suite (Couëslan, unpublished data, 2013, 2016). Rare-earth–element and trace-element profiles of the Al-Ca gneiss suite are more enriched than typical gabbro.

Rocks of the Al-Ca gneiss suite are spatially associated with discontinuous bands of mafic gneiss characterized by a distinct MORB-like trace-element signature (108-15-1202; Figure 12d). The REE and trace-element profiles of the Al-Ca gneiss suite are suggestive of an arc affinity, distinctly different from the associated mafic rocks. However, the profiles of the Al-Ca suite are similar to the majority of mafic gneiss at Sipiwesk Lake and could imply a possible co-genetic relationship (Figure 31a, b). The rocks of the Al-Ca gneiss suite are more enriched in Th, Nb, LREE and Zr, and depleted in Ti, V and Sc compared to the mafic gneiss suite, suggesting they could be derived from an intermediate to felsic protolith. This is supported by low Cr values

Table 2: Normative mineral–alteration indices calculated for selected units from the central Sipiwesk Lake area using the NORMAT method (Piché and Jébrak, 2004).

Sample	Unit/rock type	IFRAIS[1]	IPARA[2]	ISER[3]	ICHLO[4]	IPYRO[5]
	Al-Mg gneiss suite					
108-12-1079A1	Al-Mg gneiss	0	1.4	2.0	90.7	6.0
108-12-1079C	Al-Mg gneiss	0.2	8.8	15.0	48.4	27.6
108-12-1080A	Al-Mg gneiss	0	1.1	1.7	96.6	0.7
108-12-1084A	Al-Mg gneiss	8.0	31.2	14.1	46.1	0.7
108-12-1084B	Al-Mg gneiss	36.3	39.2	24.5	0	0
	Mafic gneiss suite					
108-12-1038	Leuco mafic gneiss	100.0	0	0	0	0
108-12-1111C	Leuco mafic gneiss	100.0	0	0	0	0
108-12-1023A	Leuco mafic gneiss	100.0	0	0	0	0
108-12-1055	Meso mafic gneiss	100.0	0	0	0	0
108-12-1099A	Meso mafic gneiss	100.0	0	0	0	0
108-15-1202	Meso mafic gneiss	100.0	0	0	0	0
108-12-1111D	Mafic gneiss, Grt-bearing	100.0	0	0	0	0
108-12-1146B	Mafic sand/tuff	100.0	0	0	0	0
108-12-1058	Ultramafic gneiss	100.0	0	0	0	0
	Siliciclastic rocks					
108-12-1064C	Mudstone	18.5	27.3	54.2	0	0
108-12-1146A	Mudstone	56.7	23.0	20.3	0	0
97-12-020A01	Arkosic arenite	91.1	7.2	1.7	0	0
108-12-1079B	Arkosic arenite	75.8	19.0	5.2	0	0
97-12-055	Arkosic wacke	80.2	16.1	3.6	0	0
108-12-1036	Arkosic wacke	71.6	21.7	6.7	0	0
	Al-Ca gneiss suite					
108-12-1076	Al-Ca gneiss, Qtz-rich	100.0	0	0	0	0
108-12-1202A	Al-Ca gneiss, Qtz-poor	100.0	0	0	0	0
108-12-1202B	Al-Ca gneiss, Qtz-poor	100.0	0	0	0	0
	Mafic-ultramafic dikes					
108-12-1014	Diabase	100.0	0	0	0	0
108-12-1032	Diabase	100.0	0	0	0	0
108-12-1019	Gabbro	100.0	0	0	0	0
108-12-1073	Gabbro	100.0	0	0	0	0
108-12-1118	Peridotite	100.0	0	0	0	0

[1] Index of alkali-element depletion; lower numbers indicate increase intensity of depletion (alteration)
[2] Index of paragonitization; higher numbers indicate increasing intensity
[3] Index of sericitization; higher numbers indicate increasing intensity
[4] Index of chloritization; higher numbers indicate increasing intensity
[5] Index of pyrophyllitization; higher numbers indicate increasing intensity
Abbreviations: Grt, garnet; Leuco, leucocratic; Meso, mesocratic; Qtz, quartz.

and plotting of the Al-Ca gneiss suite in the andesite to dacite fields on the Zr/Ti–Nb/Y diagram of Pearce (1996; Figure 31c).

The Al-Ca gneiss suite could represent intensely carbonate-altered volcanic rocks that were completely decarbonized during high-grade metamorphism. The low MgO and Mg# values would imply that carbonate minerals were dominated by calcite±siderite, and relatively high Al_2O_3 concentrations would suggest the presence of an aluminous phase such as Fe-chlorite or pyrophyllite. If sericite was present, the low concentrations of Na_2O and K_2O suggest these elements must have been removed by the CO_2-rich fluid during decarbonization. It is also possible that a CO_2-rich fluid could have been oxidizing and resulted in the relatively high $Fe^{3+}/(Fe^{3+}+Fe^{2+})$ ratio of this rock.

Alternatively, the Al-Ca gneiss could be the result of intense epidotization of a volcanic protolith. Epidosites are typically depleted in Na^+, K^+ and Mg^{2+}, while being enriched in Ca^{2+}, Al^{3+} and Fe^{3+} (Galley, 1993). NORMAT (Piché and Jébrak, 2004) was used to calculate normative mineral assemblages for this unit and yielded major rock-forming–mineral assemblages of 6–7% albite, 6–7% actinolite, 12–33% quartz and

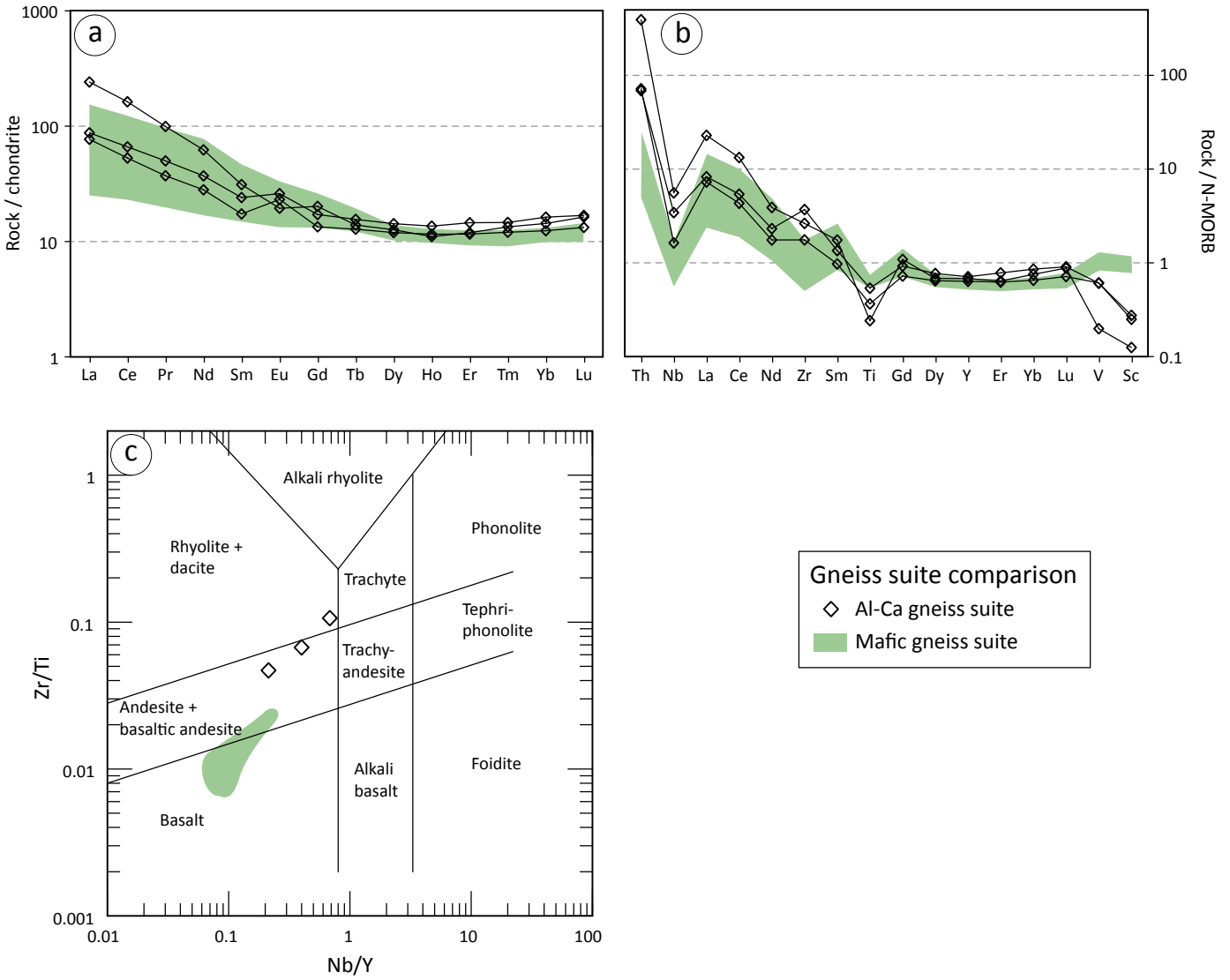

Figure 31: *Geochemical diagrams comparing the mafic gneiss suite and Al-Ca gneiss suite:* ***a)*** *chondrite-normalized rare-earth–element profiles;* ***b)*** *N-MORB–normalized multi-element profiles;* ***c)*** *Zr/Ti–Nb/Y diagram of Pearce (1996). Normalizing values for chondrite from McDonough and Sun (1995) and N-MORB values from Sun and McDonough (1989).*

51–69% epidote (Table 3; Appendix 1, Table 16). Similar results were obtained using the Theriak phase-equilibrium modelling software of de Capitani and Petrakakis (2010) in the system Na_2O-CaO-K_2O-FeO-MgO-Al_2O_3-SiO_2-H_2O-TiO_2-Fe_2O_3 (NCKF-MASHTO). Mineral assemblages were calculated using the bulk compositions of samples 108-12-1202A and B at conditions of 400°C and 1 kbar in a water-oversaturated system. These conditions are similar to those proposed for epidotization associated with VMS systems (Galley, 1993). Samples 108-12-1202A and B are projected to contain 0.4–0.5% microcline, 1.0–1.5% titanite, 1.9–7.9% grossular, 6.8–7.0% albite, 8.0–8.7% actinolite, 14.1–14.9% quartz and 60.9–66.6% epidote. This interpretation would not require the complete decarbonization of the rock during metamorphism and it could explain the high Fe^{3+}/(Fe^{3+}+Fe^{2+}) ratio of the rock. Intense epidotization of a volcanic protolith with the above composition is therefore the preferred interpretation for this unit.

Economic considerations

Rocks underlying the central Sipiwesk Lake area appear to be continuous with rocks from the adjacent Oxford-Stull domain. Therefore, there is notional potential for any of the deposit types associated with greenstone belts in the Oxford-Stull domain, including lode Au (God's Lake, Knee Lake, Monument Bay), volcanogenic massive sulphide (VMS; Oxford Lake) and anorthosite-related Fe-Ti (Pipestone Lake). Most significant may be the Al-Mg gneiss suite of Sipiwesk Lake and its potential derivation from VMS-related hydrothermal alteration. Intense alkali-depleted and Mg- and Al-enriched alteration is typically found in close association with ore zones in VMS systems. The Al-Mg gneiss suite may therefore have formed relatively close to VMS mineralization. In addition, volcanogenic hydrothermal alteration is spatially associated with Au-bearing cherts at Utik Lake (Bernier and MacLean, 1989; Böhm et al., 2007). However, high strain and high-grade metamorphism may lower the

Table 3: Normative mineral–alteration indices and equilibrium phase assemblages calculated for rocks of the Al-Ca gneiss suite using the NORMAT method of Piché and Jébrak (2004) and Theriak software of de Capitani and Petrakakis (2010), respectively.

Sample	108-12-1076[1]	108-12-1202A	108-12-1202B
NORMAT			
Actinolite	5.00	13.51	13.46
Albite	6.33	6.35	6.59
Apatite	0.17	0.28	0.41
Calcite	0.00	1.83	0.58
Chlorite	1.66	0.00	0.00
Chromite	0.00	0.00	0.00
Epidote	51.10	64.70	66.35
K-feldspar	1.29	0.43	0.37
Pyrophyllite	0.02	0.00	0.00
Quartz	33.04	10.73	9.71
Titanite	0.66	1.01	1.47
Tremolite	0.72	1.16	1.07
Total	**100.00**	**100.00**	**100.00**
Theriak[2]			
Actinolite	N/A	8.34	8.79
Albite	N/A	6.75	6.96
Apatite	N/A	0.31	0.45
Epidote	N/A	61.40	66.48
Grossular	N/A	6.91	1.29
K-feldspar	N/A	0.52	0.44
Quartz	N/A	14.76	14.10
Titanite	N/A	1.03	1.50
Total		**100.00**	**100.00**

[1] 108-12-1076 was not analyzed for ferric iron and therefore not included in modelling with Theriak.
[2] Modelled in the chemical system NCKFMASHTO. Activities models used are listed in the 'Phase equilibrium modelling' subsection of the 'Discussion', and also includes the magnetite-spinel and ilmenite-hematite models of White et al. (2000).

preservation potential of economic ore deposits in the central Sipiwesk Lake area. Although mineral exploration in high-grade metamorphic terranes can be a daunting task, a number of world-class mineral deposits are hosted in granulite-facies rocks, most notably in Australia with the Broken Hill Pb-Zn and Challenger Au deposits (Tomkins and Mavrogenes, 2002; Frost et al., 2005, 2011; McFarlane et al., 2007). In Canada, the Werner Lake Co-Cu-Au deposit from the English River subprovince is believed to be an exhalitive-related deposit that was subjected to granulite-facies metamorphic conditions (Pan and Therens, 2000). Studies have also suggested that high-grade metamorphism may be responsible for the localized concentration of metals (upgrading) in these and other deposits (Pan and Therens, 2000; Tomkins and Mavrogenes, 2002; Tomkins et al., 2007; Frost et al., 2011).

Lode or orogenic Au mineralization in the Oxford-Stull and Island Lake domains is typically cited to occur ca. 2.7 Ga. The mineralizing systems are typically attributed to magmatic and/or metamorphic fluids moving along crustal-scale structures that were activated during docking of the Hudson Bay terrane with the North Caribou terrane. Evidence suggests that the PGD postdates and overprints this suture. Therefore, it is possible that Au mineralization occurred prior to the high-grade metamorphism and could be preserved. A number of small horizons of sulphidic iron formation are preserved in the Sipiwesk Lake area; however, none of the analyzed samples contained more than 17 ppb Au (Appendix 1, Table 2). In addition, no zones were identified as overprinted crustal-scale structures.

The Twin Lakes Au-W deposit of northeastern Manitoba occurs along the boundary between the Oxford-Stull and Island Lake domains. Crosscutting relationships at the Twin Lakes deposit constrain the timing of mineralization to between ca. 2706 Ma and ca. 2696 Ma (St. Pierre, unpublished presentation, 2014). This roughly corresponds to the onset of high-grade metamorphism in the PGD (Mezger et al., 1989; Heaman et al., 2011). Mineralization at the Musselwhite mine in northwestern Ontario was dated at ca. 2690 Ma and ca. 2665 Ma (Biczok et al., 2012; Oswald et al., 2015). Mineralization at the High Rock Island Au deposit at Island Lake, Manitoba yielded very similar ages of ca. 2687 Ma and ca. 2658 Ma (Lin and Corfu, 2002). Both of these deposits occur along the boundary between the Island Lake domain and the core of the North Caribou terrane. The timing of mineralization at Musselwhite and High Rock Island corresponds to high-grade, possibly peak metamorphism and the onset of high-temperature decompression and cooling in the PGD. Evidence suggests that the PGD represents the core of a collisional orogen. An orogen of this scale would have activated crustal-scale structures a significant distance from the core region. It is therefore quite possible that the 'Pikwitonei orogen' could have been the driving force behind at least some of the Au mineralization in the northwestern Superior province, providing both metamorphic fluids and activating pathways for fluid flow and mineralization.

The presence of ultramafic dikes related to the Molson swarm suggests a notional potential for magmatic Ni-Cu-Co-PGE in the Sipiwesk Lake area. Dikes of this swarm are believed to have been feeders to the magmatic Ni-Cu systems of the Thompson Nickel belt and Fox River sill of the Superior boundary zone (Heaman et al., 1986, 2009). Mineralization is also reported from an ultramafic dike of the Molson swarm at Cuthbert Lake (Dawson, 1952; Peck et al., 1999).

Acknowledgments

The author thanks C. Böhm and T. Martins for discussions and their contributions documenting and mapping the geology of central Sipiwesk Lake, B. Bertholet for her enthusiastic and highly capable assistance in the field, and N. Brandson and E. Anderson for logistical support. Thanks go to S. Anderson for insightful discussions on Superior province geology, P. Lenton and H. Adediran for drafting of the geological map, and J. Halcrow, J. McKay, G. Spence and the other members of the Mani-

toba Hydro boat patrol and work crew for their hospitality at the Ross Bay camp.

References

Aleinikoff, J.N., Schenck, W.S., Plank, M.O., Srogi, L., Fanning, C.M., Kamo, S.L. and Bosbyshell, H. 2006: Deciphering igneous and metamorphic events in high-grade rocks of the Wilmington Complex, Delaware: morphology, cathodoluminescence and backscattered electron zoning, and SHRIMP U-Pb geochronology of zircon and monazite; Geological Society of America Bulletin, v. 118, p. 39–64.

Anderson, S.D. 2016a: Alkaline rocks at Oxford Lake and Knee Lake, northwestern Superior province, Manitoba (NTS 53L13, 14, 15): preliminary results of new bedrock mapping and lithogeochemistry; *in* Report of Activities 2016, Manitoba Growth, Enterprise and Trade, Manitoba Geological Survey, p. 16–27, URL <https://www.manitoba.ca/iem/geo/field/roa16pdfs/GS-1.pdf> [May 2021].

Anderson, S.D. 2016b: Preliminary results of bedrock mapping at central Knee Lake, northwestern Superior province, Manitoba (NTS 53L15, 53M2); *in* Report of Activities 2016, Manitoba Growth, Enterprise and Trade, Manitoba Geological Survey, p. 1–15, URL <https://www.manitoba.ca/iem/geo/field/roa16pdfs/GS-2.pdf> [May 2021].

Anderson, S.D. 2017a: Detailed stratigraphic and structural mapping of the Oxford Lake–Knee Lake greenstone belt at southern and central Knee Lake, Manitoba (parts of NTS 53L15, 53M2); *in* Report of Activities 2017, Manitoba Growth, Enterprise and Trade, Manitoba Geological Survey, p. 1–11, URL <https://www.manitoba.ca/iem/geo/field/roa17pdfs/GS2017-1.pdf> [May 2021].

Anderson, S.D. 2017b: Preliminary geology of the diamond occurrence at southern Knee Lake, Oxford Lake–Knee Lake greenstone belt, Manitoba (NTS 53L15); Manitoba Growth, Enterprise and Trade, Manitoba Geological Survey, Open File OF2017-3, 27 p, URL <https://www.manitoba.ca/iem/info/libmin/OF2017-3.zip> [May 2021].

Anderson, S. and Martins, T. 2019a: Whole rock geochemistry compilation of the Oxford Lake–Knee Lake greenstone belt, northwestern Superior Province, Manitoba (parts of NTS 53L6, 12–15, 53M2, 63I9, 16); Manitoba Agriculture and Resource Development, Manitoba Geological Survey, Data Repository Item DRI2019007, Microsoft® Excel® file, URL <https://www.manitoba.ca/iem/info/libmin/DRI2019007.xlsx> [May 2021].

Anderson, S. and Martins, T. 2019b: Compilation of Sm-Nd isotopes from the Oxford Lake–Knee Lake greenstone belt, northwestern Superior Province, Manitoba (parts of NTS 53L6, 12–15, 53M2, 63I9, 16); Manitoba Agriculture and Resource Development, Manitoba Geological Survey, Data Repository Item DRI2019008, Microsoft® Excel® file, URL <https://www.manitoba.ca/iem/info/libmin/DRI2019008.xlsx> [May 2021].

Anderson, S.D., Kremer, P.D. and Martins, T. 2012: Preliminary results of bedrock mapping at Oxford Lake, northwestern Superior province, Manitoba (NTS 53L12, 13, 63I9, 16); *in* Report of Activities 2012, Manitoba Innovation Energy and Mines, Manitoba Geological Survey, p. 6–22, URL <https://www.manitoba.ca/iem/geo/field/roa12pdfs/GS-1.pdf> [May 2021].

Anderson, S.D., Kremer, P.D. and Martins, T. 2013: Preliminary results of bedrock mapping at Oxford Lake, northwestern Superior province, Manitoba (NTS 53L13, 14); *in* Report of Activities 2013, Manitoba Mineral Resources, Manitoba Geological Survey, p. 7–22, URL <https://www.manitoba.ca/iem/geo/field/roa13pdfs/GS-1.pdf> [May 2021].

Arima, M. and Barnett, R.L. 1984: Sapphirine bearing granulites from the Sipiwesk Lake area of the late Archean Pikwitonei granulite terrain, Manitoba, Canada; Contributions to Mineralogy and Petrology, v. 88, p. 102–112.

Barrett, T.J., MacLean, W.H. and Årebäck, H. 2005: The Paleoproterozoic Kristineberg VMS deposit, Skellefte district, northern Sweden, part II: chemostratigraphy and alteration; Mineralium Deposita, v. 40, p. 368–395.

Bell, C.K. 1971: Boundary geology, Upper Nelson River area, Manitoba and northwestern Ontario; *in* Geoscience Studies in Manitoba, A.C. Turnock (ed.), Geological Association of Canada, Special Paper 9, p. 11–39.

Bell, C.K. 1978: Geology, Wekusko Lake map-area, Manitoba; Geological Survey of Canada, Memoir 384, 84 p. and 1 map at 1:250 000 scale and 3 maps at 1:500 000 scale.

Bell, R. 1879: Report on the country between Lake Winnipeg and Hudson's Bay; *in* Report of Progress for 1877–1878, Geological Survey of Canada, p. 1cc–31cc.

Bell, R. 1880: Report on explorations on the Churchill and Nelson rivers and around God's and Island lakes 1879; *in* Report of Progress for 1878–1879, Geological Survey of Canada, p. 1c–72c.

Bernier, L.R. and MacLean, W.C. 1989: Auriferous chert, banded iron formation, and related volcanogenic hydrothermal alteration, Atik Lake, Manitoba; Canadian Journal of Earth Sciences, v. 26, p. 2676–2690.

Biczok, J., Hollings, P., Klipfel, P., Heaman, L., Maas, R., Hamilton, M., Kamo, S. and Friedman, R. 2012: Geochronology of the North Caribou greenstone belt, Superior Province Canada: implications for tectonic history and gold mineralization at the Musselwhite mine; Precambrian Research, v. 192–195, p. 209–230.

Böhm, C.O., Heaman, L.M. and Corkery, M.T. 1999: Archean crustal evolution of the northwestern Superior Province margin: U-Pb zircon results from the Split Lake Block; Canadian Journal of Earth Sciences, v. 36, p. 1973–1987.

Böhm, C.O., Heaman, L.M., Creaser, R.A. and Corkery, M.T. 2000: Discovery of pre-3.5 Ga exotic crust at the northwestern Superior Province margin, Manitoba; Geology, v. 28, p. 75–78.

Böhm, C.O., Heaman, L.M., Stern, R.A., Corkery, M.T. and Creaser, R.A. 2003: Nature of Assean lake ancient crust, Manitoba: a combined SHRIMP–ID-TIMS U–Pb geochronology and Sm-Nd isotope study; Precambrian Research, v. 126, p. 55–94.

Böhm, C.O., Kremer, P.D. and Syme, E.C. 2007: Nature, evolution and gold potential of the Utik Lake greenstone belt, Manitoba (parts of NTS 53M4, 5, 63P1, 8): preliminary field results; *in* Report of Activities 2007, Manitoba Science, Technology, Energy and Mines, Manitoba Geological Survey, p. 98–113, URL <https://www.manitoba.ca/iem/geo/field/roa07pdfs/GS-10.pdf> [May 2021].

Böhm, C.O., Kremer, P.D., Syme, E.C. and Martins, T. 2021: Compilation of Sm-Nd isotope results from Utik Lake, Superior province, east-central Manitoba (parts of NTS 53M4, 5, 63P1, 8); Manitoba Agriculture and Resource Development, Manitoba Geological Survey, Data Repository Item DRI2021003, Microsoft® Excel® file, URL <https://www.manitoba.ca/iem/info/libmin/DRI2021003.xlsx> [May 2021].

Cabanis, B. and Lecolle, M. 1989: Le diagramme La/10–Y/15–Nb/8: un outil pour la discrimination des series volcaniques et la mise en evidence des processus de mélange et/ou de contamination crustale; Comptes Rendus de l'Academie des Sciences, v. 309, p. 2023–2029.

Corkery, M.T., Davis, D.W. and Lenton, P.G. 1992: Geochronological constraints on the development of the Cross Lake greenstone belt, northwestern Superior Province, Manitoba; Canadian Journal of Earth Sciences, v. 29, p. 2171–2185.

Corkery, T.M., Cameron, H.D.M., Lin, S., Skulski, T., Whalen, J.B. and Stern, R.A. 2000: Geological investigations in the Knee Lake belt (parts of NTS 53L); *in* Report of Activities 2000, Manitoba Industry, Trade and Mines, Manitoba Geological Survey, p. 129–136, URL <https://www.manitoba.ca/iem/geo/field/roa00pdfs/00gs-22.pdf> [May 2021].

Couëslan, C.G. 2013: Preliminary results from bedrock mapping in the Partridge Crop Lake area, eastern margin of the Thompson nickel belt, central Manitoba (parts of NTS 63P11, 12); *in* Report of Activities 2013, Manitoba Mineral Resources, Manitoba Geological Survey, p. 34–45, URL <https://www.manitoba.ca/iem/geo/field/roa13pdfs/GS-3.pdf> [May 2021].

Couëslan, C.G. 2014a: Mapping progress in the Pikwitonei granulite domain: tectonic and economic implications; Manitoba Mineral Resources, Manitoba Geological Survey, Manitoba Mining and Minerals Convention 2014, Winnipeg, Manitoba, November 19–21, 2014, oral presentation, URL <https://www.youtube.com/embed/1M-9_jHzjKs> [May 2021].

Couëslan, C.G. 2014b: Preliminary results from bedrock mapping in the Armstrong Lake area, Pikwitonei granulite domain, central Manitoba (parts of NTS 63P10, 11); *in* Report of Activities 2014, Manitoba Mineral Resources, Manitoba Geological Survey, p. 7–17, URL <https://www.manitoba.ca/iem/geo/field/roa14pdfs/GS-1.pdf> [May 2021].

Couëslan, C.G. 2014c: Preliminary results from bedrock mapping in the Partridge Crop Lake area, eastern margin of the Thompson nickel belt, central Manitoba (parts of NTS 63P11, 12) – Year 2; *in* Report of Activities 2014, Manitoba Mineral Resources, Manitoba Geological Survey, p. 18–31, URL <https://www.manitoba.ca/iem/geo/field/roa14pdfs/GS-2.pdf> [May 2021].

Couëslan, C.G. 2016a: The Pikwitonei granulite domain, Manitoba, a collisional orogenic zone along the northwestern margin of the Superior craton; Geological Association of Canada–Mineralogical Association of Canada, Joint Annual Meeting, Whitehorse, Yukon, June 1–3, 2016, abstract, URL <https://gac.ca/wp-content/uploads/2018/11/2016_GAC2016_AbstractVol.pdf> [May 2021].

Couëslan, C.G. 2016b: Preliminary results of bedrock mapping in the southeastern Duck Lake–Sesep Rapids area, Pikwitonei granulite domain, central Manitoba (part of NTS 63J16); *in* Report of Activities 2016, Manitoba Growth, Enterprise and Trade, Manitoba Geological Survey, p. 40–50, URL <https://www.manitoba.ca/iem/geo/field/roa16pdfs/GS-4.pdf> [May 2021].

Couëslan, C.G. 2018: Geology of the Tower Cu-Zn-Ag-Au deposit, sub-Phanerozoic Superior boundary zone, central Manitoba (part of NTS 63G14); Manitoba Growth, Enterprise and Trade, Manitoba Geological Survey, Open File OF2018-4, 38 p., URL <https://www.manitoba.ca/iem/info/libmin/OF2018-4.pdf> [May 2021].

Dawson, A.S. 1952: Geology of the Partridge Crop Lake area, Cross Lake Mining Division, Manitoba; Manitoba Department of Mines and Natural Resources, Mines Branch, Publication 41-1, 26 p. and 1 map at 1:126 720 scale.

de Capitani, C. and Brown, T.H. 1987: The computation of chemical equilibrium in complex systems containing non-ideal solutions; Geochimica et Cosmochimica Acta, v. 51, p. 2639–2652.

de Capitani, C. and Petrakakis, K. 2010: The computation of equilibrium assemblage diagrams with Theriak/Domino software; The American Mineralogist, v. 95, p. 1006–1016.

Diener, J.F.A., Powell, R., White, R.W. and Holland, T.J.B. 2007: A new thermodynamic model for clino- and orthoamphiboles in the system Na_2O–CaO–FeO–MgO–Al_2O_3–SiO_2–H_2O–O; Journal of Metamorphic Geology, v. 25, p. 631–656.

Ermanovics, I.F. and Davison, W.L. 1976: The Pikwitonei granulites in relation to the north-western Superior Province of the Canadian Shield; *in* The Early History of the Earth, B.F. Windley (ed.), John Wiley and Sons, London, p. 331–347.

Finlow-Bates, T. and Stumpfl, E.F. 1981: The behavior of so-called immobile elements in hydrothermally altered rocks associated with volcanogenic submarine-exhalative ore deposits; Mineralium Deposita, v. 16, p. 319–328.

Frost, B.R., Swapp, S.M. and Gregory, R.W. 2005: Prolonged existence of sulphide melt in the Broken Hill orebody, New South Wales, Australia; Canadian Mineralogist, v. 43, p. 479–493.

Frost, B.R., Swapp, S.M. and Mavrogenes, J. 2011: Textural evidence for extensive melting of the Broken Hill orebody; Economic Geology, v. 106, p. 869–882.

Galley, A.G. 1993: Characteristics of semi-conformable alteration zones associated with volcanogenic massive sulphide districts; Journal of Geochemical Exploration, v. 48, p. 175–200.

Gemmell, J.B. and Fulton, R. 2001: Geology, genesis, and exploration implications of the footwall and hanging-wall alteration associated with the Hellyer volcanic-hosted massive sulphide deposit, Tasmania, Australia; Economic Geology, v. 96, p. 1003–1035.

Goldstein, S.L., O'Nions, R.K. and Hamilton, P.J. 1984: Sm-Nd study of atmospheric dusts and particulates from major river systems; Earth and Planetary Science Letters, v. 70, p. 221–236.

Guevara, V.E. 2017: How hot, how deep, how long: constraints on the tectono-metamorphic evolution of granulite terranes; Ph.D. thesis, Virginia Polytechnic Institute and State University, Blacksburg, Virginia, 303 p.

Guevara, V.E., MacLennan, S.A., Dragovic, B., Caddick, M.J., Schoene, B., Kylander-Clark, A.K.C. and Couëslan, C.G. 2020a: Polyphase zircon growth during slow cooling from ultrahigh temperature: an example from the Archean Pikwitonei granulite domain; Journal of Petrology, v. 61, art. egaa021, URL <https://doi.org/10.1093/petrology/egaa021>.

Guevara, V.E., Dragovic, B., Caddick, M.J. and Couëslan, C.G. 2020b: Slow differentiation of continental crust in an Archean granulite terrane; Geological Society of America, Annual Meeting virtual event, October 26–30, 2020, Montréal, Quebec, oral presentation.

Halls, H.C. and Heaman, L.M. 2000: The paleomagnetic significance of new U–Pb age data from the Molson dyke swarm, Cauchon Lake area, Manitoba; Canadian Journal of Earth Sciences, v. 37, p. 957–966.

Hannington, M.D., Kjarsgaard, I.M., Galley, A.G. and Taylor, B. 2003: Mineral-chemical studies of metamorphosed hydrothermal alteration in the Kristineberg volcanogenic massive sulphide district, Sweden; Mineralium Deposita, v. 38, p. 423–442.

Harley, S.L. 1998: On the occurrence and characterization of ultrahigh-temperature crustal metamorphism; *in* What Drives Metamorphism and Metamorphic Reactions?, P.J. Treloar and P.J. O'Brien (ed.), Geological Society of London, Special Publications, v. 138, p. 81–107.

Harrison, J.M. 1951: Preliminary map, Sipiwesk, Manitoba; Geological Survey of Canada, Paper 51-3, 1 map at 1:253 440 scale.

Heaman, L.M., Machado, N., Krogh, T.E. and Weber, W. 1986: Precise U–Pb zircon ages for the Molson dyke swarm and the Fox River sill: constraints for Early Proterozoic crustal evolution in northeastern Manitoba, Canada; Contributions to Mineralogy and Petrology, v. 94, p. 82–89.

Heaman, L.M., Erdmer, P. and Owen, J.V. 2002: U-Pb geochronologic constraints on the crustal evolution of the Long Range Inlier, Newfoundland; Canadian Journal of Earth Sciences, v. 39, p. 845–865.

Heaman, L.M., Peck, D. and Toope, K. 2009: Timing and geochemistry of 1.88 Ga Molson Igneous Events, Manitoba: insights into the formation of a craton-scale magmatic and metallogenic province; Precambrian Research, v. 172, p. 143–162.

Heaman, L.M., Böhm, C.O., Machado, N., Krogh, T.E., Weber, W. and Corkery, M.T. 2011: The Pikwitonei Granulite Domain, Manitoba: a giant Neoarchean high-grade terrane in the northwest Superior Province; Canadian Journal of Earth Sciences, v. 48, p. 205–245.

Holland, T.J.B. and Powell, R. 1998: An internally-consistent thermodynamic dataset for phases of petrological interest; Journal of Metamorphic Geology, v. 16, p. 309–344.

Hollings, P. and Wyman, D. 2005: The geochemistry of trace elements in igneous systems: principles and examples from basaltic systems; *in* Rare-Element Geochemistry and Mineral Deposits, R.L. Linnen and I.M. Samson (ed.), Geological Association of Canada, GAC Short Course Notes 17, p. 1–16.

Holness, M.B. and Sawyer, E.W. 2008: On the pseudomorphing of melt-filled pores during the crystallization of migmatites; Journal of Petrology, v. 49, p. 1343–1363.

Holness, M.B., Cesare, B. and Sawyer, E.W. 2011: Melted rocks under the microscope: microstructures and their interpretation; Elements, v. 7, p. 247–252.

Hoskin, P.W.O. and Schaltegger, U. 2003: The composition of zircon and igneous and metamorphic petrogenesis; *in* Zircon, J.M. Hanchar and P.W.O. Hoskin (ed.), Mineralogical Society of America, Reviews in Mineralogy & Geochemistry, v. 53., p. 27–62.

Hubregtse, J.J.M.W. 1977: Sipiwesk Lake–Wintering Lake area (parts of NTS 63P3, 4E1/2, 5, 63J16N1/2); *in* Report of Field Activities 1977, Manitoba Energy and Mines, Mineral Resources Division, p. 73–79, URL <https://www.manitoba.ca/iem/geo/field/roa77.pdf> [May 2021].

Hubregtse, J.J.M.W. 1978: Sipiwesk Lake–Landing Lake–Wintering Lake area (parts of NTS 63P3, 4, 5, 6, 63J16 and 63I13 and 14); *in* Report of Field Activities 1978, Manitoba Department of Mines, Resources and Environmental Management, Mineral Resources Division, p. 54–62.

Hubregtse, J.J.M.W. 1980: The Archean Pikwitonei Granulite Domain and its position at the margin of the northwestern Superior Province; Manitoba Department of Energy and Mines, Mineral Resources Division, Geological Paper GP80-3, 16 p., URL <https://www.manitoba.ca/iem/info/libmin/GP80-3.pdf> [May 2021].

Hubregtse, J.J.M.W., Kusmirski, R.T. and Charbonneau, R. 1978a: Sipiwesk Lake; Manitoba Mines, Resources and Environmental Management, Mineral Resources Division, Preliminary Map 1978N-2, scale 1:50 000.

Hubregtse, J.J.M.W., Culshaw, N.G. and Kusmirski, R.T. 1978b: Duck Lake; Manitoba Mines, Resources and Environmental Management, Mineral Resources Division, Preliminary Map 1978N-5, scale 1:50 000.

Innes, M.J.S. 1960: Gravity and isostasy in northern Ontario and Manitoba; Canada Department of Mines and Technical Surveys, Dominion Observatories, Publication of the Dominion Observatory, v. 21, no. 6., 338 p.

Jenner, G.A. 1996: Trace element geochemistry of igneous rocks: geochemical nomenclature and analytical geochemistry; *in* Trace Element Geochemistry of Volcanic Rocks: Applications for Massive Sulphide Exploration, D.A. Wyman (ed.), Geological Association of Canada, GAC Short Course Notes, v. 12, p. 51–77.

Jensen, L.S. and Pyke, D.R. 1982: Komatiites in the Ontario portion of the Abitibi belt; *in* Komatiites, N.T. Arndt and E.G. Nisbet (ed.), George Allen & Unwin, London, United Kingdom, p. 147–157.

Kadir, S., Erkoyun, H., Eren, M., Huggett, J. and Önalgil, N. 2016: Mineralogy, geochemistry, and genesis of sepiolite and palygorskite in Neogene lacustrine sediments, Eskişehir Province, west central Anatolia, Turkey; Clays and Clay Minerals, v. 64, no. 2, p. 145–166.

Kelsey, D.E. 2008: On ultrahigh-temperature crustal metamorphism; Gondwana Research, v. 13, p. 1–29.

Kelsey, D.E. and Hand, M. 2015: On ultrahigh-temperature crustal metamorphism: phase equilibria, trace element thermometry, bulk composition, heat sources, timescales, and tectonic settings; Geoscience Frontiers, v. 6, p. 311–356.

Kelsey, D.E., White, R.W., Holland, T.J.B. and Powell, R. 2004: Calculated phase equilibria in K_2O-FeO-MgO-Al_2O_3-SiO_2-H_2O for sapphirine-quartz–bearing mineral assemblages; Journal of Metamorphic Geology, v. 22, p. 559–578.

Koblinger, B.M. and Pattison, D.R.M. 2017: Crystallization of heterogeneous pelitic migmatites: insights from thermodynamic modelling; Journal of Petrology, v. 58, p. 297–326.

Kooijman, E., Mezger, K. and Berndt, J. 2010: Constraints on the U-Pb systematics of metamorphic rutile from in situ LA-ICP-MS analysis; Earth and Planetary Science Letters, v. 293, p. 321–330.

Kooijman, E., Smit, M.A., Mezger, K. and Berndt, J. 2012: Trace element systematics in granulite facies rutile: implications for Zr geothermometry and provenance studies; Journal of Metamorphic Geology, v. 30, p. 397–412.

Krogh, T., Heaman, L., Machado, N., Davis, D. and Weber, W. 1986: U-Pb geochronology program: Pikwitonei-Thompson-Cross Lake area; *in* Report of Field Activities 1986, Manitoba Energy and Mines, Minerals Division, p. 178–180.

Kuiper, Y.D., Lin, S. and Böhm, C.O. 2011: Himalayan-type escape tectonics along the Superior Boundary Zone in Manitoba, Canada; Precambrian Research, v. 187, p. 248–262.

Le Maitre, R.W. 2002: Igneous Rocks: A Classification and Glossary of Terms; Cambridge University Press, Cambridge, United Kingdom, 236 p.

Lin, S. and Corfu, F. 2002: Structural setting and geochronology of auriferous quartz veins at the High Rock Island gold deposit, northwestern Superior province, Manitoba, Canada; Economic Geology, v. 97, p. 43–57.

Lin, S., Davis, D.W., Rotenberg, E., Corkery, M.T. and Bailes, A.H. 2006: Geological evolution of the northwestern Superior Province: clues from geology, kinematics, and geochronology in the Gods Lake Narrows area, Oxford-Stull terrane, Manitoba; Canadian Journal of Earth Sciences, v. 43, p. 749–765.

Ludwig, K.R. 2003: Isoplot 3.00: a geochronological toolkit for Microsoft® Excel®; Berkeley Geochronological Center, Special Publication 4, 71 p.

Macek, J.J. 1989: Sapphirine coronas from Sipiwesk Lake, Manitoba; Manitoba Energy and Mines, Geological Services, Geological Paper GP85-1, 42 p.

Maniar, P.D. and Piccoli, P.M. 1989: Tectonic discrimination of granitoids; Geological Society of America Bulletin, v. 101, p. 635–643.

Matile, G.L.D. and Keller, G.R. 2006: Surficial geology of the Sipiwesk map sheet (NTS 63P), Manitoba; Manitoba Science, Technology, Energy, and Mines, Manitoba Geological Survey, Surficial Geology Compilation Map SG-63P, scale 1:250 000, URL <https://www.manitoba.ca/iem/geo/gis/surfgeomap.html> [May 2021].

McDonough, W.F. and Sun, S.-s. 1995: The composition of the Earth; Chemical Geology, v. 120, p. 223–253.

McFarlane, C.R.M., Mavrogenes, J.A. and Tomkins, A.G. 2007: Recognizing hydrothermal alteration through a granulite-facies metamorphic overprint at the Challenger Au deposit, South Australia; Chemical Geology, v. 243, p. 64–89.

Meschede, M. 1986: A method of discriminating between different types of mid-ocean ridge basalts and continental tholeiites with the Nb-Zr-Y diagram; Chemical Geology, v. 56, p. 207–218.

Mezger, K. 1989: Dating the P-T evolution of granulites; Ph.D. thesis, State University of New York at Stony Brook, 172 p.

Mezger, K., Hanson, G.N. and Bohlen, S.R. 1989: U-Pb systematics of garnet: dating the growth of garnet in the Late Archean Pikwitonei granulite domain at Cauchon and Natawahunan Lakes, Manitoba, Canada; Contributions to Mineralogy and Petrology, v. 101, p. 136–148.

Mezger, K., Bohlen, S.R. and Hanson, G.N. 1990: Metamorphic history of the Archean Pikwitonei granulite domain and the Cross Lake subprovince, Superior province, Manitoba, Canada; Journal of Petrology, v. 31, p. 483–517.

Mohammadi, N., Fyffe, L.R., McFarlane, C.R.M., Wilson, R. and Lentz, D.R. 2019: U-Pb zircon and monazite geochronology of volcanic and plutonic rocks in southwestern, central, and northeastern New Brunswick (NTS 21G, 21J, 21P); Geological Survey of Canada, Open File 8581, 44 p. URL <https://geoscan.nrcan.gc.ca/starweb/geoscan/servlet.starweb?path=geoscan/fulle.web&search1=R=314824> [February 2021].

Oswald, W., Malo, M., Castonguay, S., Dubé, B., Mercier-Langevin, P., McNicoll, V. and Biczok, J. 2015: Geological setting of the world-class Musselwhite BIF-hosted gold deposit, Ontario, Canada; 13th SGA Biennial Meeting, August 24–27, 2015, Nancy, France, Conference Proceedings, v. 3, p. 1115–1118.

Paktunç, A.D. and Baer, A.J. 1986: Geothermobarometry of the northwest margin of the Superior Province: implications for its tectonic evolution; Journal of Geology, v. 94, p. 381–394.

Pan, Y. and Therens, C. 2000: The Werner Lake Co-Cu-Au deposit of the English River Subprovince, Ontario, Canada: evidence for an exhalative origin and effects of granulite-facies metamorphism; Economic Geology, v. 95, p. 1635–1656.

Pattison, D.R.M. and Tinkham, D.K. 2009: Interplay between equilibrium and kinetics in prograde metamorphism of pelites: an example from the Nelson aureole, British Columbia; Journal of Metamorphic Geology, v. 27, p. 249–279.

Pearce, J.A. 1996: A user's guide to basalt discrimination diagrams; *in* Trace-Element Geochemistry of Volcanic Rocks: Applications for Massive Sulphide Exploration, D.A. Wyman (ed.), Geological Association of Canada, Short Course Notes, v. 12, p. 79–113.

Peccerillo, A. and Taylor, S.R. 1976: Geochemistry of Eocene calc-alkaline volcanic rocks from the Kastamonu area, northern Turkey; Contributions to Mineralogy and Petrology, v. 58, p. 63–81.

Peck, D.C., Halden, N.M., Heaman, L.M., Corkery, M.T., Cameron, H.D.M. and Toope, K. 1999: Field, geochemical and geochronological studies of Paleoproterozoic mafic and ultramafic dykes in the northwestern Superior Province (parts of NTS 63I, 63J and 63P); *in* Report of Activities 1999, Manitoba Industry, Trade, and Mines, Geological Services, p. 97–101, URL <https://www.manitoba.ca/iem/geo/field/roa99pdfs/gs-22-99.pdf> [May 2021].

Percival, J.A., Sanborn-Barrie, M., Skulski, T. Stott, G.M., Helmstaedt, H. and White, D.J. 2006: Tectonic evolution of the western Superior province from NATMAP and LITHOPROBE studies; Canadian Journal of Earth Sciences, v. 43, p. 1085–1117.

Percival, J.A., Skulski, T., Sanborn-Barrie, M., Stott, G.M., Leclair, A.D., Corkery, M.T. and Boily, M. 2012: Geology and tectonic evolution of the Superior Province, Canada; *in* Tectonic Styles in Canada: The LITHOPROBE Perspective, J.A. Percival, F.A. Cook and R.M. Clowes (ed.), Geological Association of Canada, Special Paper 49, p. 321–378.

Piché, M. and Jébrak, M. 2004: Normative mineral and alteration indices developed for mineral exploration; Journal of Geochemical Exploration, v. 82, no. 1, p. 59–77.

Rance, H. 1966: Superior-Churchill structural boundary, Wabowden, Manitoba; Ph.D. thesis, University of Western Ontario, London, Ontario, 131 p. and 1 map at 1:126 720 scale.

Rayner, N. and Stott, G.M. 2005: Discrimination of Archean domains in the Sachigo subprovince: a progress report on geochronology; *in* Summary of Field Work and Other Activities 2005, Ontario Geological Survey, Open File Report 6172, p. 10-1–10-21.

Reinhardt, J. 1987: Cordierite-anthophyllite rocks from north-west Queensland, Australia: metamorphosed magnesian pelites; Journal of Metamorphic Geology, v. 5, p. 451–472.

Sawyer, E.W. 2008: Atlas of Migmatites; The Canadian Mineralogist, Special Publication 9, NRC Research Press, Ottawa, Ontario, 371 p.

Schmidberger, S.S., Simonetti, A., Heaman, L.M., Creaser, R.A. and Whiteford, S. 2007: Lu-Hf, in-situ Sr and Pb isotope and trace element systematics for mantle eclogites from the Diavik diamond mine: evidence for Paleoproterozoic subduction beneath the Slave craton, Canada; Earth and Planetary Science Letters, v. 245, p. 55–68.

Scoates, R.F.J. and Macek, J.J. 1978: Molson dyke swarm; Manitoba Mines, Resources and Environmental Management, Mineral Resources Division, Geological Paper GP78-1, 51 p.

Simonetti, A., Heaman, L.M., Hartlaub, R.P., Creaser, R.A., MacHattie, T.G. and Böhm, C. 2005: U-Pb zircon dating by laser ablation–MC–ICP–MS using a new multiple ion counting Faraday collector array; Journal of Analytical Atomic Spectrometry, v. 20, p. 677–686.

Skulski, T., Corkery, M.T., Stone, D., Whalen, J.B. and Stern, R.A. 2000: Geological and geochronological investigations in the Stull Lake–Edmund Lake greenstone belt and granitoid rocks of the northwestern Superior Province; *in* Report of Activities 2000, Manitoba Industry, Trade and Mines, Manitoba Geological Survey, p. 117–128, URL <https://www.manitoba.ca/iem/geo/field/roa00pdfs/00gs-21.pdf> [May 2021].

Smit, M.A., Scherer, E.E. and Mezger, K. 2013: Lu-Hf and Sm-Nd garnet geochronology: chronometric closure and implications for dating petrological processes; Earth and Planetary Science Letters, v. 381, p. 222–233.

Stern, R.A., Hanson, G.N. and Shirey, S.B. 1989: Petrogenesis of mantle-derived, LILE-enriched Archean monzodiorites and trachyandesites (sanukitoids) in southwestern Superior Province; Canadian Journal of Earth Sciences, v. 26, p. 1688–1712.

Stott, G.M., Corkery, M.T., Percival, J.A., Simard, M. and Goutier, J. 2010: A revised terrane subdivision of the Superior province; *in* Summary of Field Work and Other Activities 2010, Ontario Geological Survey, Open File Report 6260, p. 20-1–20-10.

Sun, S.-s. and McDonough, W.F. 1989: Chemical and isotopic systematics of oceanic basalts: implications for mantle composition and processes; *in* Magmatism in the Ocean Basins, A.D. Saunders and M.J. Norry, (ed.), Geological Society of London, Special Publications, v. 42, p. 313–345.

Syme, E.C., Corkery, M.T., Bailes, A.H., Lin, S., Cameron, H.D.M. and Prouse, D. 1997: Geological investigations in the Knee Lake area, northwestern Superior Province (parts of NTS 53L14, 15); *in* Report of Activities 1997, Manitoba Energy and Mines, Minerals Division, p. 37–46, URL <https://www.manitoba.ca/iem/geo/field/roa97.zip> [May 2021].

Tinkham, D.K. and Ghent, E.D. 2005: Estimating P-T conditions of garnet growth with isochemical phase diagram sections and the problem of effective bulk-composition; The Canadian Mineralogist, v. 43, p. 35–50.

Tomkins, A.G. and Mavrogenes, J.A. 2002: Mobilization of gold as a polymetallic melt during pelite anatexis at the Challenger deposit, South Australia: a metamorphosed Archean gold deposit; Economic Geology, v. 97, p. 1249–1271.

Tomkins, A.G., Pattison, D.R.M. and Frost, B.R. 2007: On the initiation of metamorphic sulphide anatexis; Journal of Petrology, v. 48, p. 511–535.

Tyrrell, J.B. 1903: Report on the northeastern portion of the District of Saskatchewan and adjacent parts of the District of Athabaska and Keewatin; *in* Annual Report, v. XIII, Geological Survey of Canada, p. 5F–37F.

Unterschutz, J.L.E., Creaser, R.A., Erdmer, P., Thompson, R.I. and Daughtry, K.L. 2002: North American margin origin of Quesnel terrane strata in the southern Canadian Cordillera: inferences from geochemical and Nd isotopic characteristics of Triassic metasedimentary rocks; Geological Society of America Bulletin, v. 114, p. 462–475.

Vry, J.K. and Brown, P.E. 1992: Evidence for early fluid channelization, Pikwitonei Granulite Domain, Manitoba, Canada; Canadian Journal of Earth Sciences, v. 29, p. 1701–1716.

Waters, D.J. 2001: The significance of prograde and retrograde quartz-bearing intergrowth microstructures in partially melted granulite-facies rocks; Lithos, v. 56, p. 97–110.

Weber, W. 1983: The Pikwitonei granulite domain: a lower crustal level along the Churchill-Superior boundary in central Manitoba; *in* A Cross Section of Archean Crust, L.D. Ashwal and K.D. Card (ed.), Lunar and Planetary Institute, Houston, Texas, Technical Report 83-03, p. 95–97.

Weber, W. and Mezger, K. 1990: An oblique cross section of Archean continental crust at the northwestern margin of Superior Province, Manitoba, Canada; *in* Exposed Cross-Sections of the Continental Crust, M.H. Salisbury and D.M. Fountain (ed.), Kluwer Academic Publishers, Netherlands, p. 327–341.

Weber, W. and Scoates, R.F.J. 1978: Archean and Proterozoic metamorphism in the northwestern Superior Province and along the Churchill-Superior boundary, Manitoba; *in* Metamorphism in the Canadian Shield, Geological Survey of Canada, Paper 78-10, p. 5–16.

White, R.W., Powell, R., Holland, T.J.B. and Worley, B.A. 2000: The effect of TiO_2 and Fe_2O_3 on metapelitic assemblages at greenschist and amphibolite facies conditions: mineral equilibria calculations in the system K_2O-FeO-MgO-Al_2O_3-SiO_2-TiO_2-Fe_2O_3; Journal of Metamorphic Geology, v. 18, p. 497–511.

White, R.W., Powell, R. and Clarke, G.L. 2002: The interpretation of reaction textures in Fe-rich metapelitic granulites of the Musgrave Block, central Australia: constraints from mineral equilibria calculations in the system K_2O-FeO-MgO-Al_2O_3-SiO_2-H_2O-TiO_2-Fe_2O_3; Journal of Metamorphic Geology, v. 20, p. 41–55.

White, R.W., Powell, R. and Holland, T.J.B. 2007: Progress relating to calculation of partial melting equilibria for metapelites; Journal of Metamorphic Geology, v. 25, p. 511–527.

Winchester, J.A., Park, R.G. and Holland, J.G. 1980: The geochemistry of Lewisian semipelitic schists from the Gairloch district, Wester Ross; Scottish Journal of Geology, v. 16, p. 165–179.